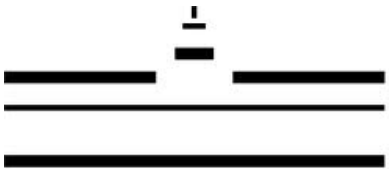

Diploma-Thesis

A Neural Network with Synaptic Plasticity: Applications to Epileptic Seizures

Daniel Ritterskamp

31. Januar 2012

Institut für Theoretische Physik

Westfälische Wilhelms-Universität Münster

Contents

1. Introduction

"It's a dangerous business [...] going out of your door, he used to say. You step into the Road, and if you don't keep your feet, there is no telling where you might be swept off to."

J. R. R. Tolkien, The Fellowship of the Ring

Complex systems always have been a point of fascination and interest in science, due to their multiplicity. For instance, the movement of one pendulum can be calculated analytically and also for two coupled pendular. But if the number increases and the coupling between them becomes more complex, the behaviour of the system is more difficult to predict and it is soon impossible to make a prediction without numerical simulations. The same situation exists for neural populations. A lot is known about the behaviour of one neuron [TDH$^+$11, HGMJ06], but little about larger cultures. Consequently, it is not astonishing that in modern neuroscience many different interdisciplinary approaches are made from a theoretical and experimental point of view. Whereas the common aim is to understand the human brain and in the last decades new knowledge was gained. It is still not yet completely understood. For instance, it is discussed how memory works [FA11, GvH92], an epileptic seizure terminates [LBH$^+$09] or information is processed [MTK05].
Due to the complexity of the human brain and the complex interactions that arise, it is necessary to develop theoretical models to understand and describe the occurring phenomena in neural networks. They are often abstract and some are at first sight not related to the observed biological system. But, they have proofed to be useful. Since the behaviour of the brain is due to the interactions between neurons, one can use this model to simulate small populations and investigate the system dynamics with nonlinear methods. Reduced models, which only consider certain aspects of a biological neuron, can be applied to pinpoint the features that lead to the emergence of a phenomenon. By this, knowledge about the system is gained that finally can be transferred to the biological system and new insights into the human brain itself can be gained.
In this diploma thesis, a theoretical neural model is considered that includes synaptic plasticity, which denotes the change of the connections between the neurons. The description takes place on a microscopic level, because the model describes each neuron of the system and the connections between them.

Since a wide range of disciplines participate in neuroscience, many different models were developed. Each of them has a different focus. Some are accessing the description from a biological point of view, others use more mathematical descriptions and some are developed to investigate special phenomena. Also the level of description differs, since models exist that simulate a network on a neuronal level or that study the behaviour of larger regions in the brain, like the Jansen Model [JR95]. In this thesis, a model is used that describes a neural network on a microscopic level.
One of the models that describes a neuron in great detail on a biological background is the Hodgkin-Huxley Model, introduced by Hodgkin and Huxley in 1990 [HH52]. But, due to its complexity, it is unsuitable to describe larger populations. This model is seen as one of the greatest achievements of theoretical neuroscience in the last century. Based on it, several neural models were developed, like the Fitz-Hugh-Nagumo model, which is obtained by applying simplifications to the Hodgkin-Huxley Model. Two other models that are also related to it are the Morris-Lecar and the Hindmarsh-Rose model. All of the last mentioned models are suitable, due to their reduced complexity, to describe larger populations.
A model mainly used for the simulation of networks is the Leaky-Integrate and Fire Model. It is also established for its exact description of neurons. An overview of the different models can be gained in a review article from Cessac and Samuelides [CS07].
The model used in this thesis is the Lighthouse Model. It was introduced by Hermann Haken [Hak06] and it describes each neuron of the network as a pulse-coupled threshold oscillator. It was developed to investigate synchronization phenomena and the main difference to other neuron models is that the response of a neuron to an input is given by a sigmoidal function. The Lighthouse Model is combined with synaptic plasticity, which was recently performed by Cornelia Petrovic and Rudolf Friedrich [PF12]. Plasticity was first described by Donald Hebb [Heb49] from a biological point of view. Since then, many attempts were made to reveal the underlying mechanism. For example, Bell et al [BHSG99] pointed out that one mechanism, responsible for synaptic plasticity, depends on the spike times of the neurons. Models were introduced to describe this spike time dependent plasticity, for example, by van Rossum et al [vRBT00] and Chun-Chung Chen and David Jasnow [CJ10]. The mechanism introduced by Chen and Jasnow is used in this work.

Since a neural network is simulated, the biological background is shortly introduced in chapter 2. In section 3, the governing equations are explained. Furthermore, the model is compared to two other neural models and the differences between them are pointed out. The aim of chapter 4 and 5 is to get more familiar with the used equations. First the long time behaviour of the coupling weight is considered in chapter 4. Afterwards the findings presented in [CC06, Coo05, GC04], which all studied bumps, are reproduced. Bumps are spatial localized areas of persistent neural activity. In chapter 5 the attributes of the neural network given by the synaptic plasticity are investigated. In addition, associative memory and travelling signals are considered.

Finally, in chapter 6 collective states of the whole system, which are linked to synchronization, are examined. Collective states in neural networks are of general interest in neuroscience and many contributions were made in this area [HH95, LHG09, MG09, RL11]. In contrast to these contributions, the focus of this work lies on the statistical attributes of the occurring states. These collective states are extreme events with distinct statistical features. The underlying dynamic is considered. The behaviour of the system is investigated in the beginning, during and at the termination of a state and explained on the system scale. Their statistical attributes are considered in chapter 6.2 and compared to recently found statistical features of epileptic seizures *et al.* [OFS$^+$10]. For example, Osorio *et al.* [OFS$^+$10] pointed out that the probability density function for the energy of an epileptic seizure is governed by a power-law, which indicates *Self-organized-criticality*. By the comparison similarities between the different systems and their underlying dynamics can be pointed out.

Part I.

Basic concepts

2. Biological background

"We feel like more than just the sum of a trillion neurons. We feel like more than just three pounds of wet flesh, and so simply describing the brain in terms of its neurotransmitters and neurons and all these chemicals and exciting ingredients doesn't fully grapple with what it feels like to be human."

Chimeras of Experience: A Conversation with Jonah Lehrer

The basic unit of the brain is the neuron and the human brain consists of up to 100 billion of them. They are connected via synapses and although the neuron itself is quite simple and well understood, a network of these is very complex and full of mysteries. The biological background in this work will be rudimentary and only the biological information that is necessary for the modelling is given. Recommended literature to get a deeper insight are *Principles of Brain Functioning* [Hak95], *Brain dynamics* [Hak06] by Hermann Haken and *Neurobiology* [She94] by Gordon M. Shephard. In the following, a general description of the neuron itself is given, that is valid for a wide range of neuron types. Secondly, the connection between them, the synapses, are investigated.

2.1. The neuron

A neuron consists of four main components that are shown in figure 2.1. One part are the dendrites that have a rootlike structure and their function is to submit the incoming currents to the soma. The soma is the cell body and the currents are processed and accumulated there. The axon hillock is part of the soma and if the sum of the incoming signals crosses a certain threshold, an action potential is generated there. Through the axon, which is basically a thin wire with a high resistance, the action potential spreads.
The neurons communicate with each other by action potentials. Their emergence is based on the summation of dendritic input currents in the soma, which takes place via a membrane potential. The potential decays if no input signal is received. All action potentials have the same shape and amplitude, whereat the amplitude is of the order of tens of millivolts. Since all produced action potentials are nearly identical, it is assumed that information is stored in the spike rate of the neurons and the exact spike times. The axon hillock has a refractory period after generating a signal. Its length depends on the type of neuron, though. During this refractory time, the hillock can not transmit another spike, independent of the input level.

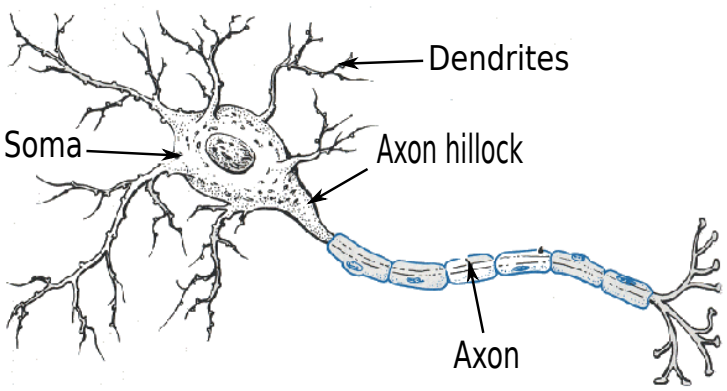

Figure 2.1.: The general structure and the main components of the neuron can be seen. This picture was taken from [Car92]

As a result of this, a maximal spike frequency exists that is around 500 up to 1000 spikes per seconds, but for some kind of neurons in higher cortical areas the maximal spike frequencies is only 30 spikes per second.

2.2. Synapses

Neurons communicate with each other via synapses. Each neuron in the human brain has up to 10^4 synaptic inputs, whereas it is unusual that one neuron receives more than one synaptic input from the same neuron. In reverse, the axon of each neuron has to have the same number of branches. The cerebral cortex, which is the largest part of the human brain, consists of billions of neurons that are densely connected. But this high density only occurs on small spatial ranges and long term connections are much sparser. Therefore, an all-to-all coupling exists between the neurons on a short scale. One has to keep this structure in mind, when a network is set up for numerical simulations.
Different kinds of synapses exist, whereat the general function is the same for all, namely to enable a neuron to pass a signal to another cell. The most common type of synapses is the chemical one and the basic setup can be seen in figure 2.2. A synapse is divided into a presynaptic and postynaptic side. Presynaptic refers to the side at that the incoming signals arrive.
A chemical synapse converts a presynaptic electrical signal into a chemical one and afterwards back into a postsynaptic electrical signal.
This transformation is based on the release of neurotransmitters, which are chemical substances. Caused by an incoming presynaptic action potential, neurotransmitters are emitted into the synaptic gap. Each time a spike arrives, these are released, whereas effects of fatigue

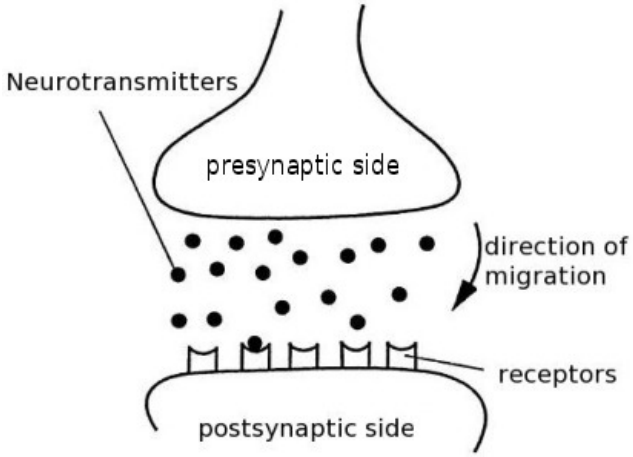

Figure 2.2.: The setup of a synapse is shown. The pre and a postsynaptic side are separated by the synaptic gap. Neurotransmitters are emitted by the presynaptic side and received by the receptors of the postsynaptic one. This figure was taken from [Hak06].

can occur. Fatigue denotes that the synapse is not able to dispense the same amount of neurotransmitters for each ensuing spike. The chemicals diffuse from the presynaptic to the postsynaptic side, where they dock and bind to the receptors. Ion-channels are opened, ion-migration takes place and this causes a depolarization. This is received by the soma of the postsynaptic neuron. In general, a synapse can be inhibitory or excitatory, which denotes that the transferred signal can either lower or enhance the activity of the postsynaptic neuron.

2.3. Propagation of a signal

So far, it was not considered how an action potential emerges and how exactly it surpasses the synaptic gap. A resting potential of -70 mV exists in the membrane of the axon and the hillock, due to an unequal distribution of ions within and outside of the membrane. This is caused by different permeabilities of the ions and the inequality in the resting state is maintained by the sodium potassium pump. The polarisation of the membrane can be changed by incoming charges. A neuron receives input currents from other neurons via the synapses and these are transmitted along the dendrites to the soma, where all incoming signals are accumulated by the polarisation of the axon membrane. If the incoming signal is excitatory, the membrane will depolarize. In reverse, the membrane hyperpolarizes and the likelihood of a spike event decreases if the synapse is inhibitory. If the depolarization surpasses a certain threshold, a short reversion of the potential takes place. The value of the

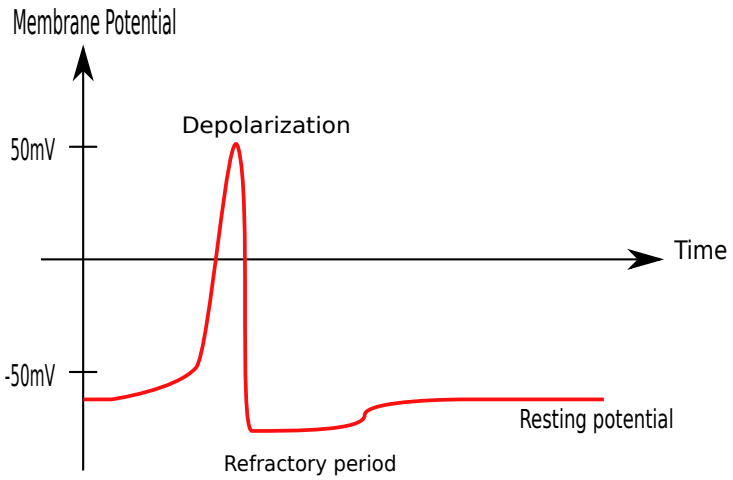

Figure 2.3.: An action potential is shown. If an input is applied, the membrane potential slowly increases starting from the resting potential of approximately -70 mV. After crossing a threshold, it depolarizes. Shortly after this, the membrane starts to repolarize and enters a refractory period. During this period, the neuron can not spike. Afterwards, the voltage increases again, until it reaches the resting potential. A neuron is going through this cycle with each generated action potential.

threshold potential is approximately -55 mV and hence the depolarization has to be larger than -15 mV. The reversal is caused by the opening of ion channels, which happens due to an enhanced voltage. Consequently, ions can migrate from the inside to the outside of the axon membrane. The inside becomes positive and the outside negative and the charges are inverted. By the opening of even more channels, the ions migrate back and the voltage decreases to the resting potential. The change of the potential and the duration of this reversal is nearly independent of the intensity and length of the received current pulse. By this, the constant shape and amplitude of the produced action potentials is explained, which is shown in figure 2.3.
The reversal starts in the axon hillock and travels down the axon, whereas the ions are moving perpendicular to it. From the axon, the action potential reaches the synapses and spreads to other neurons. Since the depolarization has to exceed a certain threshold before a signal is generated and because the shape of the produced signal does not depend on the exact value of the depolarisation, it is called an all-or-nothing signal.
A similar mechanism holds for the transfer of signals via synapses. With each incoming action potential, the presynaptic side emits neurotransmitters into the synaptic gap. The chemicals diffuse from the presynaptic to the postsynaptic side, where they dock and bind

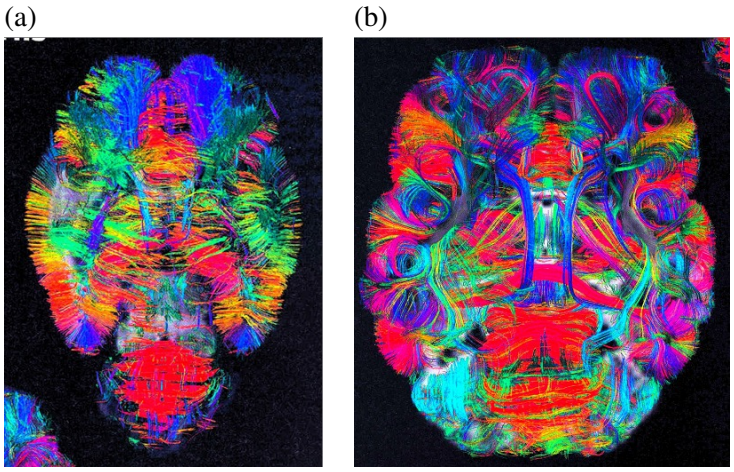

Figure 2.4.: *Diffusion tensor images* (DTI) of the brain of a cat for different ages are shown. In (a) the brain of a ten days old cat and in (b) the brain of a three month old cat is shown. The structure of the synaptic connections is visible. This picture was taken from [Spe10].

to the receptors. This causes an opening of ion channels and subsequent a migration of ions. Consequently, an ionic current penetrates through the membrane and the membrane potential depolarizes. Since neurotransmitters are decaying fast, the ion channels will close quickly. Therefore, the depolarization can not be sustained. This signal is received by the postsynaptic soma. The amount of released neurotransmitters can differ for each synapse and this defines the coupling strength between two neurons.

2.4. Synaptic plasticity

The synaptic connections in the brain are not fixed. New synapses are build, strengthened, disconnected and reconnected constantly. These effects are summarized by synaptic plasticity. For example, the brain of a newborn is quite unstructured, but with ongoing time, the synaptic connections structure, due to the different functionalities of the areas of the brain. In figure 2.4 the *diffusion tensor image* (DTI) of a cat is shown.

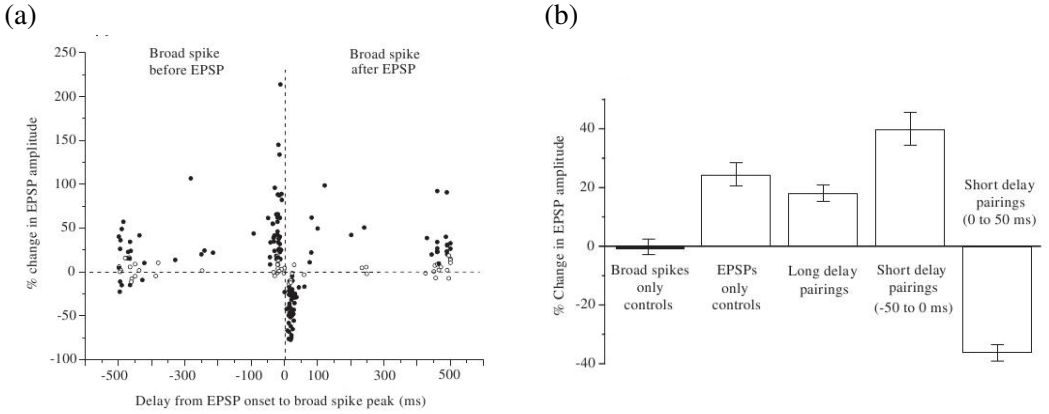

Figure 2.5.: (a) The relative change of the synaptic strength is plotted in dependency on the time difference between postsynaptic and presynaptic spike. It is observed that different kinds of spike pairings cause a change of the synaptic strength. The peaks at a delay time of $\pm$ 500 ms mostly consists of single spikes. The change caused by smaller delay times is due to short delay pairing, which is the main reason for a change of the synaptic weight. (b) A histogram of the different kind of pairings and their contributions to the alteration of the coupling weight is shown and it supports this statement. This figure was taken from [BHSG99].

As can be seen, the brain of a ten days old cat has in comparison to a three month old cat less long range connections and the synaptic connections between the different areas seem to be more unstructured. Ergo, one can conclude that the connections in the brain of a three month old cat adapted to the functionality of the different areas in the brain.
Synaptic plasticity can be explained, for instance, by a change of the number of receptors, a change in the quantity of the released neurotransmitters or by the breaking and creation of new synapses. These effects can be divided into short term plasticity (STP) and long term plasticity (LTP). Short term plasticity is a change of the synaptic strength that decays on a small time scale of a couple of seconds. It can be explained by a change of the probability and quantity, with which neurotransmitters are released. Contributions that consider STP are [AVSN97, TM97].
Long term plasticity (LTP) lasts from minutes up to days and it is linked to a change of the efficacy of synapses and a variation of the number of synaptic connections between two neurons. LTP explains synaptic plasticity in the human brain. It was first discovered and explained by D. O Hebb in his book *The Organization of Behavior: A Neuropsychological Theory* [Heb02]. The main statement is known as the Hebbian learning rule, which states:

> *"Let us assume that the persistence or repetition of a reverberatory activity tends to induce lasting cellular changes that add to its stability. [...] When an axon of cell A is near enough to excite a cell B and repeatedly or persistently takes part in firing it, some growth process or metabolic change takes place in one or both cells such that A's efficiency, as one of the cells firing B, is increased."*
>
> *The Organization of Behavior: A Neuropsychological Theory* [Heb02]

The synaptic change in LTP is due to the the different kind of pairings of the spikes of the connected neurons, as can be seen in figure 2.5. The dependency on the spike relations is called spike time dependent plasticity (STDP).
It is evident that the main mechanism for LTP is short delay pairing. If one takes a closer look at the change of the synaptic weight for small delays, like shown in figure 2.6, one observes that the time window widths, in which the pairings for potentiation and depression of the synaptic strength take place, are asymmetric. The time window for depression is larger than the one for potentiation. In addition, the alteration of the coupling weights differs in both cases. The relative change, due to potentiation, is spread over a wider range. On the opposite the relative depression is nearly constant for a fixed time distance.
These observations are used to model synaptic plasticity in the next chapter. A spike time dependent model is developed, that considers the differences in the changes due to potentiation and depression. But first of all, the underlying neural model is introduced.

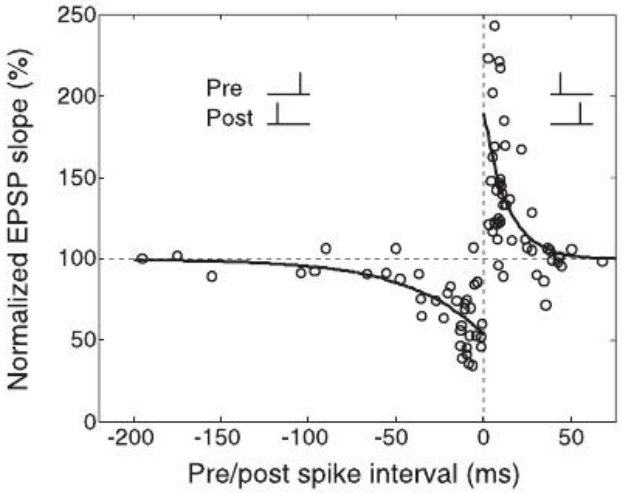

Figure 2.6: The change of the synaptic weight is shown for short time pairings. The figure was produced by [DP06]. The time axis is inverted, in comparison to figure 2.5.

3. Theory

"*Neurons that fire together wire together*"

N. Doidge. 2007 [Doi07]

A wide range of neural models exists that describe the generation of action potentials by a neuron, due to its input signal. Their focus differs and some models have the purpose to simulate the behaviour of a single neuron in a biological accurate way. Others are specialized on the description of bigger populations and therefore reduce the underlying equations, to lower the numerical costs. For instance the number of characterizing equations are downsized by approximations.
The neural network investigated in this work is based on the Lighthouse Model that has been introduced by Hermann Haken [Hak06] with the aim to study synchronization effects on the level of single neurons. It treats a neural network as a system of pulse-coupled oscillators and characterizes each neuron via a phase ϕ and a dendritic current ψ. In addition, the Lighthouse Model is extended by spike time dependent plasticity (STDP).

3.1. Common neural models

Before the Lighthouse Model is investigated, two of the most common neuron models are briefly considered. First, the Hodgkin-Huxley Model is introduced. Second, the Leaky Integrate and Fire Model is presented, which is used to investigate bigger neural populations. Both models are only reviewed briefly and more information about them can be gained in [Fen01, Hak06, HH52, Bur06].

3.1.1. Hodgkin-Huxley Model

The Hodgkin-Huxley Model was introduced by Alan Lloyd Hodgkin and Andrew Huxley in 1952 [HH52]. It models the time development of the membrane potential of a neuron. The membrane is treated as an capacitor and the change of the voltage V is characterized by inflow ion-currents of potassium and sodium ions, which are contained in the membrane.

The model is very precise in describing the generation of action potentials. The underlying equations are stated below.

$$C_M \frac{dV}{dt} = -\bar{g}_{Na} m^3 h \,(V - E_{Na}) - \bar{g}_K n^4 \,(V - E_k) - g_{leak} \,(V - E_{leak}) \tag{3.1}$$

$$\begin{aligned} \tau_m \frac{dm}{dt} &= m_\infty - m \\ \tau_h \frac{dh}{dt} &= h_\infty - h \\ \tau_n \frac{dn}{dt} &= n_\infty - n \end{aligned} \tag{3.2}$$

The constant C_M is the membrane capacitance. Each term on the right hand side of equation (3.1) describes an ionic current, whereat the term in front of the bracket models the conductance of the ion. The maximal value of the ion conductance is given by $\bar{g}_{Ion}$ and E_{Ion} is the reversal potential of the ion. m, h, n are dimensionless gating variables and their values are between zero and one. n represents the fraction of particles that are inside the membrane. m denotes the fraction of activating ions on the inside and h is the proportion of inactivating molecules outside the membrane. The constants n_∞, m_∞, h_∞ adapt the functions to experimental results.the concentration is less that , the recovery rate has to be smaller than the feeding rate
The gating variables in equation (3.1), except the one for the leak term, are governed by differential equations (3.2). These equations are physical motivated and adapted to experimental results. Their aim is to describe the conductances with a reasonable accuracy in a simple way that is suitable for the theoretical description of the action potential and refractory period. Different variations of the Hodgkin-Huxley Model exist. Some added new biological background and other reduced the complexity of the equations to be able to simulate bigger neural systems. For instance, the Hodgkin-Huxley Model was reduced to two dimensions by utilizing that the gating factors m and n are changing so fast that they are, in a good approximation, always at their extreme values. This leads to the Fitzhugh-Nagumo equations [Hak06].

3.1.2. Leaky Integrate and Fire Model

The Leaky Integrate and Fire Model (LIF) uses a more reduced description than the Hodgkin-Huxley Model, but it also describes the generation of an action potential via a capacitance. Its aim is to describe larger populations of neurons, each of which is characterized by a membrane voltage V. If the voltage V reaches a certain threshold θ, the neuron spikes and the voltage is reset to its resting potential. The underlying formula for a single neuron is shown in equation (3.3).

$$\dot{V} = -\frac{V - V_0}{\tau_V} + \frac{I_{ext}}{C} \tag{3.3}$$

$\dot{V}$ denotes the time derivative of V. The first term is the Leak-term and describes the attempt of the membrane to reach the resting potential. If V is larger than V_0, the voltage decays with the rate τ_V until it reaches the resting potential V_0. In reverse, the voltage increases if it is smaller than V_0. The change of the voltage due to input currents I_{ext} is given by the second term. C is the capacitance. The threshold θ does not have to be fixed, but it can underlie a differential equation, which can be seen in equation (3.4).

$$\dot{\theta} = \frac{(\theta_0 - \theta)}{\tau_\theta} + \delta(V - \theta)\,\Delta\theta \tag{3.4}$$

With the spiking of the neuron, the threshold increases by an amount of $\Delta\theta$ and it tends exponentially towards a resting value θ_0. In some versions of the Leaky Integrate and Fire Model, for example [CLM04], the voltage V is kept at the resting value for a period of T_R after the spiking of a neuron and thereby a refractory period is generated.

3.2. Lighthouse Model

The Lighthouse Model has been introduced by Hermann Haken [Hak06]. In opposite to the two models shown before, the Lighthouse Model is not describing a neuron via a capacitor and unlike the Hodgkin-Huxley Model, the main focus lies not on the description of a single neuron in detail, but rather to investigate the collective behaviour of a neural system. It was developed to investigate synchronization phenomena in a neural network and characterizes each neuron as a phase oscillator. These are coupled by the exchanges of delta-pulses. A model, which also considers synchronization phenomena, is the Kuramoto-Model [ABPV$^+$05]. Similar to the Lighthouse Model it describes a system of phase oscillators, but in contrast, a sinusoidal phase coupling is used. In addition, each neuron has a natural phase frequency in the Kuramoto-Model. The underlying model system of the Lighthouse Model is drafted in figure 3.1. The Lighthouse Model reduces a neuron to a phase ϕ_m and a dendritic current ψ_m. Due to the phase description, the model is called Lighthouse Model. One can imagine the beam of a lighthouse spinning and if the beam points at the observer, a flash is detected. This idea is included in the phase ϕ_m, since for each completed turn of the phase the neuron spikes. By this, the behaviour of the axon hillock and the soma are modelled. It sums up the incoming signals and if the phase reaches 2π, a neuron spikes. Therefore it characterizes the polarisation level of the membrane. The phase determines the spike times $t_m^{(n)}$ and hence the action potential $S_k(t)$ of a neuron. The phase ϕ is a 2π-periodic variable. The shape of a spike is described by a delta distribution and thus the spike train $S_k(t)$, generated by neuron k is a sum of delta distributions and reads

$$S_k(t) = \sum_n \delta(t_k^{(n)} - t) = \sum_n \delta(2\pi - \phi_k(t_n))\dot{\phi}_k = S_k(\phi_k(t))\ . \tag{3.5}$$

The derivative of the phase $\dot{\phi}_k$ is included due to normalization. The spike-form can be altered, e.g an alpha function or an Gaussian shaped spike could be used, to introduce more

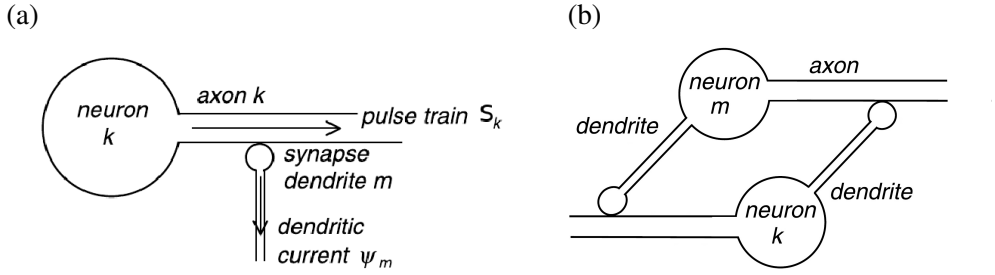

Figure 3.1.: The underlying system of the Lighthouse Model is shown. (a) sketches the generating and transmitting of a spike. (b) displays the connection of two neurons. Neuron k emits an action potential S_k into the axon. This action potential is transformed into a dendritic current ψ_m at the synapses, which is connecting neuron k and neuron m. The dendritic current ψ_m is received by neuron m. The pictures were taken from [Hak06].

realistic shapes. But due to mathematical simplicity, this spike-form is chosen. The evolution equation of the phase ϕ is determined by

$$\dot{\phi}_m(t) = \Xi\left(\sum_k c_{mk}\psi_k(t) + p_{(ext,m)}(t), \theta\right) . \tag{3.6}$$

The change depends on the dendritic current ψ_k of each neuron, times a factor c_{mk} that describes the increment of the phase ϕ_m of neuron m caused by the dendritic current ψ_k of neuron k. Therefore c_{mk} states, which dendritic current is applied to a neuron and from a biological point of view, it characterizes the connection between the dendrites and the cell bodies. The factors c_{mk} form the increment matrix $\bar{c}$. In the following numerical simulations and calculations, the matrix is chosen diagonal. It is assumed that a neuron is only linked to its own dendrites, which is mainly found for biological neurons. By this, only the current of the neuron itself leads to an increase of the phase. The other factor that influences the increment of the phase is the external input $p_{(ext,m)}(t)$. It could be for instance a mechanical or optical input.
The function $\Xi(X,\theta)$ is the Naka-Rushton relation [Hak06] and characterizes the response of a neuron to an input current. The Naka-Rushton relation is given by

$$\Xi(X,\theta) = \frac{\nu X^N}{\theta^N + X^N} . \tag{3.7}$$

It is a sigmoidal function. For high input values X, the output saturates towards a maximum firing rate ν and if the input signal is below a certain threshold value θ, the output is zero. By this, the all-or-nothing behaviour of the axon hillock is simulated. The constant N is used to fit the function to experimental data. The Naka-Rushton relation is plotted in figure 3.2.

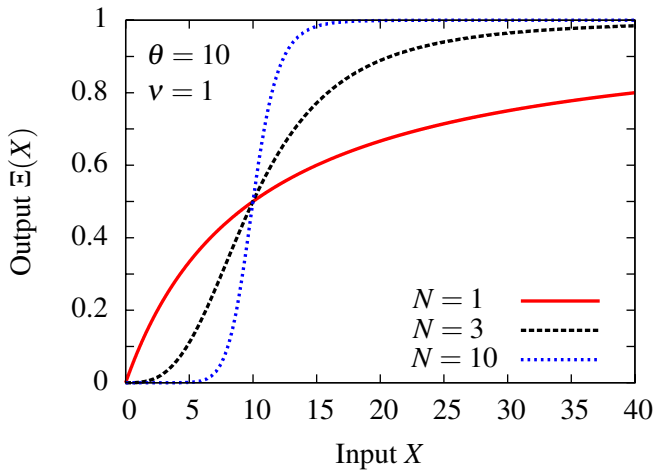

Figure 3.2.: The Naka-Rushton relation is shown for different values of N. As one can see, it saturates for large input values and is around zero for small inputs, whereas the threshold is more distinct for bigger N. For the simulations a N of 3 and a ν of 1 is chosen.

Due to the saturation of the Naka-Rushton relation for large input values, a refractory period τ, after the spiking of a neuron, is included in the system. τ states:

$$\tau = \frac{2\pi}{\nu} \,. \tag{3.8}$$

If a neuron generates an action potential, it will be received by all connected neurons and consequently the dendritic current $\psi_m(t)$ of these neurons will change. The dendritic current is governed by the differential equation

$$\dot{\psi}_m(t) = \sum_k a_{mk}\, S_k(\phi_k(t)) - \gamma\psi_m(t) \,. \tag{3.9}$$

The parameter a_{mk} is the synaptic weight and describes the connection pointing from neuron k to neuron m. Thereupon, if neuron k emits an action potential and the coupling weight a_{mk} is non zero, it will receive the spike and the dendritic current ψ_m changes. If a_{mk} has a positive sign, the current increases and the connection is denoted as excitatory coupling. A negative sign induces a decrease of the current and is called inhibitory coupling. The synaptic weights are part of the coupling matrix $\underline{a}$. It characterizes the synaptic connection of the system. Because the axon and dendrites are similar to a wire with a resistant, the dendritic current is damped exponentially with a decay constant γ. In figure 3.3 two coupled neurons are considered and the relationship between the phase ψ_m of neuron m and the dendritic current ϕ_k of neuron k is demonstrated. Like one would expect, the dendritic current of

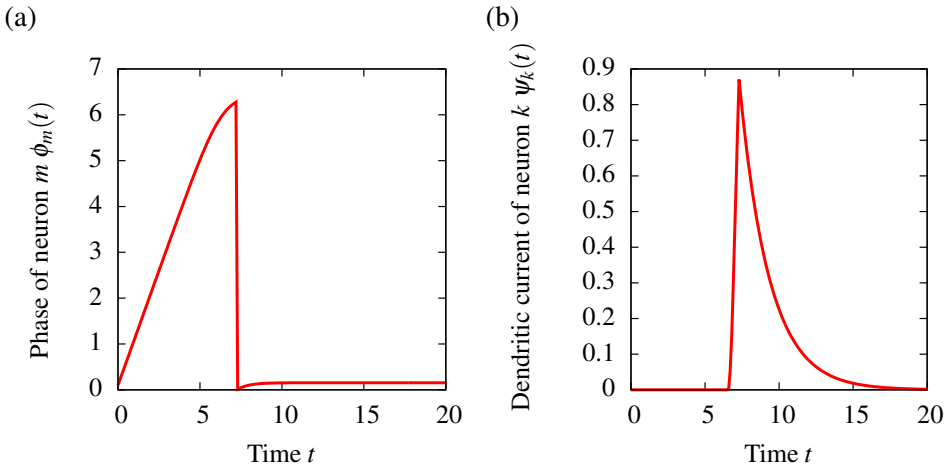

Figure 3.3.: Two neurons are observed, whereat in (a) the phase ϕ_m of neuron m and in (b) the dendritic current ψ_k of neuron k is plotted. They are linked to each other by synapses. Therefore the current ψ_k of neuron k is changing if neuron m spikes. As one can see, with the reset of the phase the dendritic current of neuron k increases rapidly and decays exponentially afterwards.

neuron k changes with spiking of neuron m. If one compares the Lighthouse Model to the Leaky-Integrate and Fire Model, it can be observed that the main difference between them is not the introduction of a phase variable, since the Leaky-Integrate and Fire Model can be transformed into a phase description [CLL$^+$11], but rather the phase relation of the Lighthouse Model. The phase velocity of a Lighthouse Neuron is given by the output of the Naka-Rushton relation, which includes the refractory period and the all-or-nothing behaviour of the neuron. Furthermore, a non-linear response to input signals of the neuron is included in the system.

3.3. Spike time dependent plasticity (STDP)

The applied mechanism for spike time dependent plasticity is based on the Hebbian learning rule and has been introduced by Chen [CJ10] and van Rossum *et al.* [vRBT00]. It depends on the relationship between the spikes of two neurons. If two neurons fire causal, the coupling weight a_{km} will strengthen and it will weaken for acausal firing. For the coupling weight a_{km} causal firing designates that neuron m spikes before neuron k. The occurring spiking can consequently be caused by the connection. Conversely, acausal firing denotes the spiking of neuron k before neuron m.
As one can see, for the same spike pattern the coupling weight a_{km} strengthens and the reverse coupling weight a_{mk} weakens. Therefore, the connection between two neurons

becomes directed by Hebbian learning. To detect a causal or acausal relationship between two neurons, Chen *et al.* [CJ10] introduced time windows by postulating the existence of a chemical reaction. This mechanism is based on the release of neurotransmitters at the synapse with the receiving of an action potential on the presynaptic side. The time window is characterized by chemical concentrations A_m and B_m at the synapse of the neuron m, whereupon A_m and B_m describe the time window of neuron m responsible for potentiation and depression, respectively. If neuron m spikes, both chemical concentrations will increase rapidly and decay exponentially with decay rates τ_A and τ_B. These decay rates define the time window widths. The differential equation for the chemical concentrations reads

$$\dot{\sigma}_m(t) = u_\sigma(1-\sigma_m(t)-I_\sigma^m(t))S_m(t) - \frac{\sigma_m(t)}{\tau_\sigma} \quad ; \quad \sigma_m = A_m, B_m \; . \tag{3.10}$$

u_σ is the mean fraction of neurotransmitters, which are released at the synapse if a neuron spikes, to the amount of transmitters that can be maximally produced without σ getting larger than its saturation value $1-I_\sigma$. Accordingly, u_σ has to be smaller than 1. The existence of a saturation concentration is due to a physiological determined maximum, since only a limited amount of neurotransmitters is available. In addition, effects of fatigue can occur. The expression $(1-\sigma_m-I_\sigma)$, contained in the first term on the right hand side, is lowering the increment of the amplitudes with increasing value of the amplitude itself. If a high spiking rate is received for a long time by the synapse, the saturation value of the chemical concentrations will decrease due to fatigue. The fatigue is represented by the inactive state I_σ and it blocks a fraction of the chemical concentration σ. The critical differential equation is

$$\dot{I}_\sigma^m(t) = \frac{\sigma_m(t)}{\tau_{l\sigma}} - \frac{I_\sigma^m(t)}{\tau_{r\sigma}} \; . \tag{3.11}$$

The inactive state increases with the chemical concentration σ itself and the increase rate is given by $\tau_{l\sigma}$. The chemical concentration regenerates with the recovery constant $\tau_{r\sigma}$. It is assumed that the feeding rate of the blocked fraction is less than the decay rate of the chemical concentration.

$$\tau_{l\sigma} \geq \tau_\sigma$$

If neuron k spikes within the time window, thus before the chemical concentration of neuron m decayed to zero, one can identify a causal or acausal relationship between two spikes and therefore the coupling weight changes.

$$\dot{a}_{km}(t) = \Delta A_m(t)S_k(t) - r a_{km}(t)B_k(t)S_m(t) \tag{3.12}$$

The first term of equation (3.12) characterizes potentiation due to causal firing. The potentiation is proportional to the potentiation constant Δ and it is larger, if the two neurons spike right after each other. This is caused by the exponential damping of the chemical concentrations. The second term causes the depression of the coupling weight. It is proportional to the

depression constant r and it contains the coupling weight a_{km} itself. Therefore the depression produces in contrast to the potentiation a relative change. This can lead to a saturation of the coupling weights a_{km}, as one will see in the next section and in chapter 4.
If one keeps in mind the discussion of synaptic plasticity from a biological point of view from chapter 2.4, it is obvious that the introduced spike time dependent plasticity mechanism can describe all kind of spike pairings. But the STDP has to be implemented for each possible kind of pairing separately, because the learning parameters have to be adapted and the algorithm has to be applied to different coupling weights. For short-delay pairing, self-coupling is neglected and consequently the STDP is not applied to the diagonal elements of the coupling weight matrix. To simulate synaptic plasticity caused by single spikes, the algorithm is just applied to the diagonal elements. In this work only short-delay pairing is simulated.
An important fact gained by the experimental data, is that the time windows for potentiation and depression are asymmetric, as can be seen in figure 2.6. The time scale, necessary for the description of synaptic plasticity, is based on the spike frequencies of the neurons. But the scales on that the plasticity influences the couplings can be adapted by the learning parameters. For instance, to slow down the change of the synaptic weights the potentiation and depression constants Δ and r can be lowered.

3.4. Extended Lighthouse Model

In this thesis the Lighthouse Model is combined with STDP, as was suggested by Cornelia Petrovic and Rudolf Friedrich [PF12]. Therefore the extended Lighthouse Model describes a neural network, whereat the connections between the neurons are not fixed, but changing in dependency of the spiking. The equations that are to solve are

$$\begin{aligned}
\dot{\phi}_m(t) &= \Xi\left(\sum_k c_{mk}\psi_k(t) + p_{(ext,m)}(t), \theta\right) , \\
\dot{\psi}_m(t) &= \sum_k a_{mk}\, S_k(\phi_k(t)) - \gamma\psi_m(t) , \\
\dot{\sigma}_m(t) &= u_\sigma(1-\sigma_m(t) - I_\sigma^m(t))S_m(t) - \frac{\sigma_m(t)}{\tau_\sigma} , \\
\dot{I}_\sigma^m(t) &= \frac{\sigma_m(t)}{\tau_{l\sigma}} - \frac{I_\sigma^m(t)}{\tau_{r\sigma}} ,
\end{aligned} \tag{3.13}$$

and

$$\dot{a}_{km}(t) = \Delta A_m(t)S_k(t) - r a_{km}(t)B_k(t)S_m(t) . \tag{3.14}$$

The equations for the blocked fraction I_σ^m and the chemical concentration σ_m has to be solved twice for each neuron. In the following, the increase matrix $\underline{c}$ is chosen diagonal and

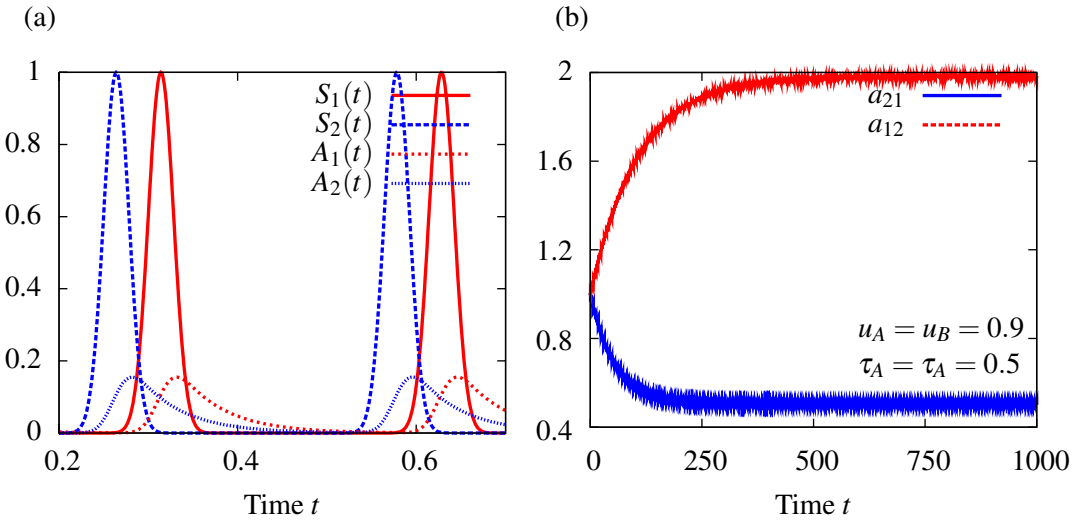

Figure 3.4.: (a) The spike train $S_1(t)$ and $S_2(t)$ of neuron one and neuron two are plotted. Furthermore, the chemical concentrations of both neurons are shown. The time window widths and the chemical fractions for potentiation and depression are set up equally. Consequently, the chemical concentrations for potentiation and depression A_i and B_i are the same. In (b) the coupling weight a_{12} and a_{21} are displayed.

therefore the neurons are interacting via the dendritic current ψ_m with each other. A network of identical neurons is considered. The Lighthouse Model is dimensionless and due to this, units are omitted. The scaling factor of the time axis is given by the saturation frequency ν included in the Naka-Rushton relation. If it is assumed that the maximal spiking frequency is 500 spikes per second, the minimal distance between two spikes of one neuron is given in milliseconds and the dynamics take place on the same time scale.

3.4.1. Demonstration STDP

In the following example, the learning algorithm is demonstrated and the fact that the coupling weights can saturate. A system of two neurons is simulated and the spike rates of the neurons are fixed. The action potential, the chemical concentrations and the coupling weights are observed. As one can see in figure 3.4 (a), the chemical concentration of neuron two increases with the spiking of it and decays exponentially. Before the concentration decays to zero, neuron one spikes and therefore the chemical concentration overlaps with the spike train of neuron one. This superposition leads, as described by equation (3.12), to an increase of the coupling weight a_{12}, because it is conform to causal firing concerning a_{21}. Reversely, the same overlap denotes acausal firing regarding coupling weight a_{21} and therefore the coupling weight decreases. This can be seen in 3.4 (b). Furthermore, one can

see that the coupling weights are tending towards a saturation value on a large time scale. It is obvious that no real saturation occurs, but an oscillation around a suspension value takes place. This can be seen in figure 3.4 (b).
This behaviour is included in the learning mechanism, since it only contains singular contributions caused by the delta distribution contained in equation (3.12). The change of the coupling weight for potentiation is absolute. On the opposite the depression contains the coupling weight a_{ij} itself and hence the depression is a relative alteration. Therefore, a coupling weight exists where the potentiation and depression annihilate each other over a spike cycle. The coupling weight is in this case on a periodic orbit and an oscillation of the coupling weights around the saturation value occurs.

3.5. Neural Mass Model

A neural model, based on a neuronal level description, underlies limitations in the simulation of large populations. Therefore models that are able to simulate large networks, for example a cortical column, are briefly introduced, by taking the example of the Neural Mass Model developed by Oliver David *et al.* [DHF05]. It is based on the Jansen Model, which was introduced by Ben H. Jansen and Vincent G. Rit [JR95]. The following discussion follows [HO11]. The model is describing an area of the brain and the considered system variables are averaged values. The aim of this model is to reproduce the output signal, like EEG or MEG readings, of a large population in the brain. Since the output signal of the model can be directly compared to experimental data, one is able to investigate the effects that lead to the behaviour of the experimental data. The described population is tripartitioned into an excitatory sub-population, an inhibitory sub-population and an excitatory output sub-population of pyramidal cells. The general setup of the model system can be seen in figure 3.5. Each neural population has an average membrane potential, which is altered by the incoming average pulse density of action potentials. The response of the membrane potential is given by the convolution of $H_{i,e}$ and the incoming pulses. $H_{i,e}$ reads

$$H(t) = \begin{cases} H_{i,e} t e^{\frac{t}{\tau_{i,e}}} & t \geq 0 \\ 0 & t < 0 \end{cases} . \tag{3.15}$$

The function differs for excitatory (e) and inhibitory (i) populations. $H_{i,e}$ is the maximal post-synaptic potential and $\tau_{i,e}$ is a delay constant. The average membrane potential produces an average pulse density of action potentials, whereat the transformation S between the membrane potential and the pulse density is a sigmoidal function. The population of pyramidal cells produces an output signal, which can either be send to another cortical column or be measured as an EEG or MEG signal, whereas a transformation regarding the kind of output signal has to be performed. The model can be extended to describe two connected columns, whereat the coupling between these underlies restrictions [DHF05].

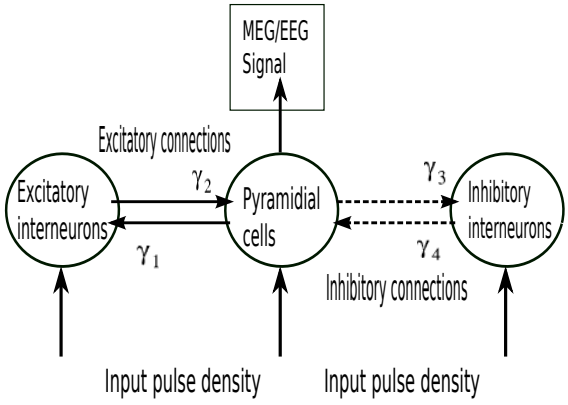

Figure 3.5.: The setup of the Jansen Model is drafted. The system consists of three sub-populations that are connected with each other via synapses. The connections are described by the connectivity constants γ_i. These describe the number of synapses between the systems. An external pulse density is applied on the system. Only the population of pyramidal neurons is producing an output signal and the inhibitory and excitatory sub-populations are coupled bidirectional to the the pyramidal population. This draft is based on a figure of [DHF05].

The model does not use a microscopic description of the neuronal population, but applies a macroscopic depiction. Therefore the mathematical model averages over all neurons of the population. The interior behaviour of the neural population is contained in the parameter settings and in the tripartitioning. In contrast to this, the Lighthouse Model focuses on the inner structure of the population and the dynamic of the single elements.
These two different kinds of models are therefore supplementing each other. Both systems have similarities in their response functions to incoming pulses and in the production of pulses. In the Lighthouse Model an incoming pulse, leads to an increase of the dendritic current, which decays exponentially in time. A similar behaviour is described by equation (3.15). Furthermore, the produced pulse density of action potentials in both systems is given by a sigmoidal function. Consequently, if a large population is simulated with the Lighthouse Model and if it is set up in a similar way as shown in figure 3.5, the produced output should be similar to the one produced by the Jansen Model. Since the extended Lighthouse Model includes synaptic plasticity one could use this model to figure out how the response functions of the neural population in the Jansen Model have to change in time to include synaptic plasticity.

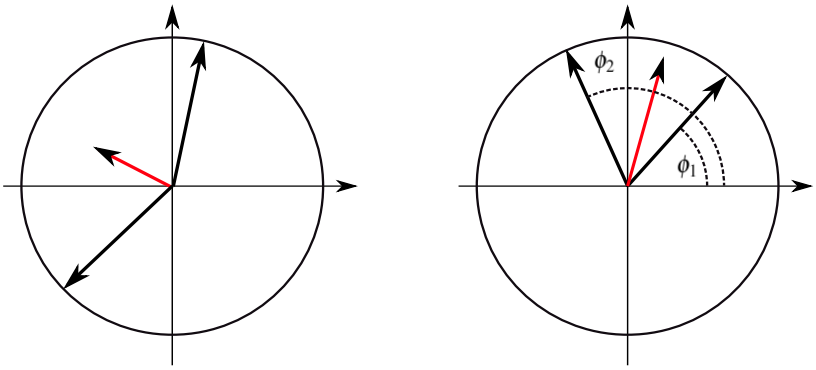

Figure 3.6.: The system vector is calculated for two different setups of the phase vectors and is marked in red. As one can see, the length of the system vector is larger if the two vectors are pointing into similar directions. This indicates that their phases are similar and therefore their synchronization is higher.

3.6. Methods and Numerics

3.6.1. Synchronization

In the following, it is necessary to calculate the synchronization between neurons. It is calculated via the phase vector $\vec{r}_{\phi_i}$ of each neuron. Each vector has a length of one and is given by:

$$\vec{r}_{\phi_i} = \begin{pmatrix} cos(\phi_i) \\ sin(\phi_i) \end{pmatrix} . \tag{3.16}$$

The average phase vector is calculated, which is denoted as system vector. If all phase vectors point in the same direction, which indicates that the phases of the neurons are similar, the length κ of the resulting system vector is larger. In reverse, the length of the vector is smaller if all vectors point in random directions. Therefore, the length κ of the system vector is a measure for the synchronization of the phases and is determined by:

$$\kappa = \frac{1}{N} \left| [\sum_i \vec{r}_{\phi_i}] \right| . \tag{3.17}$$

The calculated synchronization parameter is equivalent to the coherence K of the Kuramoto-Model [ABPV$^+$05].

3.6.2. Runge-Kutta-method

The time step procedure, used to solve the equations introduced above, is the Runge-Kutta-method. The method was developed in the beginning of the 20th century by C. Runge

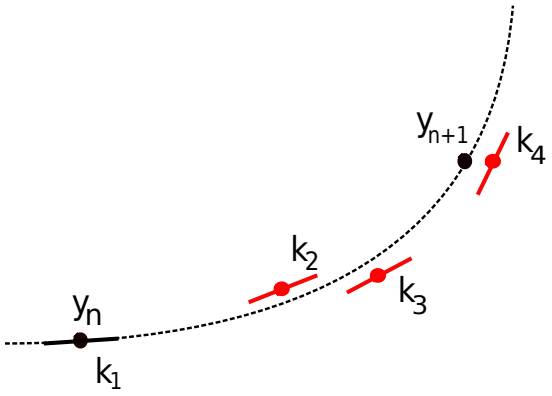

Figure 3.7.: The main idea of the Runge-Kutta-method is shown. The function is evaluated at different times between the discrete time steps.

and M. W. Kutta and it is a common procedure for solving ordinary differential equations nowadays [Pre07]. The classical Runge-Kutta-method is numerically stable and exact, since the global error of this method is of the fourth order of the time step size Δt. The classical Runge-Kutta-method and the general approach to solve an equation numerically are shortly introduced. The equation that is to solve has the form

$$\frac{d}{dt}y(t) = f(t, y(t)). \tag{3.18}$$

First one has to discretize the time, whereas the time step is referred to as Δt. The used equations for the classical Runge-Kutta-method are shown below.

$$y_{n+1} = y_n + \frac{h}{6}\,(k_1 + 2k_2 + 2k_3 + k_4) \tag{3.19}$$

$$\begin{aligned} k_1 &= f(t_n, y_n) \\ k_2 &= f(t_n + \frac{\Delta t}{2}, y_n + k_1\frac{\Delta t}{2}) \\ k_3 &= f(t_n + \frac{\Delta t}{2}, y_n + k_2\frac{\Delta t}{2}) \\ k_4 &= f(t_n + \Delta t, y_n + k_3\Delta t) \end{aligned} \tag{3.20}$$

The Runge-Kutta-method evaluates the right hand side of equation (3.18) at four different times per step. Once at the initial point (y_n, t_n), twice at midpoints and once at the endpoint ($y_n + \Delta t$, $t_n + k_3\ \Delta t$), which is the next point in time on the discrete scale. Afterwards a weighted mean value is calculated to gain the next function value. The method is sketched in figure 3.7.

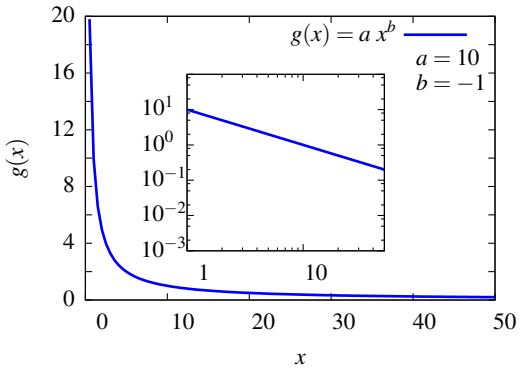

Figure 3.8.: A power-law is plotted. The scaling of both axes in the inset is logarithmic.

3.6.3. Probability density function

Since the probability density function (*PDF*) is calculated in chapter 6, it is briefly introduced. A complete description can be found in [Pop00]. Consider a dynamical system with a dynamic variable $x(t)$ that depends only on time. All possible values of this variable $x(t)$ describe the set of events Ω. The function value $f(y)$ states the probability to find the system in the state $y \in \Omega$. Since the *PDF* denotes a probability, it has to fulfil two conditions.

$$f(x) \geq 0 \quad \text{and} \quad \int_{\Omega} f(x)\,dx = 1 \tag{3.21}$$

A probability can not be smaller than zero and the probability of the dynamic variable to take any value of Ω has to be one, since the variable can not be outside of the event set. The *PDF* is gained by averaging all possible realisations y of the dynamic variable $x(t)$ over all times.

$$f(y) = \lim_{T\to\infty} \frac{1}{T} \int_0^T \delta(y - x(t))\,dt = < \delta(y - x(t)) > \tag{3.22}$$

As can be seen, the integral is non-zero if the dynamic variable $x(t)$ takes the value of y. Therefore $f(y)$ states the probability that the system reaches the value y. By this, a histogram for all elements is created with an infinitesimal bin-size.
Consider the case that the time series of a dynamical system is given, but the *PDF* is unknown. The data is in the time interval $[0 : T_{max}]$. One is able to estimate the *PDF* of $x(t)$ with equation 3.22. If the system is stationary and the time series represents the dynamics of the system well, the estimated *PDF* is close to the real one. This is applied in chapter 6.

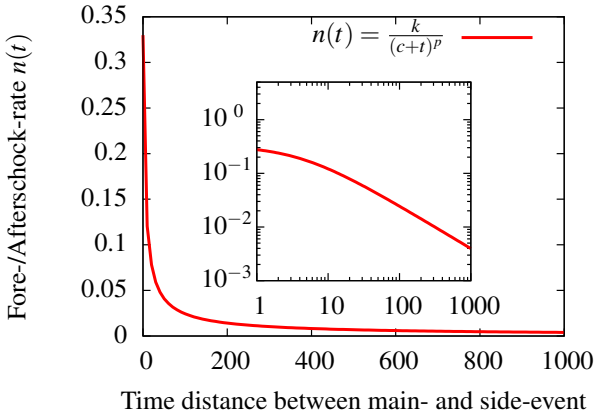

Figure 3.9.: The Omori-Law is plotted in this figure for random parameter settings.

3.6.4. Power-law

In chapter 6, power-laws are fitted into the received probability density functions. A power-law is described by the following equation:

$$g(x) = \beta \cdot x^{\alpha}. \tag{3.23}$$

β is a pre-factor and α the scaling coefficient. The power-law is plotted in figure 3.8. As can be observed, it tends asymptotic to the x-axis for bigger x-values. For small x-values it increases rapidly and it is going towards infinity for x tending to zero.

3.6.5. Omori-Law and Inverse Omori-Law

Earthquakes are rare events in time. They are discharges of tension that accumulate in the earth crust. A discharge is often followed or headed by another discharge. This behaviour is described by the Omori- and inverse Omori-Law, whereat the inverse Omori-Law predicts the foreshock-rate and the Omori-Law describes the aftershock-rate $n(t)$ in dependency of the time difference from the main shock. Both are empirical laws, which are described by equation (3.24), whereas the parameters are different. It was originally introduced by Omori *et al.* [Omo94] and extended by Utsu *et al.* [UOM95].

$$n(t) = \frac{k}{(c+t)^p} \tag{3.24}$$

$$\Leftrightarrow \log(n(t)) = \log(k) - p\ \log(c+t) \tag{3.25}$$

k is an amplitude, c is an offset parameter and p describes the decay rate. For aftershocks it is typically between 0.7 and 1.5. t is the time-difference between the main event and the foreshock or aftershock. The Omori- and inverse Omori-Law are shown in figure 3.9. For earthquakes an asymmetric foreshock- and aftershock-rate is observed. This can be explained by the fact that it is not unequivocal to determine if the event is an aftershock or already a foreshock to the next main-event [STR04].

Part II.

Results

4. Analytical approaches

4.1. Saturation of the coupling weights

In this section the behaviour of the coupling weights on a large time scale is investigated. Due to the governing equations (3.12), one would suspect that saturation occurs. However, saturation does not denote an asymptotic stability, but rather an oscillation about a resting point. This behaviour is included in the learning mechanism and was explained in section 3.4.1 by the example of two neurons. In the following, a similar system is considered and the saturation value for the coupling weights is calculated analytically. The system consists of N neurons and the phase velocity $\dot{\phi}_i$ for all neurons is fixed and given by ω. Accordingly, the phase of each neuron is denoted by:

$$\phi_i = \phi_i^{(0)} + \omega t \ . \tag{4.1}$$

$\phi_i^{(0)}$ is the initial value of the phase ϕ_i. The spike-times $t_i^{(n)}$ are determined by the phase ϕ_i and are given by:

$$t_i^{(n)} = t_i^{(0)} + n\Delta_T. \tag{4.2}$$

$t_i^{(0)}$ is the initial spike time and denotes the point in time, at which the neuron spikes the first time. It can be calculated by $2\pi \stackrel{!}{=} \omega\, t_i^{(0)} + \phi_i^{(0)}$. Δ_T is the time between two spikes of neuron i and is consequently given by $\Delta_T = \frac{2\pi}{\omega}$. Accordingly, the action potential $S_i(t)$ is completely determined by the initial phase $\phi_i^{(0)}$ and the spike frequency ω. An additional assumption is that all initial spike times $t_i^{(0)}$ are in the time interval $[0\ ;\ \Delta_T]$.
To find the saturation value of the coupling weights, a self-consistency check is performed. The dendritic current is determined by means of the calculated coupling weights. By this current, the phase velocity $\dot{\phi}_i$ is calculated to see if it is consistent with the assumed initial phase velocity ω. The scheme is shown in figure 4.1.

4.1.1. Basic equations

The learning algorithm contains differential equations for the chemical concentrations, their fatigue and the actual change of the coupling weight. In the following, the fatigue is neglected to simplify the calculations. Therefore the remaining differential equations is the evolution

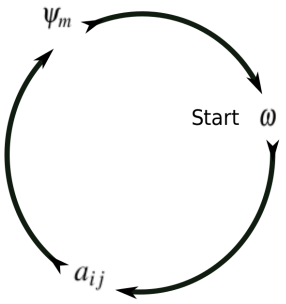

Figure 4.1.: The self-consistency scheme for the phase velocity $\dot{\phi}$ is shown

equation for the chemical concentration $\sigma_m(t)$ and for the coupling weight $a_{ij}(t)$ that are shown below.

$$\dot{\sigma}_j(t) = u_\sigma[1-\sigma_j(t)]\ \omega\ \delta\left(t - t_j^{(0)} - \Delta_T n\right) - \frac{\sigma_j(t)}{\tau_\sigma} \tag{4.3}$$

$$\dot{a}_{km}(t) = \Delta A_m(t) S_k(t) - r a_{km}(t) B_k(t) S_m(t) \tag{4.4}$$

Both equations contain delta distributions and hence for the analysis Poincare-maps are used, whereby the planes are given by the delta distributions. The coupling weight a_{ij} does not change between two spikes, but the chemical concentration $\sigma_j(t)$ is not fixed over an interval, due to the contained damping term.

4.1.2. Chemical concentrations

First the chemical concentration is calculated. The equation is shown in (4.3). For the calculation, one neuron is considered and its spike times are given by $t_i^{(n)}$. Time is decomposed into equal intervals of the length Δ_T, whereupon the edges are given by spikes. Each interval has to contain one spike and therefore the right interval-border is close and the left border is open. The setup is shown in figure 4.2. Equation (3.10) splits into two parts, because the term including the delta-distribution is only non zero at the right interval border. The solution of the ordinary differential equation between the spike is

$$\sigma_j\left(t + (n-1)\Delta_T + t_j^{(0)}\right) = \sigma_j\left(\Delta_T(n-1) + t_j^{(0)}\right) e^{-\frac{t}{\tau_\sigma}} \quad ;0 < t < \Delta_T\ . \tag{4.5}$$

The chemical concentration is decaying exponentially between two spikes. Only if the neuron spikes, the chemical concentration receives a positive input. At time $t_j^{(n)}$, the decay

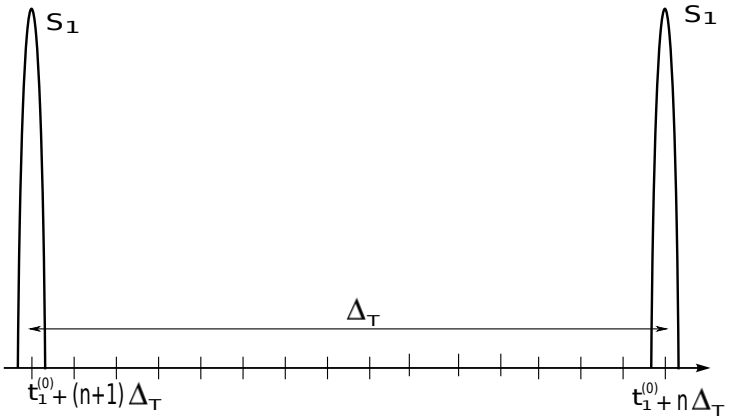

Figure 4.2.: The setup of the analytical calculations can be seen. Time is divided into equal intervals of the length Δ_T, whereas the edges are given by the spikes of the neuron.

term is not considered, since it is already contained in expression (4.5). The change $\Delta\sigma_j$ of the chemical concentration at $t_j^{(n)}$ is constituted by:

$$\Delta\sigma_j = -\frac{\sigma_j}{\tau_\sigma} + \omega\, u_\sigma[1-\sigma_j] \approx \omega\, u_\sigma\left[1-\sigma_j\left(\Delta_T(n-1)+t_j^{(0)}\right) e^{-\frac{\Delta_T}{\tau_\sigma}}\right] . \tag{4.6}$$

The chemical concentration at the right border of the interval is accordingly characterized:

$$\sigma_j\left(\Delta_T n + t_j^{(0)}\right) = \omega\, u_\sigma + \left[1-u_\sigma\omega\right]\, \sigma_j\left((n-1)\Delta_T + t_j^{(0)}\right) e^{-\frac{\Delta_T}{\tau_\sigma}} . \tag{4.7}$$

A recursive expression is gained for the chemical concentration σ_j. If one reinserts the expression n-times, an expression that depends on the initial conditions of the neurons is received. The middle terms can be expressed by a sum. The equation for σ_j reads

$$\sigma_j\left(\Delta_T n + t_j^{(0)}\right) = \omega\, u_\sigma + \sum_{m=1}^{n-1} \omega\, u_\sigma\left[(1-u_\sigma\omega)e^{-\frac{\Delta_T}{\tau_\sigma}}\right]^m + \sigma_j\left(t_j^{(0)}\right)\left[(1-u_\sigma\omega)e^{-\frac{\Delta_T}{\tau_\sigma}}\right]^n . \tag{4.8}$$

By absorbing the first term into the sum, the index can be rewritten and a geometric series is received. Consequently, if the expression in the brackets of the second term is smaller than one and larger than minus one, the limit of the series is well known. For the beginning, it is hypothesized that this condition is satisfied and it is discussed later. The same expression occurs in the last term of the equation (4.8). Since the long time behaviour of the system is considered, it is assumed that $n \gg 1$ and therefore this term is zero in a good approximation. Its basis is smaller than one and $\lim_{n\to\infty} q^n = 0$ for $|q| < 1$. In addition to this, the limes of the

geometric series for $n \to \infty$ is used. The resulting expression for the chemical concentration is

$$\sigma_j\left(t_j^{(0)}\right) = \omega\, u_\sigma \frac{1}{1-\left[1-\omega\, u_\sigma\right] e^{-\frac{\Delta_T}{\tau_\sigma}}} \tag{4.9}$$

As one can see in equation (4.9), the chemical concentration is independent of the initial value and only depends upon the frequency ω and the learning parameters τ_σ and u_σ. It states the chemical concentrations at the spike times of neuron j. The concentration between two spikes is given by

$$\sigma_j\left(t_j^{(0)}+t\right) = \omega\, u_\sigma \frac{1}{1-\left[1-\omega\, u_\sigma\right] e^{-\frac{\Delta_T}{\tau_\sigma}}}\, e^{-\frac{t}{\tau_\sigma}} = \sigma_j\left(t_j^{(0)}\right) e^{-\frac{t}{\tau_\sigma}} \quad ;0 \le t < \Delta_T\ . \tag{4.10}$$

The explicit form of $\sigma_j\left(t_j^{(0)}\right)$, which is the maximal amplitude of the chemical concentration, for depression B_j and potentiation A_j is

$$\begin{aligned} A_j &= \omega\, u_A \frac{1}{1-\left[1-\omega\, u_A\right] e^{-\frac{\Delta_T}{\tau_A}}}\ , \\ B_j &= \omega\, u_B \frac{1}{1-\left[1-\omega\, u_B\right] e^{-\frac{\Delta_T}{\tau_B}}}\ . \end{aligned} \tag{4.11}$$

4.1.3. Coupling weight

After determining an expression for the chemical concentrations, the coupling weights a_{km} are calculated. Each weight depends on the spiking of two neurons and a system of two neurons is considered. Since, the coupling weight does not change between two spikes, it only has to be calculated at the spike times $t_l^{(n)}$.
Time is decomposed in intervals of the length Δ_T as shown in figure 4.3. Each interval contains one spike of each neuron. The interval-borders are given by the spikes of one neuron and as before one edge is open and the other one is close. In the following, it is assumed that neuron j spikes before neuron i. Because, the change of the coupling weight depends on the relation between the spikes of the two neurons, one has to calculate the coupling weight a_{ji}, which is under these conditions depressed and the coupling weight a_{ij} that is potentiated. Before the coupling weights are calculated, some notations are introduced.

$$t_i^{(n)} = \Delta_T n + t_i^{(0)}, \tag{4.12}$$

$$t_j^{(n)} = \Delta_T n + t_j^{(0)}, \tag{4.13}$$

$$t_i^{(n)} - t_j^{(n)} = t_i^{(0)} - t_j^{(0)} = t_{ij}^{(0)} \quad ; \quad t_{ij}^{(0)} > 0, \tag{4.14}$$

$$t_j^{(n)} - t_i^{(n-1)} = t_j^{(0)} - t_i^{(0)} + \Delta_T = \Delta_T - t_{ij}^{(0)}. \tag{4.15}$$

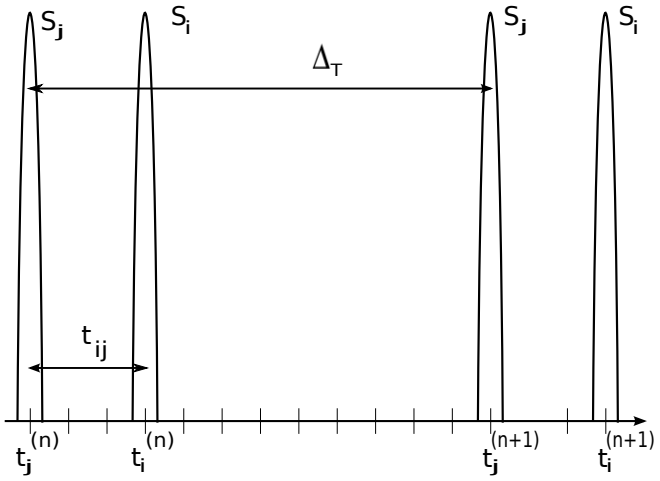

Figure 4.3.: The setup of the alculations for the coupling weights can be seen here. Time is divided into equal intervals of the interval Δ_T, whereas each interval contains two spikes. The edges are determined by the spikes of one of the neurons.

Equations (4.12) and (4.13) state the spike times of neuron i and j, respectively and equations (4.14) and (4.15) denote the time distance between two subsequent spikes.

Depressed coupling weight a_{ji}

The general setup of the calculations is drafted in figure 4.3. The initial value of the coupling weight for the interval is given by $a(t_j^{(n-1)})$. The chemical concentrations are already known (see equation (4.10)), whereas the time index n is kept for the beginning. It will be dropped if long time behaviour is considered. The change of the coupling weight a_{ji} at time $t_j^{(n)}$ and $t_i^{(n)}$, characterized by equation (4.4), is given by:

$$\begin{aligned} t_j^{(n)}: \quad & \Delta_j^{(n)} a_{ji} = \omega\, \Delta\, A_i^{(n-1)}\, e^{-\frac{t_j^{(n)} - t_i^{(n-1)}}{\tau_A}} = \omega\, \Delta\, A_i^{(n-1)}\, e^{-\frac{\Delta_T - t_{ij}^{(0)}}{\tau_A}}, \\ t_i^{(n)}: \quad & \Delta_i^{(n)} a_{ji} = -\omega\, r\, a_{ji}\left(t_j^{(n)}\right) B_j^{(n)} e^{-\frac{t_i^{(n)} - t_j^{(n)}}{\tau_B}} = -\omega\, r \left[a_{ji}\left(t_i^{(n-1)}\right) + \Delta_j^{(n)} a_{ji}\right] B_j^{(n)}\, e^{-\frac{t_{ij}^{(0)}}{\tau_B}}. \end{aligned} \tag{4.16}$$

The expression $\Delta_i^{(n)} a_{ji}$ denotes the change of the coupling weight, caused by the n-th spiking of neuron i at $t_i^{(n)}$. The coupling weight at the right border of the interval is given by the sum over $a(t_j^{(n-1)})$ and the changes stated in equation (4.16). If one considers large times and

inserts the chemical concentrations given by equation (4.10), the coupling weight at time $t_i^{(n)}$ is

$$a_{ji}\left(t_i^{(n)}\right) = a_{ji}\left(t_i^{(n-1)}\right) + \omega\,\Delta\,A_i\,e^{-\frac{\Delta_T - t_{ij}^{(0)}}{\tau_A}} - \omega\,r\left[a_{ji}\left(t_i^{(n-1)}\right) + \omega\,\Delta\,A_i\,e^{-\frac{\Delta_T - t_{ij}^{(0)}}{\tau_A}}\right] B_j\,e^{-\frac{t_{ij}^{(0)}}{\tau_B}}. \tag{4.17}$$

To reduce the complexity of the equation, notations are introduced that will be helpful to find a series expression.

$$\begin{aligned} \kappa_A^{(ij)} &= e^{-\frac{\Delta_T - t_{ij}^{(0)}}{\tau_A}} \\ \kappa_B^{(ij)} &= e^{-\frac{t_{ij}^{(0)}}{\tau_B}} \\ \beta &= \omega\,r\,B_j\,\kappa_B^{(ij)} \\ \alpha &= \omega\,\Delta A_i\,\kappa_A^{(ij)} \\ \nu &= 1-\beta \end{aligned} \tag{4.18}$$

These expressions are inserted in (4.17) and it follows:

$$a_{ji}\left(t_i^{(n)}\right) = \nu\,a_{ji}\left(t_i^{(n-1)}\right) + \nu\,\alpha\,. \tag{4.19}$$

If the equation is solved recursively, one finally gains, in a similar way as for the chemical amplitudes, a series expansion:

$$a_{ji}\left(t_i^{(n)}\right) = \nu^n\,a_{ji}\left(t_i^{(0)}\right) + \alpha\sum_{m=0}^{n}\nu^m - \alpha. \tag{4.20}$$

As mentioned before, large n are considered. By this, it is a valid approximation that the first term of equation (4.20) is going towards zero and the sum converges towards the limes of the infinite geometric series if $|\nu|$ is smaller than 1. For the following calculations, it is assumed that these convergence condition is fulfilled and it is considered later. It follows

$$a_{ji} = \alpha\frac{1}{1-\nu} - \alpha\,. \tag{4.21}$$

If the used notations are substituted in equation (4.21), an expression for the depressed coupling weight is received.

$$a_{ji} = \kappa_A^{(ij)}\,\Delta\,A_i\,\frac{1}{\kappa_B^{(ij)}\,r\,B_j} - \omega\,\kappa_A^{(ij)}\,\Delta A_i \tag{4.22}$$

As can be seen, the saturated coupling weights do not depend on the initial values of $a_{ji}^{(0)}$, but on the initial spike times $t_l^{(0)}$ of the neurons and the spike frequency ω.

Potentiated coupling weight a_{ij}

The same calculations have to be done for the coupling weight a_{ij}. It is done in the same manner as above and therefore the calculations are outlined briefly. Again one starts with equation (4.4) and the change of the coupling weight is thereupon:

$$a_{ij}\left(t_i^{(n)}\right) = a_{ij}\left(t_i^{(n-1)}\right) - \omega\, r\, a_{ij}\left(t_i^{(n-1)}\right) B_i^{(n)}\, e^{-\frac{\Delta_T - t_{ij}}{\tau_B}} + \omega\, \Delta\, A_j^{(n)}\, e^{-\frac{t_{ij}}{\tau_A}} \tag{4.23}$$

The equation is inserted recursively and the received expression can be summed up by a geometric series. The convergence criteria is

$$\left|\left[1 - \omega\, r\, B_i^{(n)}\, e^{-\frac{\Delta_T - t_{ij}}{\tau_B}}\right]\right| < 1. \tag{4.24}$$

If n is large, a_{ij} is given by:

$$a_{ij}\left(t_i^{(n)}\right) = \frac{\Delta\, A_j}{r\, B_i} e^{-\frac{t_{ij}}{\tau_A}} e^{\frac{\Delta_T - t_{ij}}{\tau_B}}. \tag{4.25}$$

4.2. Convergence criteria

In total, four assumptions are made for the convergence of the occurring geometric series.

$$\begin{aligned}
|1 - \frac{2\pi}{\Delta_T}\, r\, B_i\, e^{-\frac{\Delta_T - t_{ij}}{\tau_B}}| &< 1 \\
|1 - \frac{2\pi}{\Delta_T}\, r B_j e^{-\frac{t_{ij}^{(0)}}{\tau_B}}| &< 1 \\
|[1 - u_A \frac{2\pi}{\Delta_T}]\, e^{-\frac{\Delta_T}{\tau_A}}| &< 1 \\
|[1 - u_B \frac{2\pi}{\Delta_T}]\, e^{-\frac{\Delta_T}{\tau_B}}| &< 1
\end{aligned} \tag{4.26}$$

By these inequations, the validity of the approximations are given. If not all inequalities are fulfilled at once, the chemical concentrations or the coupling weights diverge and no saturation takes place. The considered equations depend on seven different parameters if one keeps in mind that ω is equal to $\frac{2\pi}{\Delta_T}$. Five of these parameters are system parameters and two are initial conditions. To see if the different conditions do not exclude each other, the system parameters are kept fixed and the initial conditions are varied. The results are shown in figure 4.4 and the red points indicate that the inequation is fulfilled for the given parameters. As one can observe, in certain areas all assumptions are valid at once. Consequently, the calculations are feasable in this overlapping areas. The domain is nearly independent of the time distance t_{ij}, since the chemical concentrations do not count on it and the other inequations are nearly independent of the time distance. This indicates that the validity

(a) $\tau_B = \tau_A = 0.09$, $r = 1$, $u_B = u_A = 0.8$ (b) $\tau_B = \tau_A = 10.0$, $r = 1$, $u_B = u_A = 0.8$

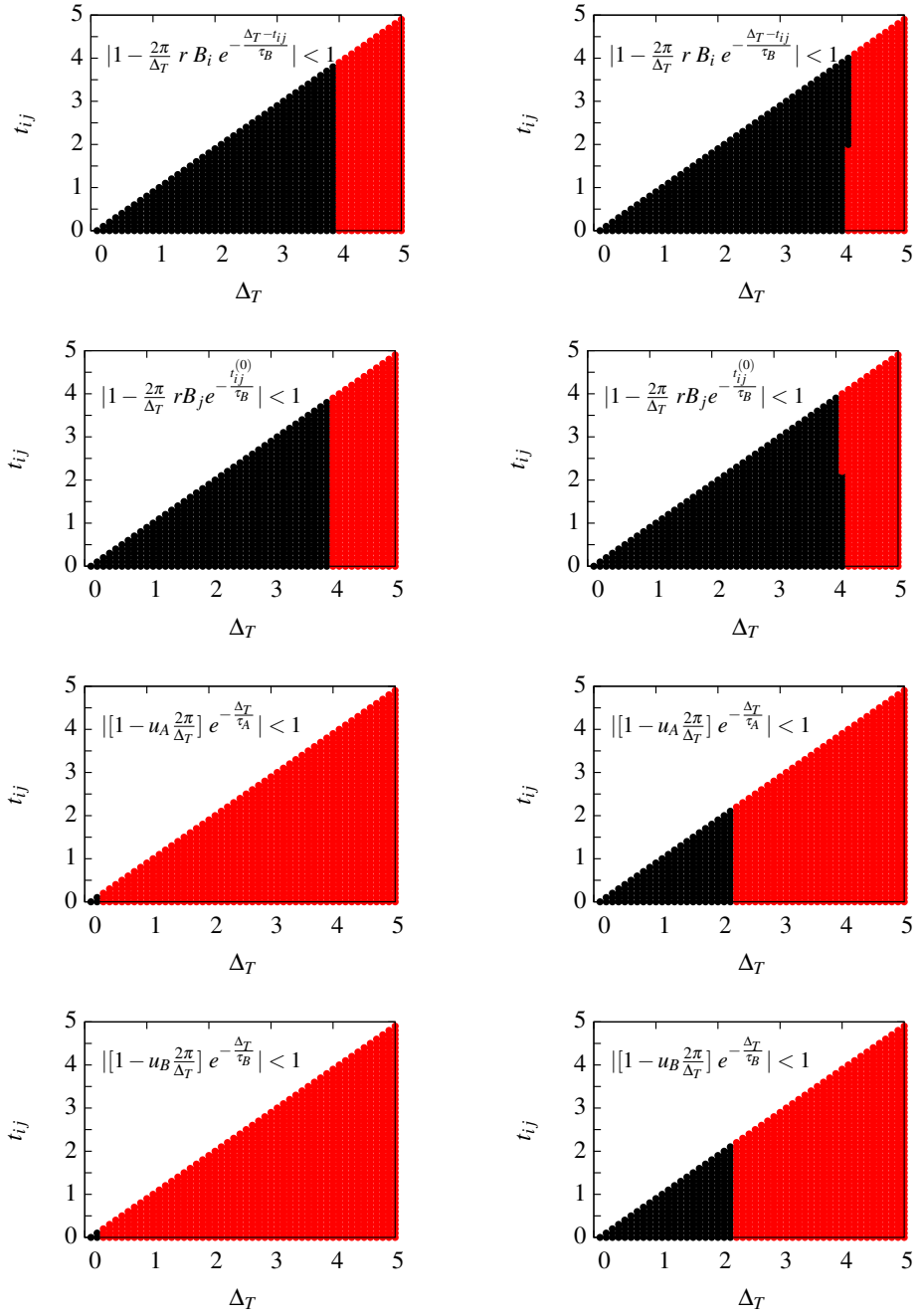

Figure 4.4.: The functions stated in equation (4.26) are plotted. The red points indicate that the inequation is fulfilled and therefore the approximation is valid in these areas. Two different parameter settings are used in (a) and (b).

does not depend on the distribution of the initial spike times $t_i^{(0)}$. Therefore, no minimal or maximal distance between the spike times of the neurons has to be considered. However the frequency can not exceed a certain value, due to the conditions stated by the convergence of the coupling weights. The change of the coupling weight over an interval would not annihilate each other and hence no periodic equilibrium point is reached. Other parameters that are important for the validity are the time window widths τ_A and τ_B. If the time window widths are to large, the chemical concentration does not decay fast enough. Consequently, the increase of the time window width, reduces the allowed range of the frequency.

4.3. Dendritic current

After obtaining an expression for the saturated coupling weights in the chapter above, the self-consistency check is performed. The dendritic current ψ_i of each neuron is calculated. Finally these currents are used to calculate the spiking frequencies of the neurons, which are determined by the Naka-Rushton relation. The dendritic current has to be calculated for a system of N neurons and it reads

$$\dot{\psi}_m\Big(t\Big) = \sum_{k=0}\sum_{i}^{N} a_{mi}\ \delta\Big(2\pi - \phi_k\Big(t_i^{(k)}\Big)\Big)\ \dot{\phi}_k(t) - \gamma\ \psi_m(t)\ . \tag{4.27}$$

The initial spike times $t_i^{(0)}$ of the neurons can be sorted in an increasing order, so that neuron one has the smallest initial spike time and neuron N the largest. It was assumed that $t_N^{(0)}$ is not larger than Δ_T and therefore the largest possible time distance t_{ij} between two spikes is Δ_T:

$$t_1^{(0)} < t_2^{(0)} < t_3^{(0)} < t_4^{(0)} < ... < t_N^{(0)} \leq \Delta_T\ . \tag{4.28}$$

As stated in equation (4.27), the dendritic current ψ_i decays exponentially between two spikes and increases with the spiking of a neuron. For reasons of convenience, the time axis is decomposed in the following way:

$$t = \bar{t} + \Delta_T\ n\ .\quad \bar{t} < \Delta_T \tag{4.29}$$

This denotes that the time axis consists of intervals of the length Δ_T, which includes one spike event of each neuron, and an interval of the length $\bar{t}$. This interval contains the spikes of all neurons that have an initial spike time $t_i^{(0)}$ smaller than $\bar{t}$. The expression for the dendritic current is

$$\begin{aligned}\psi_m\Big(\bar{t} + \Delta_T\ n\Big) = \psi_m\Big(0\Big)\ e^{-\gamma(\bar{t}+\Delta_T\cdot n)} + \omega \sum_{k=0}^{n-1}\sum_{i=1}^{N} a_{mi}\ e^{-\gamma(\bar{t}+\Delta_T\ n - t_i^{(0)} - k\cdot\Delta_T)} \\ + \omega \sum_{i=1}^{t_i^{(0)}+\Delta_T n<t} a_{mi}\ e^{-\gamma(\bar{t}+\Delta_T\ n - t_i^{(0)} - \Delta_T\ n)}\ .\end{aligned} \tag{4.30}$$

The first term is the dendritic current, determined by the initial conditions. The second term is the dendritic current caused by the action potentials of the neurons generated in a closed interval. The last term includes the contribution of the neurons with an initial spike time $t_i^{(0)} \leq \bar{t}$. Similar to the calculations above, the second term of equation (4.30) can be rewritten as a geometric series. First, one has to rescale the index k to $l = n - k$. Second, the sum has to be expanded to include $l = 0$. The additional term can be partially absorbed into the third term, whereas the remaining expression includes all spikes with an initial spike time that is larger than $\bar{t}$. The operation leads to

$$\begin{aligned}\psi_m\Big(\bar{t} + \Delta_T\ n\Big) = &\psi_m\Big(0\Big)\ e^{-\gamma \bar{t}}\ (e^{-\gamma\ \Delta_T})^n + \omega \sum_{l=0}^{n} \sum_{i=1}^{N} a_{mi}\ e^{-\gamma(\bar{t} - t_i^{(0)})}\ e^{-\gamma \Delta_T \cdot l} \\ &- \omega \sum_{i=1}^{t_i^{(0)} > \bar{t}} a_{mi}\ e^{-\gamma(\bar{t} - t_i^{(0)})}\ .\end{aligned} \tag{4.31}$$

As before, long time behaviour is considered and hence $n \gg 1$. As a result, the first term of equation (4.31) is tending towards zero and the second term converges a fixed value if $|e^{-\gamma \Delta_T}|$ is smaller than 1. Since the damping γ and the size of the time interval Δ_T are strictly positive, this condition is always fulfilled and it follows:

$$\psi_m\Big(\bar{t}\Big) = \frac{\omega}{1 - e^{-\gamma \Delta_T}} \sum_{i=1}^{N} a_{mi}\ e^{-\gamma(\bar{t} - t_i^{(0)})} - \omega \sum_{i=1}^{t_i^{(0)} > \bar{t}} a_{mi}\ e^{-\gamma(\bar{t} - t_i^{(0)})}\ . \tag{4.32}$$

In the next step, only the points in time that are multiples of Δ_T are considered and therefore $\bar{t}$ is given by Δ_T. Consequently, the last term of equation (4.32) vanishes. To simplify the resulting equation, a new notation is introduced.

$$\kappa_\gamma = \frac{1}{1 - e^{-\gamma \Delta_T}} \tag{4.33}$$

Equation (4.32) reduces to

$$\psi_m = \omega\ \kappa_\gamma \sum_{i=1}^{N} a_{mi}\ e^{-\gamma(\Delta_T - t_i^{(0)})}\ . \tag{4.34}$$

At this point, the coupling weights a_{mi} are inserted, but a case differentiation has to be performed, since the coupling weights depend on the spike times. If the initial spiking time $t_i^{(0)}$ of neuron i is larger than the initial spike time $t_m^{(0)}$ of neuron m, the coupling weight is depressed and the expression given in equation (4.22) has to be used. The index has to be changed so that j is replaced by m. In the reverse case, which denotes that $t_i^{(0)} < t_m^{(0)}$, the coupling weight given in equation (4.25) is used. This time, i is substituted by m and j is replaced by i. In addition to this, a rescaling is done to reduce the number of free parameters.

The damping constant γ is absorbed into the time constants, into the mean fraction u_σ and into the potentiation constant Δ. All parameters containing the damping constant γ are marked with a tilde. Using the notation

$$\widehat{\tau} = \frac{1}{\tilde{\tau}_A} + \frac{1}{\tilde{\tau}_B}, \tag{4.35}$$

a complete equation for the dendritic current is received.

$$\begin{aligned}
\psi_m = & \frac{\tilde{\omega}\, A\, \tilde{\Delta}\, \kappa_\gamma}{r\, B}\, e^{-\tilde{\Delta}_T(\frac{1}{\tilde{\tau}_B}+1)}\, e^{-\tilde{t}_m^{(0)}\left[\widehat{\tau}-1\right]} \sum_{i=1}^{\tilde{t}_i^{(0)}<\tilde{t}_m^{(0)}} e^{\tilde{t}_i^{(0)}\widehat{\tau}} \\
& + \frac{\tilde{\omega}\, A\, \tilde{\Delta}\, \kappa_\gamma}{r\, B}\, e^{-\tilde{\Delta}_T(\frac{1}{\tilde{\tau}_A}+1)}\, e^{-\tilde{t}_m^{(0)}\,\widehat{\tau}} \sum_{i=1}^{\tilde{t}_i^{(0)}>\tilde{t}_m^{(0)}} e^{\tilde{t}_i^{(0)}\left[\widehat{\tau}+1\right]} \\
& - \tilde{\omega}^2\, \kappa_\gamma\, A\, \tilde{\Delta}\, e^{-\tilde{\Delta}_T(\frac{1}{\tilde{\tau}_A}+1)}\, e^{-\frac{\tilde{t}_m^{(0)}}{\tilde{\tau}_A}} \sum_{i=1}^{\tilde{t}_i^{(0)}>\tilde{t}_m^{(0)}} e^{\tilde{t}_i^{(0)}(\frac{1}{\tilde{\tau}_A}+1)}
\end{aligned} \tag{4.36}$$

To calculate the sums, contained in equation (4.36), further assumptions have to be made. A distribution for the spike time has to be chosen. For instance, a Gaussian distribution can be used, but than no self-consistent solutions are found. For the following calculations, a homogeneous distribution of the spike times is applied, whereas it is assumed that the spike times are dense over an interval. By this assumption, the sums can be replaced by an integral and the calculations simplify. Since it is assumed that the distribution is dense, the considered system has to contain a large number of neurons N, because the interval size Δ_T has a lower border. The dendritic current of neuron m is given by:

$$\begin{aligned}
\psi_m = & \frac{\tilde{\omega}\, A\, \tilde{\Delta}\, \kappa_\gamma}{r\, B}\, e^{-\tilde{\Delta}_T(\frac{1}{\tilde{\tau}_B}+1)}\, \frac{1}{\widehat{\tau}} \left[e^{\tilde{t}_m^{(0)}} - e^{-\tilde{t}_m^{(0)}[\widehat{\tau}-1]} \right] \\
& + \frac{\tilde{\omega}\, A\, \tilde{\Delta}\, \kappa_\gamma}{r\, B}\, e^{-\tilde{\Delta}_T(\frac{1}{\tilde{\tau}_A}+1)}\, \frac{1}{\widehat{\tau}+1} \left[e^{\tilde{\Delta}_T[\widehat{\tau}+1]-\tilde{t}_m^{(0)}\widehat{\tau}} - e^{\tilde{t}_m^{(0)}} \right] \\
& - \tilde{\omega}^2\, \kappa_\gamma\, A\, \tilde{\Delta}\, e^{-\tilde{\Delta}_T(\frac{1}{\tilde{\tau}_A}+1)}\, \frac{1}{\frac{1}{\tilde{\tau}_A}+1} \left[e^{\tilde{\Delta}_T(\frac{1}{\tilde{\tau}_A}+1)-\frac{\tilde{t}_m^{(0)}}{\tilde{\tau}_A}} - e^{\tilde{t}_m^{(0)}} \right].
\end{aligned} \tag{4.37}$$

By the integration, an expression for the dendritic current is gained that only depends on the initial spike time $t_m^{(0)}$ of the neuron itself and not on the spike times of all neurons. The initial parameters are therefore reduced to the interval length Δ_T and the initial spike time. Due to reasons of simplicity, it is assumed that the time window widths $\tilde{\tau}_A$ and $\tilde{\tau}_B$ are symmetric and given by $\tilde{\tau}$. Accordingly, $\widehat{\tau}$ is $2/\tilde{\tau}$. Additionally, it is assumed that the chemical fractions $\tilde{u}_A$ and $\tilde{u}_B$ are equal, too. By this, equation (4.37) reduces to an expression with six free parameters. To find self-consistent solutions, dendritic currents have to be found, for which the output of the Naka-Rushton relation is equal to the assumed spike frequency. Since the

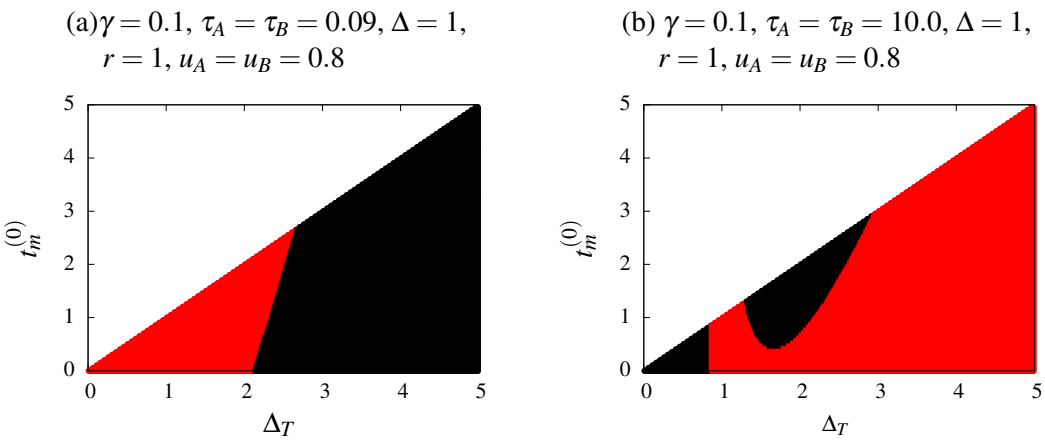

Figure 4.5.: The calculated dendritic current is inserted into the Naka-Rushton relation, whereas the matrix $\underline{c}$ is given by the identity $\mathbb{1}$. The red points mark the parameter settings, in which the output of the Naka-Rushton relation is in its saturation regime.

aim is to demonstrate that self-consistent solutions exists in general, it is assumed that the initial frequency is equal to the maximum spike frequency of the Naka-Rushton relation. This reduces the solution set, but also the complexity of the task. The remaining parameters can be separated into system and initial parameters. Therefore, the system is set up with the same values for Δ, r, τ and u as in figure 4.4. Afterwards, the initial parameters are varied, which can be seen in figure 4.5. The self-consistent solutions, which are compatible with the assumption of the homogeneous distribution of the spike times, are the parameter settings for that the Naka-Rushton relation saturates for all possible initial spike times.
As can be seen, parameter settings exists, for which self-consistent solutions are found.
If one considers the previous stated conditions in chapter 4.2 that already reduced the parameter space, it is obvious that there is no overlapping area for case (a). For larger time windows (b) an overlapping area exists and therefore self-consistent solutions are obtained. The overlap indicates that the initial frequency is equal to the saturation phase velocity of the Naka-Rushton relation. It has to be mentioned that the solutions shown here are just a subset of the complete solutions. Self-consistent solutions exist for which the initial frequency ω is not the saturation frequency of the Naka-Rushton relation.
It was shown that for the given parameter settings the coupling weight has the same value at all points in time that are multiples of the interval length Δ_T. But the coupling weight is not fixed, if the neurons are active, due to the underlying mechanism. This implies that the coupling weights are in the above scenario on an periodic orbit, which could be for instance an oscillation of the coupling weight, similar to the occurring behaviour in chapter 3.4.1.

5. Phenomenological investigation

"*Memory is the storehouse in which the substance of our knowledge is treasured up.*"

Charles Bridges, An Exposition of Psalm 119

In this chapter some phenomenological findings are discussed. All three of them are linked, in an abstract way, to memory and signal processing in the human brain. First of all one has to get familiar with the concept and definition of memory.
It has been observed that organisms change their reaction to events during their lifetime. Furthermore, it is documented that they modify their nervous system and by this their behaviour is altered. However, memory does not only refer to conditional reflexes, but also to the ability to memorize an equation, a name or a face. It is obvious that learning and memory are closely connected to each other and thusly memory can not exist without learning. The following definitions of memory and learning are taken from [Squ87].

Definition of Memory: Memory is the persistence of learning in a state that can be revealed at a later time.
Definition of Learning: Learning is the process of acquiring new information.

As one can deduce from the definitions, learning is an element of memory, since memory is a consequence of learning. It is stated that memory is not a thing, though a process. But different definitions exist for memory, which emphasize other aspects. For example, Kandel *et al.* [KSJ00] stated that memory is the process of storing information and retrieving it at a later point in time. This definition is similar to the one above, but Kandel [KSJ00] did not highlight the link between learning and memory in the same way as Squire [Squ87].
Despite the definitions stated above, one is not able to identify learning or memory on a neuronal level. For this reason, the focus has to be shifted to the biological aspects of these processes.
Biologist assume that memory is due to synaptic plasticity. The main idea is that memory comprehends a persistent change in the synaptic connections between the neurons and by this the information is stored in the system.

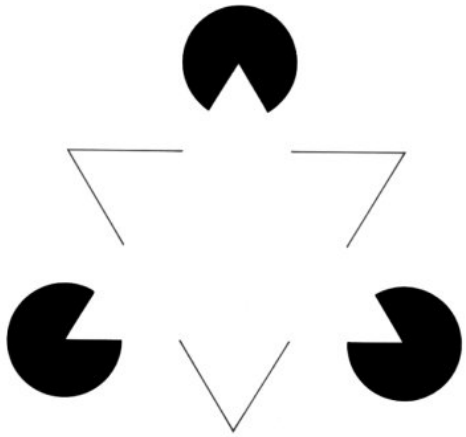

Figure 5.1.: A Kanisza figure is shown. It seems that a white triangle is overlapping with the triangle framed by the black lines. The picture was taken from [Hak06]

In the following, two special kinds of memory are considered, namely associative memory and working memory. Associative memory describes the linking of different pieces of information and conduces the completion of data. Working memory is the process of holding information or storing it for a short period in time to make it available for information processing. These two kinds of memory are investigated in more detail in the following sections.

5.1. Associative memory

Associative memory is the linking of different pieces of information and serves to complete data. This section is motivated by the work of Herman Haken [Hak06]. He investigated, if a network of Lighthouse Neurons can be set up in a way that the system develops an associative memory. First some examples are given to get a better understanding of the principles.
A common one is a telephone book [Hak06]. If one looks up a name, the book provides the conjoined telephone number. Consequently, the telephone book associates a name with a number. Another popular example is a Kanisza figure, which is shown in figure 5.1.
Even if no triangles are entirely drawn, two complete triangles can be seen, since the human brain has memorized the shape and associates it with the visual input. On the neuronal level, this can be described by the completion of spike patterns by the neurons. An input signal is received that is similar to a memorized signal. The memorized signal is in the following denoted as prototype pattern. The neurons start to spike, evoked by the external

signal. Caused by the synaptic connections between the neurons, the resulting spike pattern is completed and therefore it is equal to the one produced by the prototype signal. Hence, the brain recognizes the prototype pattern and in the case of the Kanisza figure, two triangles can be seen.
Herman Haken [Hak06] demonstrated this behaviour by examining a system of three neurons, whereat the connections between them were fixed. The prototype pattern was a line and the used input signal an interrupted one. The neurons completed this input signal and the spike pattern of the neurons showed a complete line. It has to be pointed out that the coupling weights had to be calculated analytically.
The analytical calculations performed in chapter 4 have shown that the coupling weight matrix $\underline{a}$ can saturate under STDP if the the spike pattern of the neurons is preserved. Therefore the matrix can be structured and information can be stored in the coupling weight matrix.
In the beginning of this chapter, the ability of the coupling weight matrix to saturate under the influence of an external signal is validated by numerical simulations. In contrast to the analytical and numerical results performed before, the spike times are not determined by initial conditions, but rather by an external forcing of the system. A periodic external signal, the so called prototype pattern, is driving the system and determines the spike pattern.
Afterwards, the occurring saturation is used to alter the synaptic connections of a system so that the applied prototype signal is stored in the structure of the coupling weight matrix. By this, the coupling weight matrix develops a characteristic pattern. Linked to this, the system projects the input signal on a characteristic shape in the phase and the corresponding spike pattern. If the input signal is similar to the prototype signal, similar spike patterns are produced, which is denoted as associative memory as was explained before. This behaviour occurs, because the neural network projects a wide range of signals on the shape of the prototype pattern. Subsequent, the ability of the network is compared with an untrained one.

5.1.1. Setup of the network

In the following sections, the neural network is aligned on a grid for reasons of visualization. Therefore, each grid point describes a neuron and its spatial position, whereon the coupling of the neurons is independent of their positions. The network consists of hundred neurons (10×10). The coupling weight matrix is set up randomly, whereat the values are uniformly distributed. A periodic prototype signal is applied to the network of extended Lighthouse Neurons to train the coupling weight matrix. In the used visualization the prototype signal is a horizontal line that includes ten neurons, as can be seen in figure 5.2. The spatial arrangement does not influence the connections of the neurons and consequently all torsi that consist of ten neurons are equivalent.

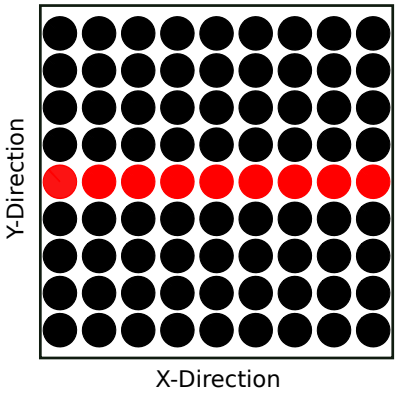

Figure 5.2: The setup of the network, used in this chapter, is drafted. The neurons are aligned on a two dimensional grid for visualization. Each neuron has a spatial component, but the connections between the neurons do not depend on the spatial alignment. The red marked points are the neurons, which receive the prototype signal. It has the shape of a line in this visualization.

5.1.2. Convergence of the coupling weight matrix

To demonstrate the saturation of the coupling weight matrix under an applied external signal, a network as described above is simulated. The external signal is received by the phase ϕ of the neurons, as can be seen in equation (3.6). The signal causes the neurons to spike and consequently the spike pattern is dominated by this. A change in the coupling weight matrix $\underline{a}$ is induced. Hence, the development in time of the coupling weight matrix is observed, whereas the examined variable is the mean value $< \Delta a_{ij} >$ of the absolute value of the differences between the matrix elements of two subsequent time steps.

$$< \Delta a_{ij}(n) >= \frac{1}{N^2} \sum_{i,j=0}^{N} |a_{ij}(n+1) - a_{ij}(n)| \tag{5.1}$$

In figure 5.3 one can observe that $< \Delta a_{ij} >$ decays exponentially and tends towards a minimal value c that is close to zero. The fact that $< \Delta a_{ij} >$ does not become zero indicates that the coupling weight values is not static, but change with a minimal rate. Since a constant structure is visible in the coupling weight matrices for larger times, it can be assumed that the coupling weights a_{ij} are oscillating about a suspension point. This is consistent with the results of chapter 4.

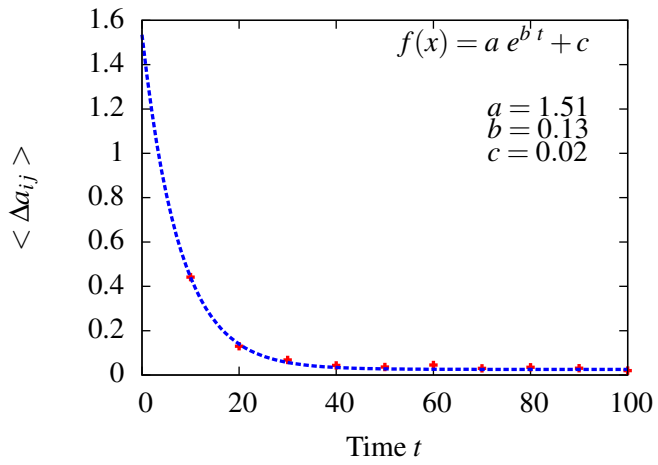

Figure 5.3.: The change of the coupling weight matrix is shown over time, caused by an applied periodic external signal. An exponential function is fitted into the calculated data, to emphasize the exponential decrease of the change $< \Delta a_{ij} >$.

5.1.3. Structuring of the matrix

The system is set up as explained in section 5.1.1. The prototype signal is fed in and hence the system produces a characteristic spike pattern. This in return, modulates the coupling weight matrix and distinctive structures emerge, as shown in figure 5.4.
Horizontal lines are visible in the coupling matrix. They are composed of the coupling weights that are directed to the neurons, which are part of the prototype pattern. The values of the coupling weights increase with progressing time. The vertical lines that consist of the connections pointing from a neuron on the line to any other neuron, are decreasing and tending towards zero on large time scales. The areas between the lines have the same behaviour, but they decay slower. Accordingly, all connections of the system are focused on the neurons on the line, since all synapses that are not pointing at these are disconnected. Hence if any neuron spikes, all neurons that are part of the pattern receive a pulse and get activated. By this mechanism, an input signal is projected onto the shape of the prototype signal.
The intensity of the different areas in the matrix are changing in dependency of the used system parameters. If the damping γ of the dendritic current ψ exceeds a certain level, no structure will occur in the coupling weight matrix. This is due to the fact that the external signal can not spread through the system and cause other neurons than these on the line to spike. If the potentiation constant Δ or the depression constant r is increasing, the intensity of the lines mentioned above is changing.

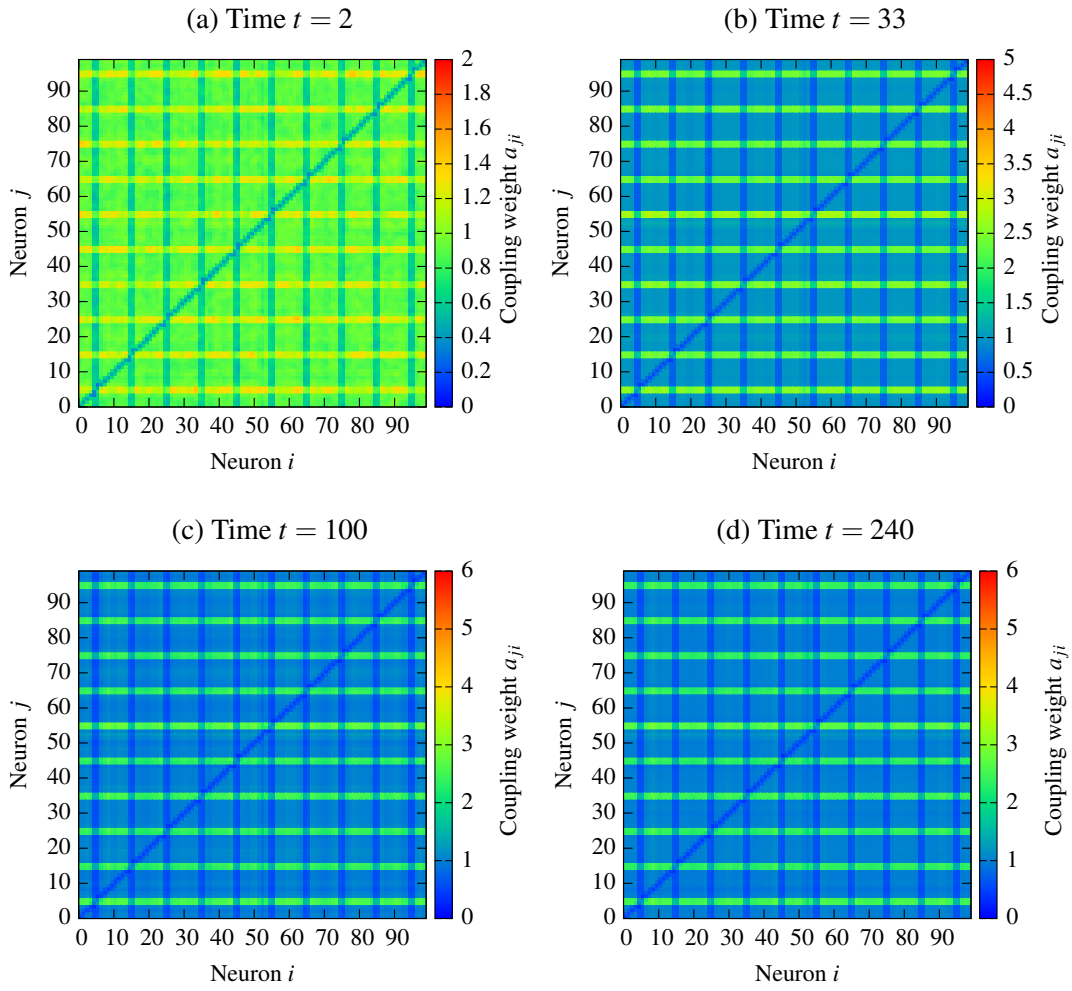

Figure 5.4.: The coupling weight matrix $\underline{a}$ is shown for different times. With progressing time the matrix changes and characteristic lines emerge that get more intense. The coupling weights in the areas between these lines tend towards zero. The visible diagonal line is due to the fact that the self-coupling elements are set to zero.

5.1.4. Occurring phase structure

A signal is associated with the learned pattern if the produced spike patterns and consequently the phase structures are similar. Therefore the phase structure produced by the prototype signal is considered. The signal is applied to the system and the learning algorithm is switched off. The trained coupling matrix characterises the connections of the system. The resulting structure in the phase and dendritic current of the network is presented in figure 5.5.

A line is visible in the structure of the dendritic current and the phase. All neurons on the line receive the same input signal and ergo their phase velocity is the same. On the opposite, the phase velocities of the surrounding neurons is zero. This explains the visible line in the phase structure for an early time step.
With the spiking of the first neuron on the line, the connected neurons receive a pulse and their dendritic current accrue. Since only the neurons within the line are strongly connected, just their dendritic current increases. Due to the fact that the increment matrix $\underline{c}$ is diagonal, only their phase velocities grow. Therefore, the line is contained in the phase and the dendritic current. By this mechanism, the produced pattern has the same structure as the prototype signal. As the coupling weights between the surrounding neurons and the neurons that are part of the prototype pattern are not exactly zero, the dendritic current and phases of the background neurons increases. In comparison to the neurons on the line, their phase velocity is low. But nevertheless, this will cause the neurons to spike on a larger time scale.

5.1.5. Pattern association

In the following it is investigated, if the trained neural network is able to associate the prototype pattern with input signals that slightly differ from it. The system associates these signals with the prototype signal if the emerging structure is similar to the shape shown in figure 5.5. Therefore, a completion of the spike pattern has to take place. The behaviour of the system, due to associative memory is drafted in figure 5.6.

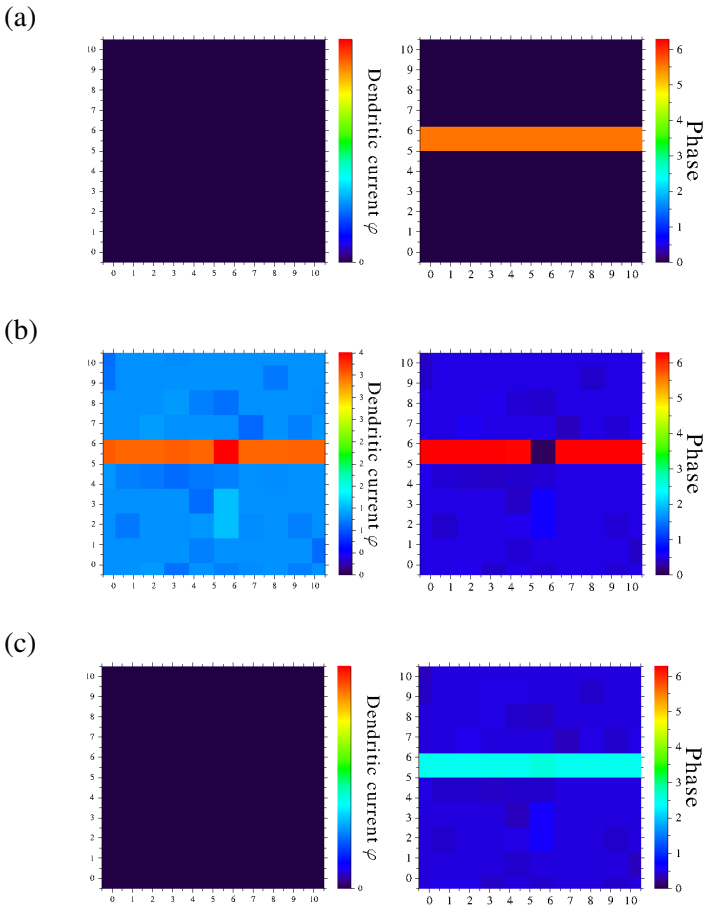

Figure 5.5.: A neural network is simulated, whereas a trained matrix is describing the connections of the system. The learning algorithm is turned off and the prototype signal is used as an input signal. A snapshot of the phase (right) and dendritic current (left) is shown a few time steps before (a), directly afterwards (b) and some time steps (c) after the external signal caused the neurons on the line to spike. By the spiking, all neurons that receive the external signal have a non zero dendritic current. On the opposite, the currents of the surrounding neurons are close to zero. Since only the current of a neuron influences its phase, the phases of the neurons on the line are changing rapidly and the phases of the surrounding neurons are nearly constant. Therefore a line is visible in the dendritic current and the phase structure. The resulting spike pattern is a nearly synchronous spiking of the neurons that receive the signal and thus the prototype signal and the spike pattern have the same shape.

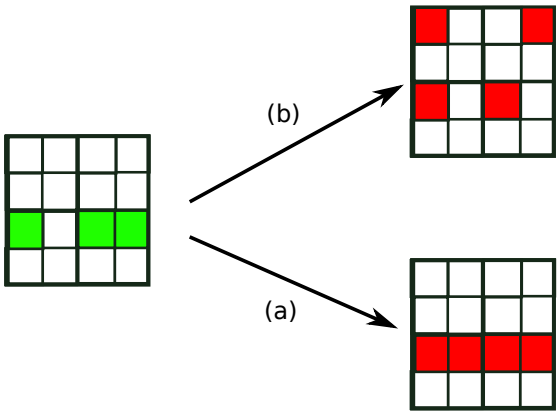

Figure 5.6.: The mechanism of associative memory is sketched. Each square represents one neuron. On the left hand side, the input signal is shown. It is an interrupted line and each neuron that is marked green receives an input signal bigger than zero. On the right hand side, the phases of the neurons are shown. Red squares indicate that the neuron has a different phase than the other neurons (white). In the case of associative memory (a), the spike pattern is completed to a line and it is equivalent to the spike pattern produced by the prototype signal. Case (b) denotes non-associative memory and therefore a random spike pattern emerges.

A completion of spike patterns is occurring if the parameters, under which the matrix is created, are chosen properly. The quality of the spike pattern strongly depends on the parameter setting. If the matrix shown in figure 5.4 is used, an interrupted line will produce a similar spike pattern as the prototype signal.
To demonstrate completion, the system is set up in the same way as explained above. But this time an interrupted line is fed in. In figure 5.7 snapshots of the system are shown.
It can be observed that the neurons, which do not receive an external input, but are part of the original prototype pattern, do not have exactly the same phase, as the other neurons on the line. The phases of these neurons are lagging, but nevertheless their phase differs from the surrounding neurons. The underlying mechanism is based on the direction of the connections caused by the spike time dependent plasticity. If any neuron spikes, the neurons on the line will receive a pulse and their phases increase. By this, the lack of an external input is partially compensated and a neuron spikes in a similar way as it would if an external signal is applied.

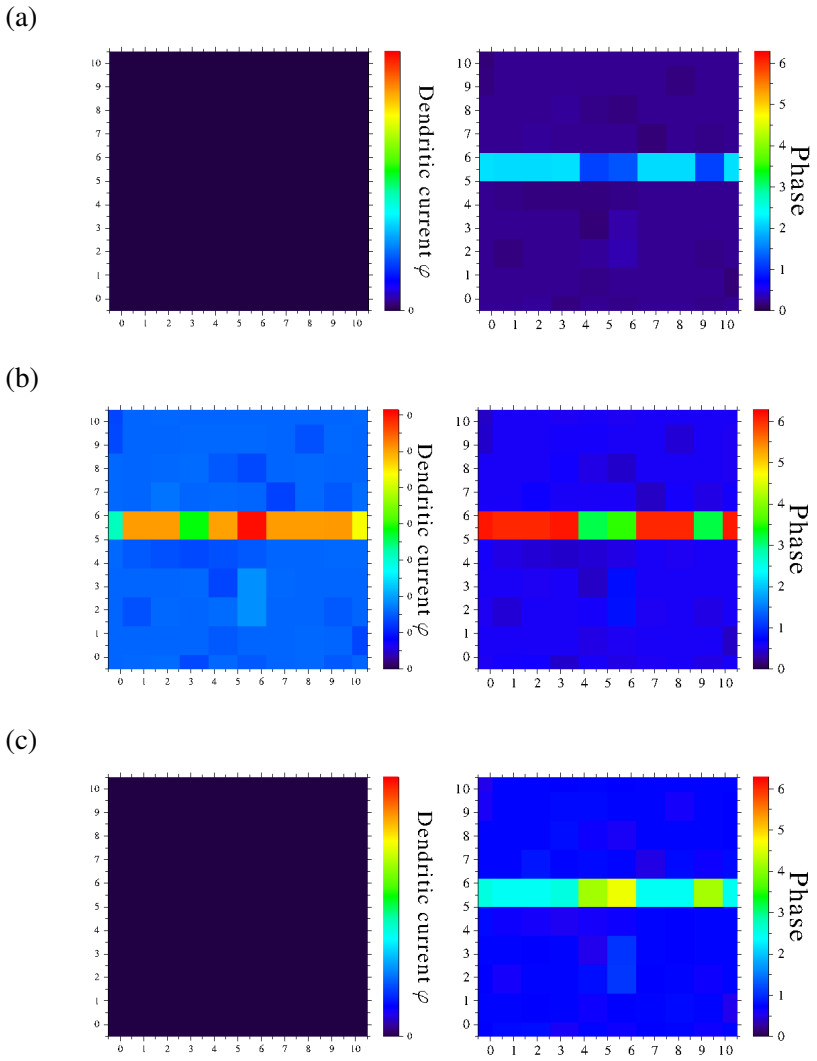

Figure 5.7.: The same setup as in figure 5.5 is used. The input signal consists of an incomplete line instead of the trained signal. (a) shows the dendritic current and the phase of the system closely before the spiking. After the firing (figure b,c) a line is visible, whereat the quality of the projection is lower as in 5.5. Nevertheless, the spike patterns are similar and therefore it can be assumed that the system associates the interrupted line with the prototype pattern.

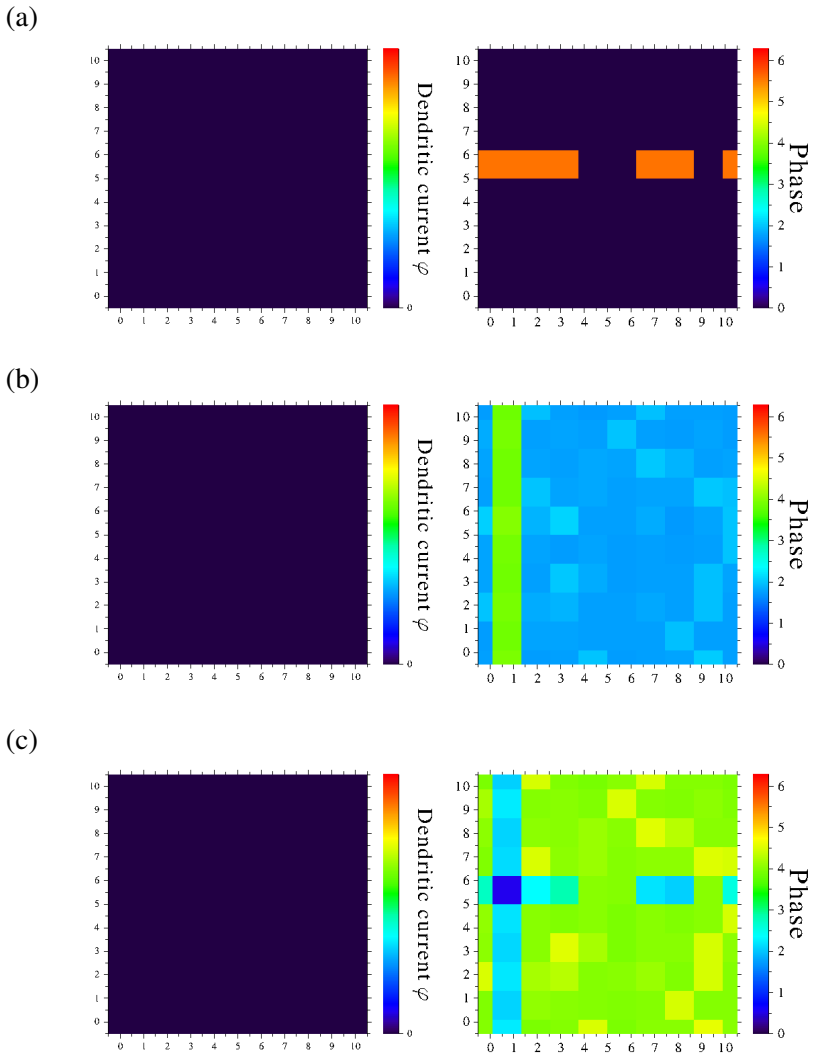

Figure 5.8.: The network is set up with a coupling weight matrix $\underline{a}$ trained by a vertical line, instead of the prototype pattern. The input signal is an interrupted horizontal line. After applying the input signal, a vertical line is visible in the phase next to a horizontal line. This demonstrates that the network projects the input on a vertical line.

To demonstrate the improved ability of the network to reconstruct the prototype pattern, it is compared to other networks. For this aim a network is set up as before, but in contrast, the coupling weight matrix was trained by a vertical line. In the following, this network is referred to as reference system and the original network is denoted as prototype system. First, the reference network is investigated by feeding a signal into the system that is similar to the original prototype pattern. It is to expect that a vertical line emerges in the phase structure, since the system projects on a vertical line. In figure 5.8 snapshots of the network are shown. It can be observed that after the spiking, a vertical line is visible in the phase of the system. With increasing time, the structure becomes noisy, since the difference between the input signal and the learned pattern is to large and by this the background neurons are activated. As one can see in figure 5.7 and 5.8 ,the ability of the prototype system to complete an interrupted horizontal line is better than of the reference system.

5.1.6. Discussion

In the beginning, the saturation of the coupling weight matrix under a periodic external signal was demonstrated. By this, it was shown that information can be stored in the synaptic connections between the neurons. The aim of this chapter was to investigate the ability of a neural network to develop an associative memory.
It was shown that a trained system projects a wide range of signals on the structure of the used prototype signal. Furthermore, it was demonstrated that a completion of spike patterns takes place, so that different signals produce equivalent spike patterns. Therefore, they are recognized by the neural system as identical input signals.
The underlying mechanism is based on the characteristic structure in the coupling weight matrix. Different input signals produce different structures. The occurring structure is based on the fact that the coupling weights become directed to the neurons that are receiving the external signal. Since the coupling weights do not depend on a spatial component, the alignment of the neurons can be altered and by this, the shape of the prototype signal changes, All torsi that consist of the same amount of neurons are equivalent and therefore more complex patterns are possible.

5.2. Working memory and bumps

After investigating associative memory, working memory is considered. The task of working memory is to store information on a time scale of seconds so that it can be used for complex tasks. These tasks are for instance language comprehension, learning and reasoning.
The storage of information takes place via bumps. A bump is a spatial localized area of persistent neural activity. Therefore, it is equivalent to a contiguous area in the brain in that neurons spike and the surrounding neurons stay inactive. It is assumed that these bumps are vital for the temporal back up of information and transmission of these in the human brain [CC06]. Because it is known that spike patterns contain information, bumps could be encoded signals that are for example, received from other areas of the brain or caused by an optical input. By the spiking of the neurons, which are part of the bump, the structure of the connections in this areas of the brain is altered and information can be stored as explained before.
Bumps were already investigated by [CC06, Coo05, GC04] and some definitions proposed in these contributions can be used. This chapter closely follows Carson C. Chow *et al.* [CC06], because the Lighthouse Model was used in their work, even if the version differs from the one stated in chapter 3. For example, the Naka-Rushton relation was substituted by the Heavyside-function. A learning algorithm was not applied. First they considered slow synapses, which is equivalent to a damping constant γ of zero and ergo the dendritic current is not damped. It was pointed out that spatial stationary bumps occurred. In the end, a system with fast synapses was considered and accordingly the damping γ was non-zero. In addition, it was demonstrated that for non-zero γ a bump begins to wander and with increasing γ, the bump collapses. If the parameter is above a certain threshold, bumps can not even emerge any more.
First, these results are reproduced to gain a better insight into the underlying mechanism and get more familiar with the Lighthouse Model. Afterwards, it is demonstrated that wandering bumps become stationary, by spike time dependent plasticity. In the beginning, the definition of a bump has to be clarified. Definitions stated by [CC06] are used.

Definition 1: A bump at time t is the set of all contiguous neurons that fired in the time interval $[t - dt; t]$.

Definition 2: A stationary bump is a bump, which persists in a single location for all time i.e. the same set of neurons continue to fire indefinitely.

Definition 3: The edge of a bump is the neuron that is next to a neuron that is not part of the set. Therefore it divides the system into an inner region and an outer region.

Definition 4: A bump is wandering if the position of the edge is neither time stationary nor periodic.

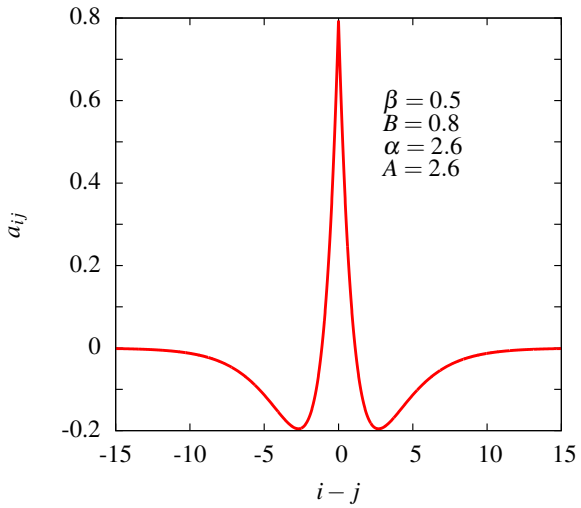

Figure 5.9: The plotted function describes the coupling weight between two neurons in dependency of the spacial distance between them. It is called *Wizard Hat* [Coo05] and the connections are excitatory for small distances, inhibitory for medium distances and close to zero for larger distances between the neurons. The used parameter settings are shown in the figure.

To sum up, a bump is a region within a neural system in which all neurons are active. To produce them, the neurons of the considered system are aligned on a line. The coupling between the neurons depends on the spatial difference between them and is like in [CC06, GC04] given by the *Wizard Hat*. The coupling weight function is plotted in figure 5.9 and the governing equation is

$$a_{ij} = A\, e^{-\alpha|i-j|} - B\, e^{-\beta|i-j|}\,. \tag{5.2}$$

The coupling between the neurons is excitatory for small spacial distances, which is basically the next neighbour and the next but one neighbour. This donates that the coupling weight a_{ij} between adjoined neurons causes these to spike. If the spacial distance increases, the coupling weights become negative and therefore inhibitive. Consequently, the spiking of the neurons is suppressed. For larger time distances, the coupling weight is tending towards zero and the neurons are not influencing each other.
But other possibilities exist to select the coupling function than the *Wizard Hat*. Necessary attributes of the coupling function are that the excitatory and inhibitory parts are spatial localised. As will be seen, a bump emerges in the centre of the the line, since the central neurons have more short range connections and as a result more excitatory coupling weights and less inhibitory than the border neurons.
To reproduce the results shown by Chow *et al.* [CC06] the learning algorithm is turned off, the increment matrix $\underline{c}$ is chosen diagonal and the coupling weights are set up as described above. The used parameter settings were: $\alpha = 3.5$, $a = 0.05$, $b = 0.01$, $A = 2$ and $B = 1$. Three different behaviours of bumps were found for different damping constants γ and in the following sections, it is demonstrated that all of them are contained in the used version of the Lighthouse Model.

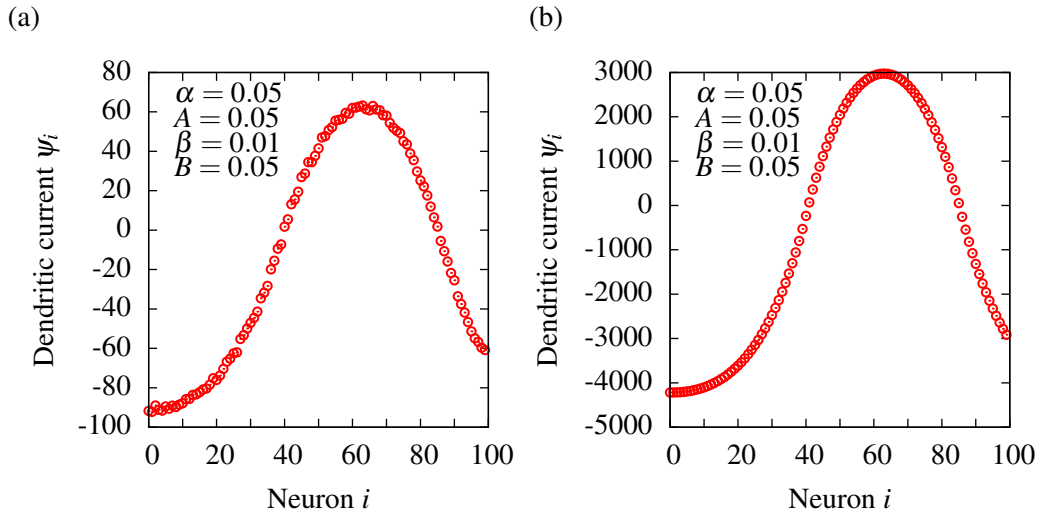

Figure 5.10.: The dendritic current of a system containing a stable bump is shown for different times. (a) is a snapshot at an early point in time and (b) is taken at a later time. Obviously, the scales of the dendritic currents in (a) and (b) are different, which is due to the non existing damping. Furthermore the bump is stretched in (b).

5.2.1. Stable Bumps

The first considered case, is a system of Lighthouse Neurons with slow synapses. In figure 5.10 the dendritic current of the neurons is shown. It can be seen that the absolute value of the dendritic current increases in time for all neurons if it is non-zero. The neurons that are in the border region of the system have a negative dendritic current ψ, which is caused by the fact that their coupling is mainly inhibitory. These neurons can not spike, because their input is below the threshold contained in the Naka-Rushton relation. The neurons in the centre of the line have a strictly positive current that is increasing in time. Consequently, due to the choice of $\underline{c}$ and the saturation of the Naka-Rushton relation for large input values, the spike rates of these neurons will reach their maximum after a short time. This frequency is the same for all neurons and stays constant, since the dendritic current does not decrease. Therefore these neurons have a persistent activity. On account of this and the inactivity of the borders, the occurring state fulfils the definition of a bump. If one looks at the activity of the neurons in figure 5.11, one can see that the state does not change in time and hence the set of the neurons that are part of the bump is conserved. Consequently the bump is stationary. The activity of the neurons is calculated by applying a threshold function on the dendritic current of each neuron. If the current is above this threshold θ_C, which is in this case zero, the activity is set to one and if it is below, the neuron is inactive and the activity is set to zero.

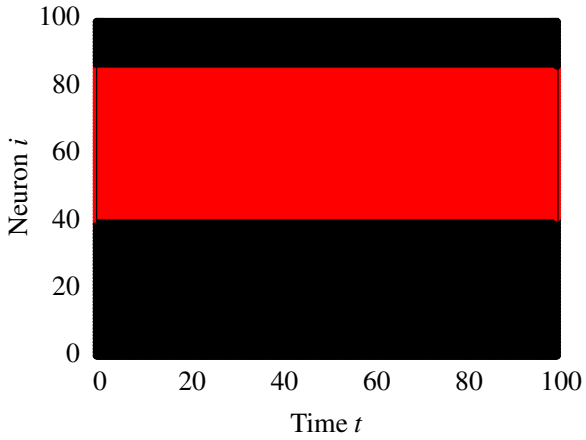

Figure 5.11: The activity of the neurons is shown, whereby red denotes activity and black inactivity. The neurons that are part of the bump are active and as can be seen, the set of the active neurons is not changing in time, which indicates that the position of the bump is not changing.

In figure 5.10 it can also be observed that the bump stretches with increasing time. This is explained by the fact that the neurons in the middle of the bump have more excitatory connections to the active neurons, caused by their centrality. Their dendritic current will increase by a larger amount than the current of the neurons at the edges of the bump. By this mechanism, the shape of the bump is stretched.

5.2.2. Wandering Bumps

As stated above, a bump is wandering if the edges of the bumps are neither stationary nor periodic. In the following case, the damping γ is set to a value of 0.5 to simulate fast synapses. The dendritic currents of the system gained in the numerical simulations are shown in figure 5.12 and the activity of the neurons is plotted in figure 5.13.
In contrast to the stationary case, it can be observed in figure 5.12 that the range of the dendritic current is the same for different times. This is caused by the damping of the current. The activity of the neurons shows, that a contiguous area of persistent activity occurs. The number of neurons, participating in it, is constant, but the position varies in time. Thus, following definition one and four, the emerging state is a wandering bump. The movement of the bump is underlying a double well potential as was pointed out by [CC06].

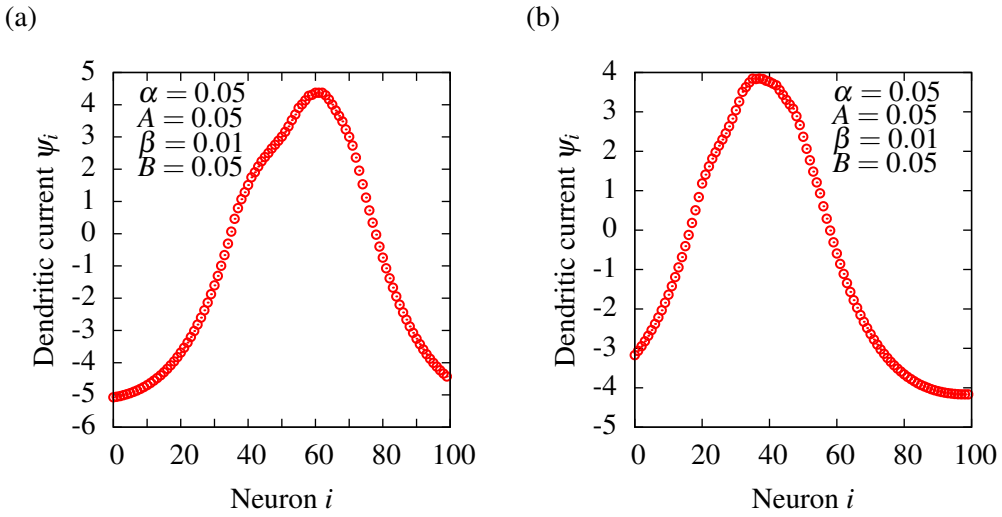

Figure 5.12.: A snapshot of the dendritic currents of the system is shown in (a) and (b), for a damping constant γ of 0.5. Both are taken at different points in time. (a) is taken at an early time and (b) at a larger system time. As can be observed, the shape and position of the bump is not conserved.

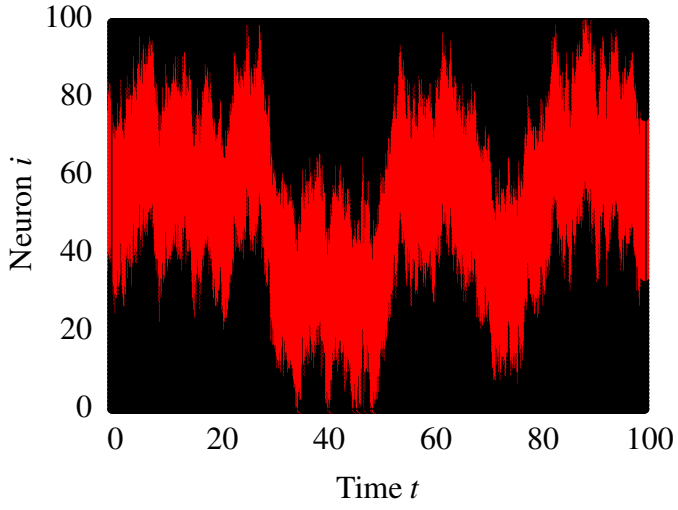

Figure 5.13: The evolution of the activity of the neurons in time is shown for $\gamma =$ 0.5. Each active neuron has at least one adjacent active neuron. Consequently a bump is moving through the system.

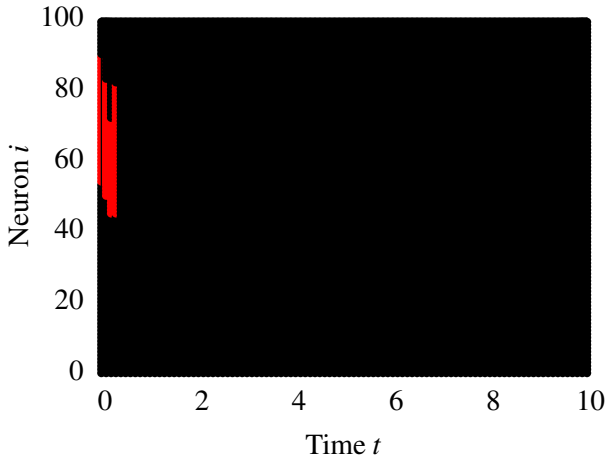

Figure 5.14: The activity of the system is plotted for $\gamma = 2$. It can be observed that in the beginning a bump emerges, but it decays soon.

5.2.3. Unstable Bumps

A stationary bump starts to wander, if the damping γ increases. Chow *et al.* [CC06] pointed out that if the damping increases further, a bump becomes unstable and starts to decay. If γ passes a certain threshold, the bump degenerates immediately and a stable or wandering bump can not emerge anymore. This is due to the fact that the dendritic currents of the neurons decay so fast that the phase velocities quickly tend towards zero. Consequently, the neurons do not spike and they are getting inactive. The system is overdamped and hence no activity can be sustained. For the simulations, γ was set to 2.0. As one can see in figure 5.14, the number of active neurons is decreasing in time and after a few time steps all neurons are inactive.

5.2.4. Stationarity through learning

The aim is to stabilize a wandering bump, by synaptic plasticity, in a way that it becomes stationary. Hence the same setup is used as before, but STDP is introduced. Furthermore the damping constant γ is set to 0.5 as for wandering bumps.
If the activity of the neurons in time is considered, which is plotted in figure 5.15, one can notice that the position of the centre of the bump is fixed. In the beginning, the edges of the bump are oscillating with a decaying amplitude and the bump becomes stationary after a short period in time. In contrast to the bumps investigated before, the shape of the bump is different and a snapshot of the dendritic current is shown in figure 5.16. The dendritic current is not continuous any more, but there is a gap between the inactive and active neurons in the dendritic current. The gap occurs at the edges of the bump. Nevertheless, for larger times this state fulfils the definition of a stationary bump. To explain the occurring stationarity of the bump, the dynamic coupling weight matrix has to be considered.

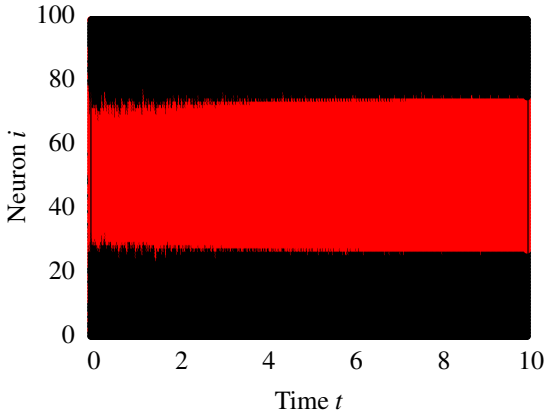

Figure 5.15: The activity of the neurons is shown over time for $\gamma = 0.5$ with the learning algorithm turned on. As one can see, in the beginning, the edges are oscillating, but these stabilize after a short time.

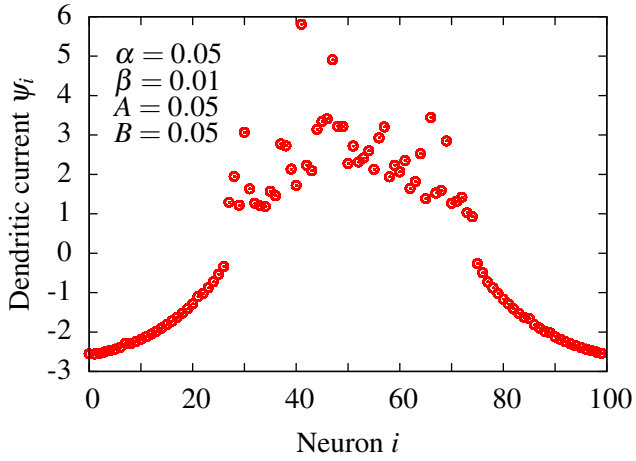

Figure 5.16: A snapshot of the dendritic currents of all neurons is shown. It can be observed that the shape of the bump is different than the shape of the bumps shown before. A gap in the dendritic current is occurring, whereby it separates the active and inactive neurons from each other.

It is plotted in figure 5.17 for different times. The initial coupling matrix contains a diagonal line given by the *wizard hat*. This line vanishes and a square like structure emerges in the centre of the matrix. Within this structure some coupling weights have a larger value. The coupling weights that are not contained in the square tend toward zero. The neurons belonging to the coupling weights, which are part of the structure, are all located in the centre of the system and are therefore part of the bump. To sum up, the connections between the neurons inside the bump strengthens and in contrast the connection between the outside and inside weakens and also between neurons, which are stationed outside of the bump. The connections of the system are becoming directed and only neurons inside the bump are connected with each other and receive spikes. Consequently, no neuron outside of the bump can get activated and hence the set of neurons that are active and part of the bump can not change anymore. By this, the wandering bump becomes stationary.

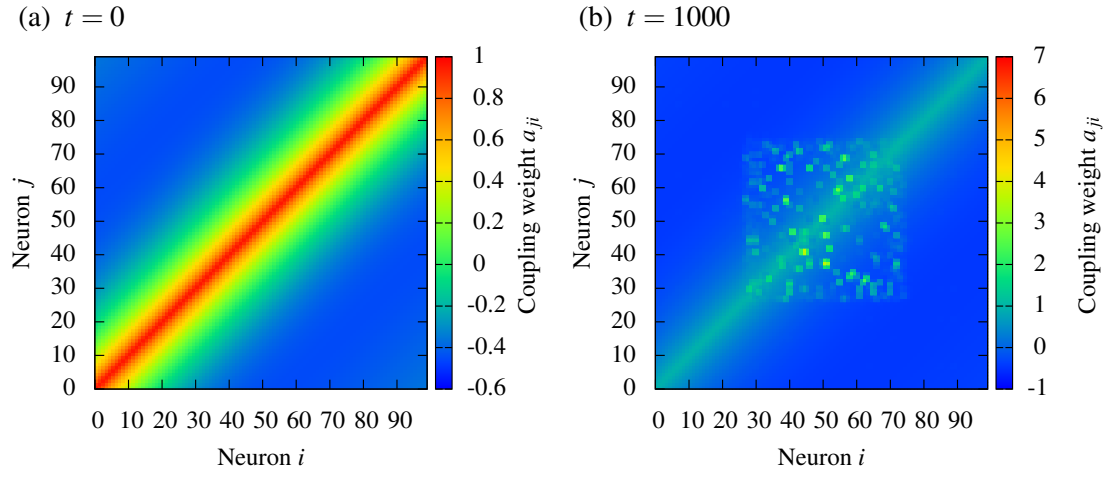

Figure 5.17.: The coupling weight matrix is shown for two different times. (a) shows the coupling weight matrix at time $t = 0$, therefore it is described by the Wizzard Hat. In (b) the coupling weight matrix at time $t = 1000$ is plotted. As one can see, the structure of the matrix changes. The original diagonal line vanishes and a square emerges in the center of the coupling weight matrix.

5.2.5. Discussion

In the beginning of this chapter, the results of [CC06] were reproduced. Bumps occur in the Lighthouse Model, whereat their behaviour depends on the damping parameter γ.
In the end, it was demonstrated that a wandering bump becomes localized and stationary if a learning algorithm is applied, since the synaptic connections between the outer and inner region of the bump disconnect. This is an interesting discovery if one keeps in mind the functionality of bumps. Bumps encode signals and store them in the short time memory and therefore they have to move to certain areas in the brain and stay there. Exactly this happened, in the case of stationary by STDP. An interesting point to investigate is if one could steer the movement of the bump by adjusting the learning parameters.

5.3. Moving spike patterns

Information is stored in spike patterns and is transmitted by these through the brain. Therefore, moving spike patterns, which are also referred to as travelling signals, are investigated. These states also fulfil the definition of wandering bumps, but on the contrary they decay with increasing time. The number of neurons participated in it are not constant. Furthermore, more than one signal emerges.
Between different areas of the brain propagating signals are transmitted in order to communicate with each other and to react to external stimuli similar to working memory. Hence in this chapter, it is investigated how travelling signals propagate through the system and interact with each other. The neurons of the observed system are aligned on a ring, whereat the system consists of hundred neurons. The setup can be seen in figure 5.18. Each neuron is only coupled to its next neighbours by a bidirectional connection. The synaptic connections are strong and of the same amount for all connections. Consequently, a neuron will receive a strong pulse if one of its neighbours spikes. The synaptic connections are fixed. The increment matrix $\underline{c}$ is diagonal, whereby the diagonal elements have the same value. To avoid that all neurons of the system spike persistently, the damping constant γ is slightly below the overdamped regime. Therefore the activity of each neuron decays quickly if it does not receive a high input from the other neurons. To produce moving spike patterns, the initial values of the phases and currents are set up randomly. Their evolution in time is observed, which is shown in figure 5.19. As one can see in figure 5.19 (a), the distribution of the current has a maximum around zero. This implies that only a couple of neurons are active, since they have a non-vanishing current. The other neurons are inactive. The distribution of the phases shows that most are close to 2π. After looking at the distributions of the phases and currents, the dynamic of the system is investigated. Therefore, three neurons of the system

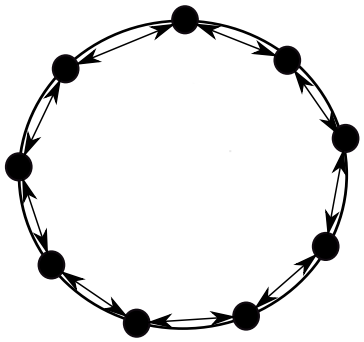

Figure 5.18: The neurons of the simulated network are aligned on a ring. Each neuron is coupled to its two nearest neighbours. The coupling strength is the same for all connections and stays fixed.

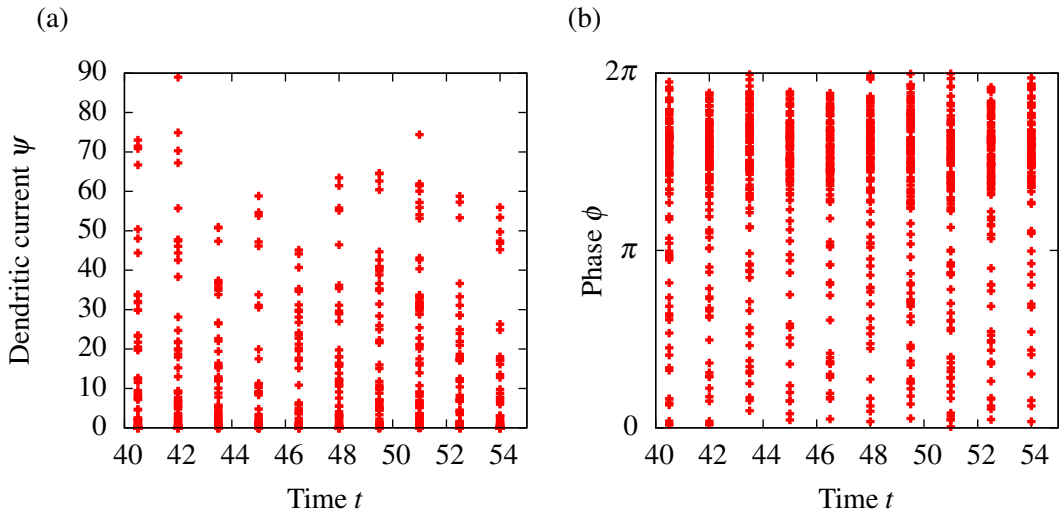

Figure 5.19.: (a) The dendritic currents ψ of all neurons of the system is shown. The maximum of the current distribution is close to zero. (b) The phase ϕ of each neuron is plotted. It can be observed that the distributions of the phases has the highest density close to 2π for all times.

are considered and their phases and currents are shown in figure 5.20. The neurons are chosen in a way that two of them are close to each other and the third one has a larger spatial distance with a position opposed on the ring. Figure 5.20 shows that for each neuron, time intervals exist in that the dendritic current ψ is close to zero and the phase is not changing. The resting value of the phase is close to 2π. The firing pattern and the dendritic current of neuron one and two are nearly synchronized, but in contrast neuron three is completely out of phase. All neurons have the same behaviour and hence it is to assume that a signal is travelling through the network.
This statement is supported by the snapshots of the phases and the dendritic currents of the system at different points in time, shown in figure 5.21. The travelling signals are not self-sustaining. In the beginning, several signals are propagating through the system, but these decay in time. The two signals contained in the network are moving into opposite directions and can move through each other. Each signal has a small tail at its backside, which is encircled in figure 5.21(c). The tail is due to the fact that the input at the backside of the neurons decreases as will be explained below.
It can be perceived that the width of the signal is degenerating with progressing time and consequently the signals are not self-sustaining. This leads to the conclusion that a neuron needs the input of both of its next neighbours to stay in the excited state. Another observation is that a signal is not propagating in both directions, but in one. This is unexpected, because

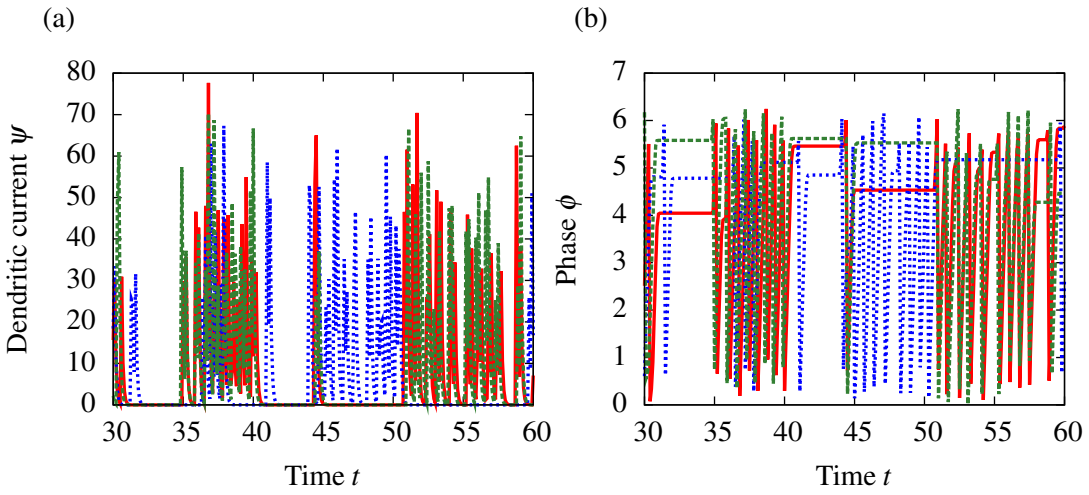

Figure 5.20.: (a) The dendritic current ψ of the neurons is shown. (b) The phase ϕ of the three neurons is plotted. The phase and dendritic current of neuron one is plotted in red, neuron two is shown in blue and neuron three is plotted in green. Neuron one and neuron two are close to each other and neuron three is arranged on the opposite side of the ring. The figures show that for each neurons intervals of inactivity occur, whereon these intervals are shifted in time.

all connections between the neurons are bidirectional and of the same size and therefore it was to expect that each point of the signal is the source of the signal itself, similar to spreading of spherical waves.
Most of the neurons have a phase close to 2π. If a neuron is in the front of the travelling signal, it receives an input signal from the neighbour that is already part of the signal. The neuron spikes, by which its phase is reset and a pulse is send to both neighbours. The signal moves along the ring and the observed neuron is now at the back of the signal. It receives a pulse from the neighbour that is now in the front of the signal. Its current and phase increase, but due to the damping γ, the current decays quickly and the phase velocity tends to zero. By this, the phase stops at a value close to 2π. This mechanism explains, first the propagation of the signal into one direction and secondly the emerging structure in the phases of the neurons. Furthermore, the occurring tail at the back of the signal, visible in the dendritic current, can be understood.

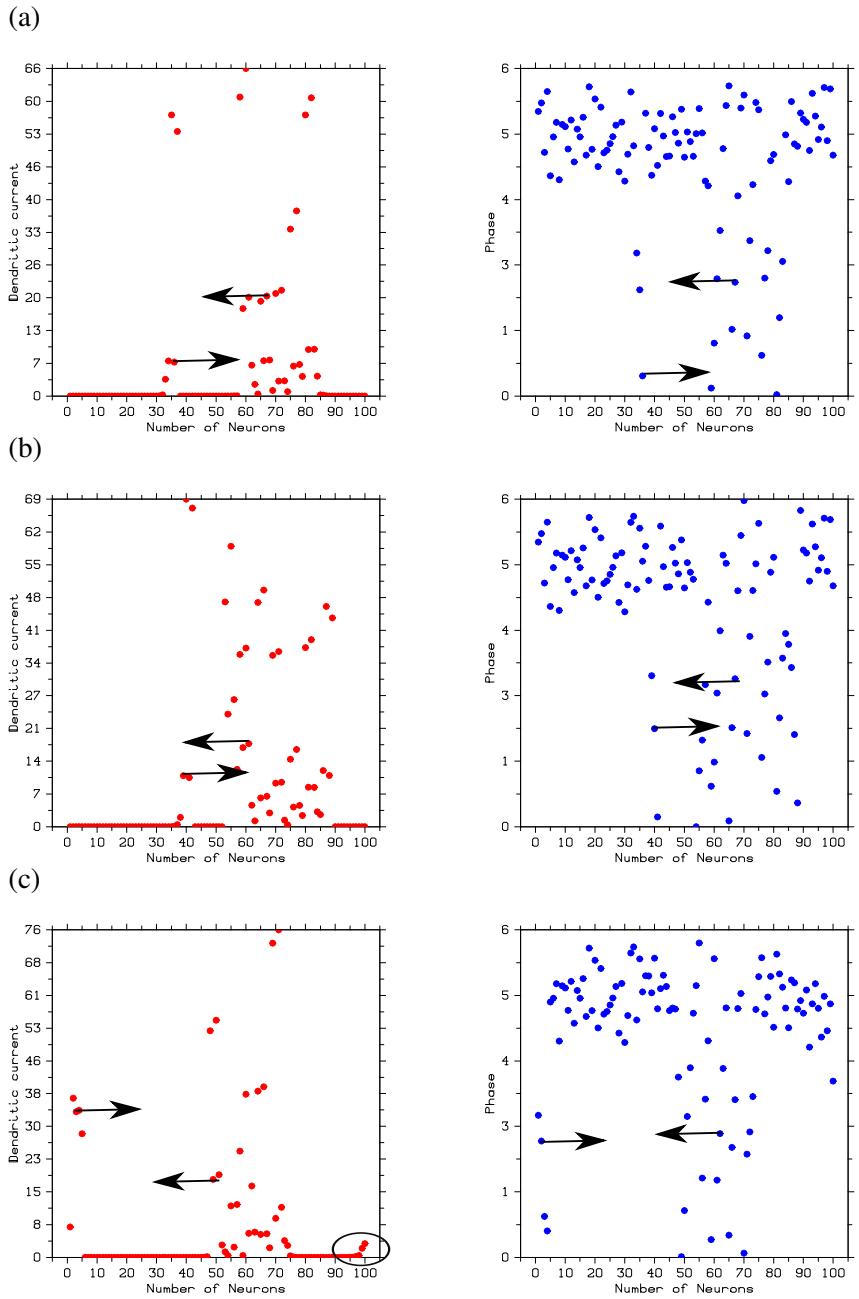

Figure 5.21.: The dendritic current of all neurons of the system is shown on the left hand side and the phase is plotted on the right hand side. The time is increasing from (a) to (c). As one can see the phase of the neurons that are not part of the signal are on the same level, which is close to 2π. The dendritic current is close to zero for these neurons. The directions of the signals are marked with arrays.

6. States of enhanced activity

6.1. Introduction

The motivation for the following investigation are the experimental works of [OFS$^+$10, Sor10]. In the contribution of Osorio *et al.* [OFS$^+$10] the statistical attributes of earthquakes and epileptic seizures were considered. The empirical data for epilepsy was raised in in-vitro-experiments on humans. The probability distributions of the energy, duration and the time interval between the single events, for earthquakes and epileptic seizures, were calculated and compared. It was not only pointed out that all distributions underlay a power-law, but also that the scaling-exponents for the same attributes are similar. In addition, they demonstrated that the Omori- and Inverse-Omorio-Law, which is valid for earthquakes, applies to epileptic seizures, too. In the end, they examined the conditional waiting time of both events and pointed out an equivalent behaviour. Therefore they showed that epileptic seizures and earthquakes are similar in certain aspects. These results are demonstrated below.
The aim of this work is to develop a mathematical model for a neural network, in which states with similar statistical attributes occur. The requirement to this model is that a microscopic description is used. By this, the underlying dynamic that leads to the statistical features might be revealed. Additionally, the creation and termination of the states can be understood in detail.
Since some contributions exist [HH95, LHG09, MG09, RL11] that either had a similar aim or that discovered states that are related to the states introduced in this work, these will be shortly presented. One of the earliest contributions was made by Hohn J. Hopfield and Andreas V. M. Herz [HH95]. They simulated a neuronal network based on a Leaky-Integrate and Fire model as introduced in equation (3.3). No learning algorithm was used and therefore the synaptic strength was fixed. Only the four nearest neighbours were linked and the coupling was homogeneously, which denotes that the coupling strength was the same for all connections. In the network, the action potentials of the neurons started to synchronize partially.
A more recent contribution in this area was made by Christian Meisel *et al.* [MG09]. They considered a network of pulse-coupled oscillators that were linked by dynamic synapses with a time averaged threshold spike time dependent synaptic plasticity. They observed that the system tends towards a self-organized state, in which the coupling weight distribution was governed by a power-law and the action potentials of the neurons synchronized. The occurring states did not terminate in the system.
A contribution that included termination was submitted by Anna Levina *et al.* [LHG09].

They considered a network of pulse-coupled oscillators, which were again linked via dynamic synapses. The synapses underlay short time depression and facilitation. An analytically description of the transition scenario to *Self-organized-criticality* (SOC) was made and the coexistence of the SOC and a sub-critical phase for certain parameters was found. These results were supported by numerical simulations. Furthermore, the distribution of the number of neurons that are part of the avalanches was investigated and it was pointed out that it is described by a power-law. The termination of an avalanche was explained by the fact that a huge activity, leads to synaptic short time depression and after a longer period of persistent activity the neurons can barely exchange signals. The main difference to the work introduced in this chapter is that an avalanche is a propagative reaction and not all neurons anticipate in the state at once. On the opposite, the states discovered in the extended Lighthouse network are collective.
Another contribution that investigates terminating states of synchrony was made by Alexander Rothkegel and Klaus Lehnertz [RL11]. They introduced a network of pulse-coupled oscillators, but in contrast to the two contributions before no learning algorithm was implemented. The used network was a small world network. Recurrent events of partial synchrony occurred, whereas all events had the same length. It was pointed out that the distribution of the interevent waiting time is described a power-law.

These contributions cover some of the statistical attributes discovered by Osorio *et al.* [OFS$^+$10]. In the following, a network of extended Lighthouse Neurons is set up and collective states of the network are produced . The statistical attributes are investigated and compared with the features, which were pointed out by Osorio *et al.* [OFS$^+$10]. If their features are similar, the gained knowledge of the dynamic of the states in the Lighthouse Network could be transferred to epileptic seizures.
Seizures are a point of discussion in the modern neuroscience. They are a symptom of epilepsy, which is a disease of the human brain that affects at this moment around 50 million people worldwide [oA12]. A person suffers from epilepsy, if seizures occur repeatedly over time. In combination to this an enduring alteration of the synaptic connection in the brain takes place, which increases the likelihood of future seizures [FBB$^+$05].
It is not exactly understood how seizures occur and why they terminate. Other unresolved questions are why seizures are not produced constantly and why they are in many cases just singularities. Furthermore, seizures are often linked to a certain level of synchronisation of spike times. But it is not known whether the synchronisation creates the seizure or if it is created by the seizure and the synchronisation terminates it [DWG$^+$05, LBH$^+$09].

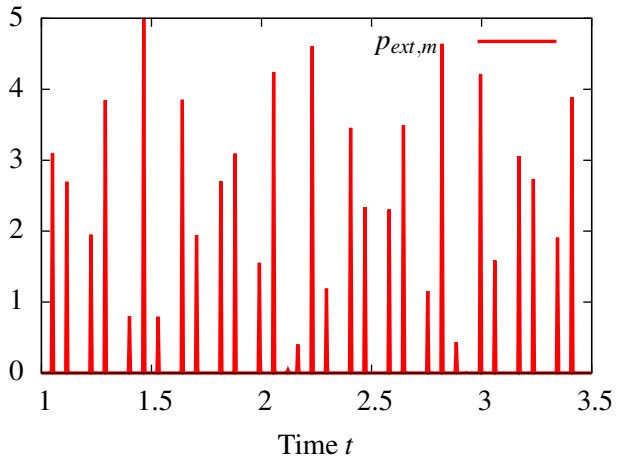

Figure 6.1.: The external signal is shown in this figure. It consists of delta-peaks that vary in height.

6.1.1. Initiation of states of enhanced activity

In the extended Lighthouse Model collective states of enhanced activity are produced. The states have in common that all neurons are active and spike with a frequency close to the saturation frequency ν. A basic level of synchronization occurs, whereupon it is very important to mention that the synchronization is varying in time.
In the beginning a network of fifty neurons is simulated. The damping constant γ is set to 0.7 and the coupling weights are initialized randomly, whereas they are uniformly distributed. By this, an all-to-all coupling exists, so that all neurons of the network are linked to each other. Self-coupling is neglected, i.e $a_{ii} = 0.0$ and hence a neuron will not receive its own spike. This is a reasonable assumption from a biological point of view. Furthermore a diagonal increment matrix $\underline{c}$ is used and the elements c_{ii} are set to 5. The learning parameters are set ups as follows: $\Delta = r = 1$, $\tau_{l\sigma} = \tau_{r\sigma} = 10.0$, $\tau_A = \tau_B$ and $u_A = u_B = 0.9$. Therefore the time windows are symmetric. To create states of enhanced activity, one neuron of the system is receiving an external signal $p_{(ext,m)}$. This could be, for instance, periodic flashes of light. The used external signal can be seen in figure 6.1. In the following, fluctuations are not implemented.
The phase and the dendritic current of one neuron of the network is shown in figure 6.2. As can be observed, time intervals exists in which the neuron has a non-vanishing dendritic current and its phase changes rapidly. Consequently, the neuron spikes and the frequency is close to the saturation frequency ν contained in the Naka-Rushton relation. On the other hand, time intervals occur in that the neuron is inactive. The dendritic current is close to zero

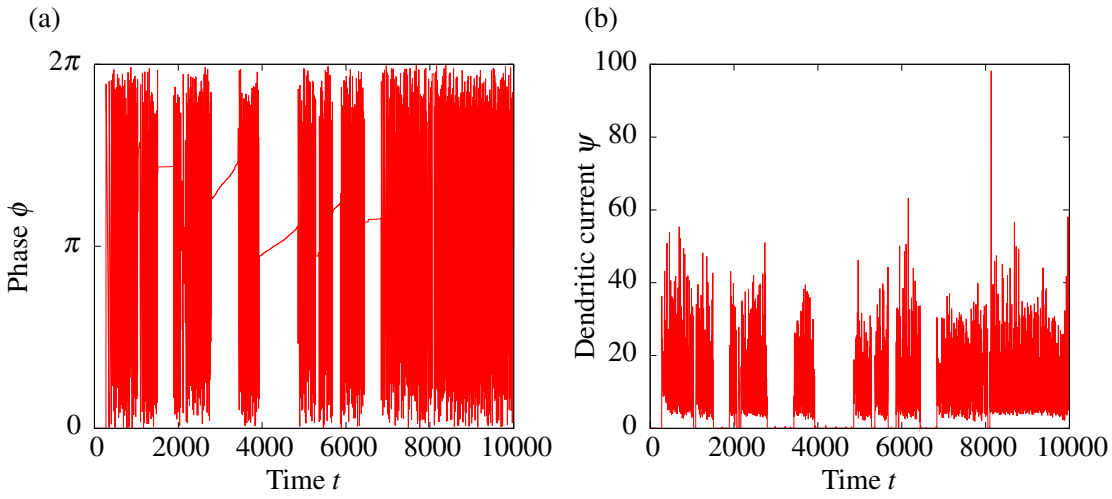

Figure 6.2.: (a) The phase of one neuron of the system is shown. (b) The dendritic current of the same neuron of the network is plotted in time. As one can see in figures (a) and (b) time-intervals occur, in which the neuron is at rest and intervals when it is higly active.

and the phase is only increasing slowly. All neurons have the same behaviour and the time intervals are the same. In the inactive intervals only the driven neuron is spiking, but with a very low frequency. Therefore collective states of the system occur, during which all neurons are highly active. At some point the state terminates and all neurons are getting inactive. In the following, these collective states are referred to states of enhanced activity.

6.1.2. Emergence and termination

First, the emergence of these states is considered. The phases of all neurons close to the beginning of a state of enhanced activity are plotted in figure 6.3. The phase of the neuron, receiving the external signal, increases and it will spike occasionally. By this all neurons that are linked to it receive pulses that are proportional to the coupling weight. The phases of them pile up, until the phase of one reaches 2π. This neuron spikes and sends a signal to the linked neurons. This causes in turn an increase of the phases of the other neurons. If more phases are close enough to 2π, other neurons will spike and a chain reaction is initiated and the state of enhanced activity starts.
The chain reaction is inhibited, if the damping constant is above a critical value $\gamma_c^{\mu p}$ that depends on the system size. The driven neuron would cause the other neurons to spike, but only once at a time, since the dendritic current decays quickly and by this the phase velocity is low. Therefore the necessary spiking frequency of the neurons to preserve and initialize a state of enhanced activity can not be reached.

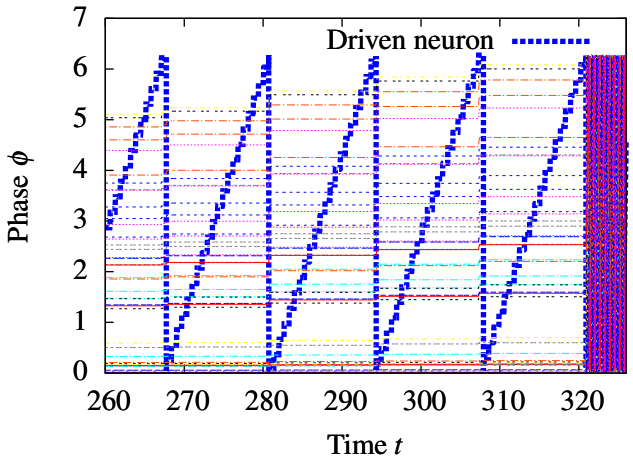

Figure 6.3: The phase of all neurons is shown in this plot. If the phase of the driven neuron reaches 2π, an action potential is generated by which the phase of the other neurons increases. Slowly, these phases pile up and if several are close enough to 2π, a chain reaction will start.

Another interesting point to investigate is the behaviour of the neurons during a state of enhanced activity. The dendritic current of all neurons is non-zero and the firing rate $\dot{\phi}_m$ is close to the saturation value. To get a better insight, a close-up of the phases of all neurons at different points in time of a state of enhanced activity is shown in figure 6.4.
One observes that the structure of the phases changes in time. First, the neurons are unordered (see Fig. 6.4 (a)), then groups form until only two bundles remain. They dissolve and the group forming starts repeatedly. Again two groups shape (Fig. 6.4 (c)) and these are getting closer to each other until the state of enhanced activity terminates (Fig. 6.4 (d)).
Since it was pointed out that the synchronization of the phases is important for these states, the synchronization of them during a state of enhanced activity is investigated. It is calculated as described in section 3.6.1 and shown in figure 6.5.
After a state is initiated, all neurons start to spike with a high frequency. The phases of the neurons become unordered as can be seen in figure 6.4 (a) and the coupling weights change, due to the occurring spiking. The level of synchronization drops down rapidly in the beginning of a state of enhanced activity. Afterwards, the phases of the neurons adapt, groups shape, and by this the synchronisation of the phases increases (see Fig. 6.4 (b)). This happens due to the learning mechanism, because the coupling between two neuron becomes directed. The different groups start to melt and therefore the synchronization increases further. If the system exceeds a certain level, the bundles dissolve again and the synchronization decreases. But directly afterwards, new groups are shaping in the phase. At one of the maxima of the synchronization, the state of enhanced activity terminates and the system gets inactive. As one can see, the maxima are unstable points of the observed states.
To understand the underlying mechanism, a system of two neurons is considered as shown in figure 6.6. It is assumed that neuron two spikes before neuron one. Consequently, the coupling weight a_{12} strengthens and in reverse a_{21} is depressed. Since the increment matrix $\underline{c}$ is diagonal, the phase velocity caused by the received spike is proportional to the

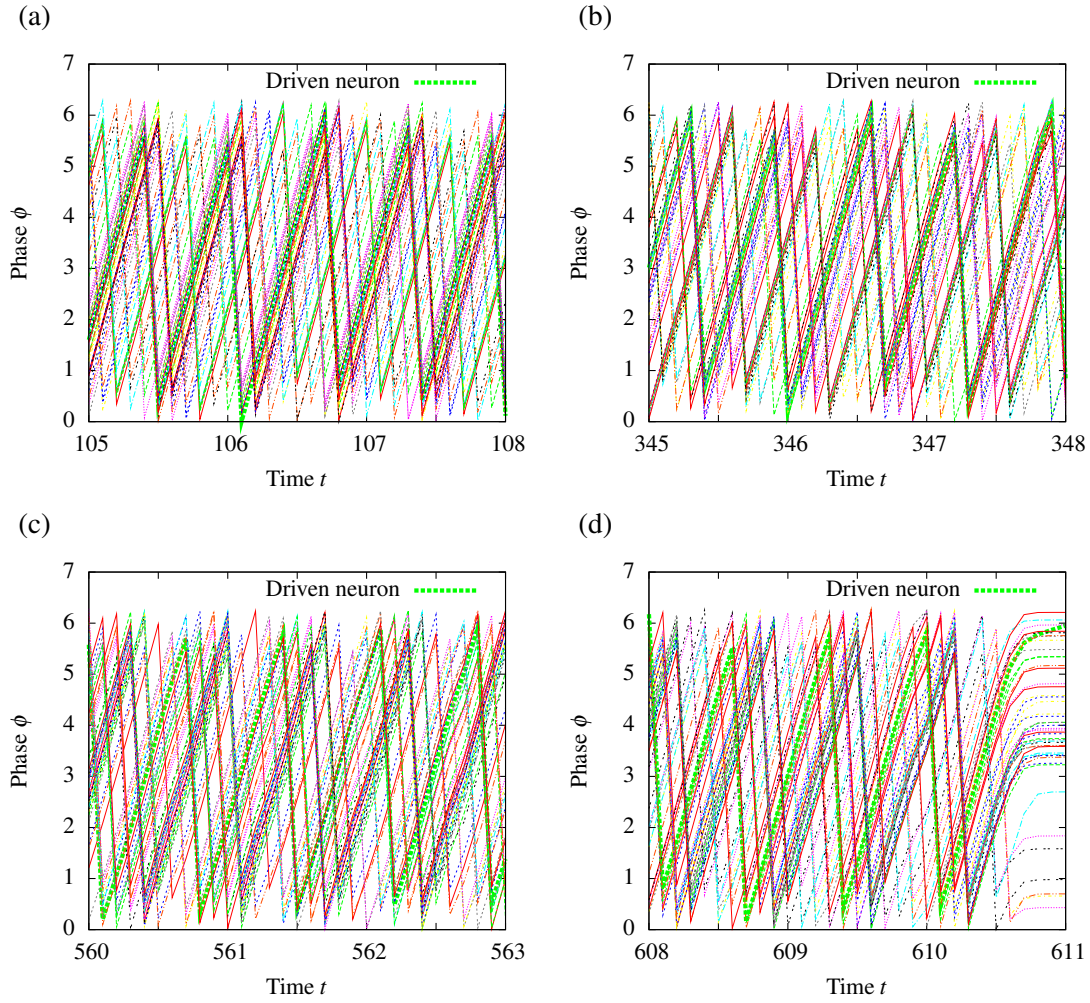

Figure 6.4.: A close-up of the phases of all neurons during a state of enhanced activity is shown at different points in time. (a) shows a close-up of the start. In (b) and (c) the phases are plotted during the state and in figure (d) a close-up of the termination is shown. One can see that the structure of the phases changes in time.

corresponding coupling weight. Therefore the phase velocity $\dot{\phi}_1$ of neuron one increases and $\dot{\phi}_2$ decreases. This is drafted in figure 6.6 (b). By the changed velocities, the phase ϕ_1 of neuron one increases faster than the phase of neuron two. The difference between the phases becomes larger and their synchronization decreases. If the spikes of the neurons moved out of the same time window, the coupling weights stay constant. At this point, one coupling

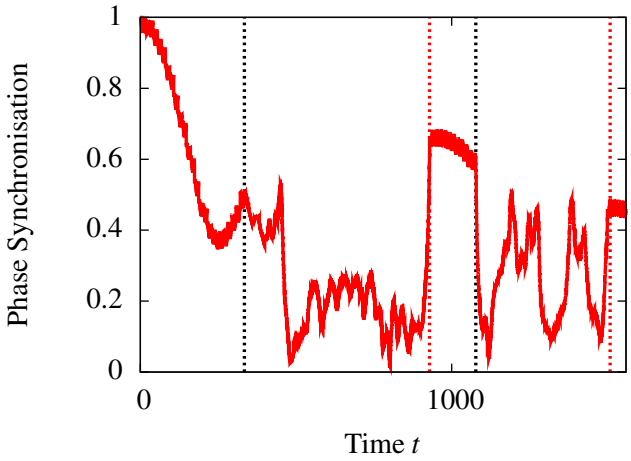

Figure 6.5.: The phase synchronisation of the whole network is plotted. The beginning of the state of enhanced activity is marked with a vertical dashed black line and the termination with a vertical red line. During a state of enhanced activity, the synchrony first reaches a minimum, increases to an local maximum and drops down again, until the state decays at a local maximum of the synchrony. Therefore, the system reaches an unstable state at the local maxima of the synchronization, at which the system can either stay in the state of enhanced activity or decay to the resting state.

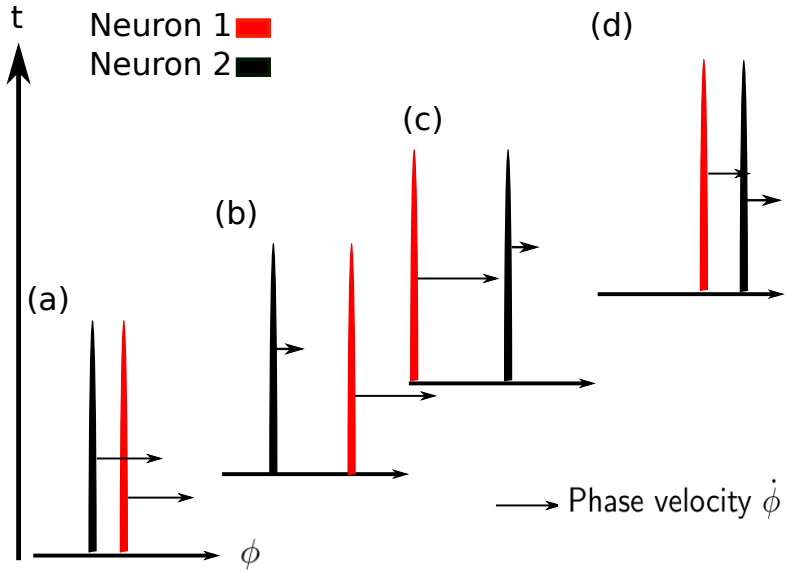

Figure 6.6: A system of two neurons is considered. The position of the phases ϕ of the two neurons and the phase velocity $\dot{\phi}$ is drafted over time.

weight is at its maximum and the other one at its minimum. Since the phase ϕ is a periodic variable, the neurons are getting closer to each other after the maximal distance of π is exceeded, but the position of the spikes to each other is swapped. The synchronization starts to increase again and after the neurons entered the same time window τ_σ, the connection between them is altered by the STDP. Since the spike pattern is swapped, the coupling weight a_{12} decreases and a_{21} increases and respectively the phase velocities. It has to be considered that a_{12} is depressed by a relative amount and a_{21} is potentiated by an absolute amount. With the given system settings the depression is larger than the potentiation and as a result both coupling weights are small and accordingly the phase velocity due to the received spikes. At the maximum of the synchronization, the phase velocity reaches its minimum. If the damping constant γ is low enough, the dendritic currents can therefore compensate the lack of input signals, since they do not decay fast enough and the phase velocity stays close to the saturation frequency.

If this knowledge is applied to a network of neurons, one can understand the group forming and the instability that occurs at a local maximum of the phase synchronization. The mean coupling weight of the system has a minimum at this point and the phase velocity decreases. If it is below a certain value, the neurons participated in the state of enhanced activity can not spike and the chain reaction, which is sustaining the state, stops. For this mechanism a lower critical damping constant γ_c^{low} exists, that depends on the system size. The damping constant has to be below this value, otherwise the chain reaction responsible for the state of enhanced activity could sustain itself.
It was shown that the change of the coupling weights is essential for the termination and consequently a state would not terminate without synaptic plasticity. If the made assumptions are valid, the level of phase synchronization during an event has to be below the level of synchronization during a state of enhanced activity produced in a system with learning. To proof this, an external driven system without learning is considered and the synchronization is calculated, which is shown in figure 6.7.
A state of enhanced activity occurs in the system, since the initiation is only linked to the piling of the phases. But in contrast to the system with learning, the state of enhanced activity does not terminate. The synchronization during a state of enhanced activity without plasticity shows no distinct maxima, like the maxima occurring with synaptic plasticity. To sum up, the start of a state of enhanced activity is due to the piling of the phase and this mechanism occurs in both kind of systems. On the opposite, the termination does not take place in a system without synaptic plasticity, since the grouping of the neurons and the synchronization is essential for the termination of a state of enhanced activity. If this findings are compared with experimental results from Marie-Therese Schindler *et al.* [SBH$^+$08] and Klaus Lehnertz *et al.* [LBH$^+$09], one can see that states of enhanced activity and seizures have a similar behaviour. [LBH$^+$09] stated that for a certain kind of epileptic seizures the synchronization and the instability occurs together, whereat the synchronization towards the end of the seizure may be a self-regulatory mechanism to catalyse the seizure termination.

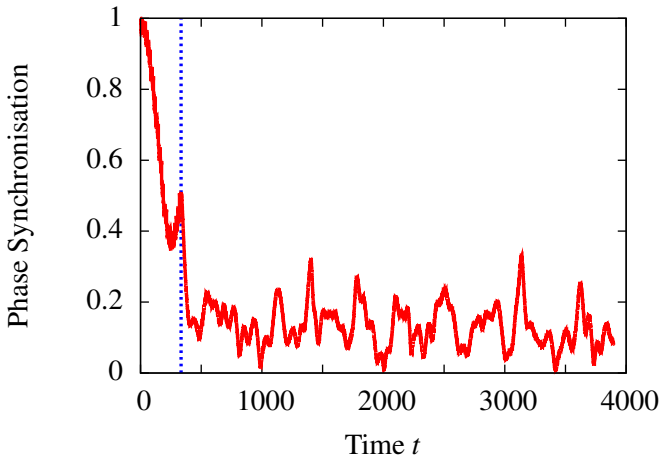

Figure 6.7: The phase synchronisation of a network without learning is plotted. The starting point of the state of enhanced activity is marked with a vertical dashed line. In comparison to the case with synaptic plasticity, the state does not terminate.

6.2. Statistical behaviour

In the following, the statistical behaviour of states of enhanced activity are investigated and compared with the experimental findings of Osorio *et al.* [OFS+10] for epileptic seizures and earthquakes, to show the similarity between them. The experimental data for epileptic seizures, used by [OFS+10], was recorded by the *University of Kansas Medical Center* between 1996 and 2000 from 60 human subjects. These suffered from mesial temporal or frontal lobe pharmacoresistant epilepsy. Data from 6032 seizures was received by continuous multiday voltage recordings, whereby $48-256$ electrodes were used for each measurement. These electrodes were either directly inserted into the brain or placed directly over the cortex. Osorio *et al.* [OFS+10] defined seizures as paroxysmal increases in the relative power in the frequencies between 8 and 42 Hz, whereas the relative power has to be above a threshold T for a certain time D, to be counted as a seizure. With this data, the interevent time, the seizure duration, and the intensity of a seizure were calculated, whereat the seizure energy E is defined as the product of the peak seizure intensity and duration.
The earthquake data of 81977 earthquakes between 1984 and 2000 with a magnitude larger than two were used, which was supplied by the Southern California Seismic Network catalog. The data was collected from 300 seismic sensors.
Since the results gained by Osorio *et al.* [OFS+10] are important for the theoretical investigation, these are shortly introduced.
Out of the experimental data, the energy E for epileptic seizures and the seismic moments S for earthquakes were calculated. These are equivalent observables between the systems. The distribution of the seismic moments S underlies the Gutenberg-Richter-Law [CDSB02, Run89]. It states that the probability density function $f(S)$ underlies a power-law, whereas the scaling-factor depends on the tectonic environment of the area.

(a) (b)

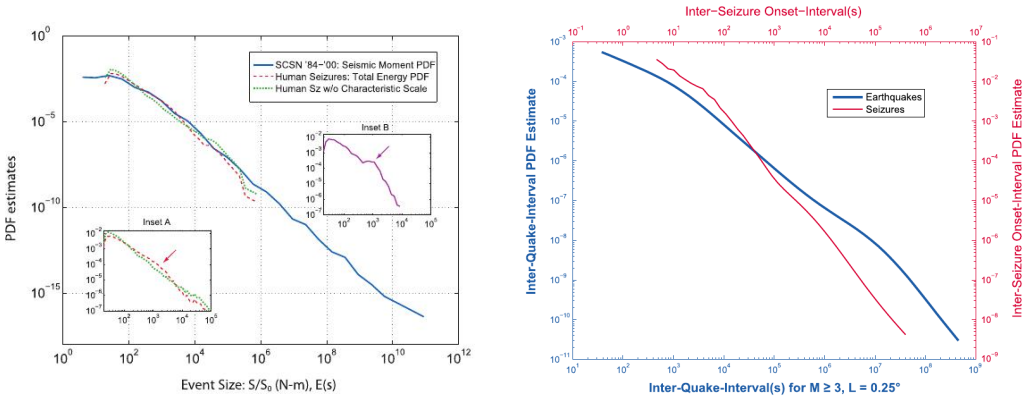

Figure 6.8.: (a) shows the *PDFs* of the seizure energy and the seismic moment. The *PDFs* are governed by a power-law, whereby both scaling coefficients, determined by Osorio *et al.* [OFS$^+$10], are similar namely $\alpha^{(E)}_{\text{Epi}} \approx \alpha^{(E)}_{\text{Earth}} \approx -5/3$. In (b) the probability density functions for the interevent waiting time are shown. These are governed by a power-law, too. But the scaling coefficients for earthquakes $\alpha^{(I)}_{\text{Earth}} = -1.1$ and epileptic seizures $\alpha^{(I)}_{\text{Epi}} \approx -3/2$ differ. Both figures are taken from [OFS$^+$10].

In addition, the *PDF* for the interevent waiting time for both systems is determined and are shown in figure 6.8. As one can see, all *PDFs* are governed by power-laws. The scaling coefficient for the *PDFs* of the energy and seismic moment are similar, but the scaling coefficients for the interevent waiting time differ. Despite this, it is astonishing that the *PDFs* of both properties of seizures are governed by a power-law and that the scaling coefficients are similar to the ones for earthquakes. This indicates that the underlying dynamics of both systems have similar features, since states of *Self-organized-criticality* (SOC) occur in both systems [BCDS02, Jen98, OFS$^+$10].

If a person suffers from epilepsy, it is most likely that he will undergo several seizures. These are reoccurring events in time, like earthquakes, whereupon their occurrence takes place on different time-scales. Osorio *et al.* [OFS$^+$10] showed that the inverse Omori-Law and the Omori-Law is valid for epileptic seizures, too. A problem that occurred is that the duration of an earthquake is in comparison to its interevent waiting time a point event, which denotes that the starting and end point are in a good approximation identical. This is not the case for epileptic seizures. To calculate the aftershock rate, Osorio *et al.* [OFS$^+$10] only considered the endpoints of the epileptic seizures. They locked an indicator function to one endpoint and calculated the time distance to the other endpoints. This was done for each endpoint and a histogram was created. The same is done for the foreshock-rate,

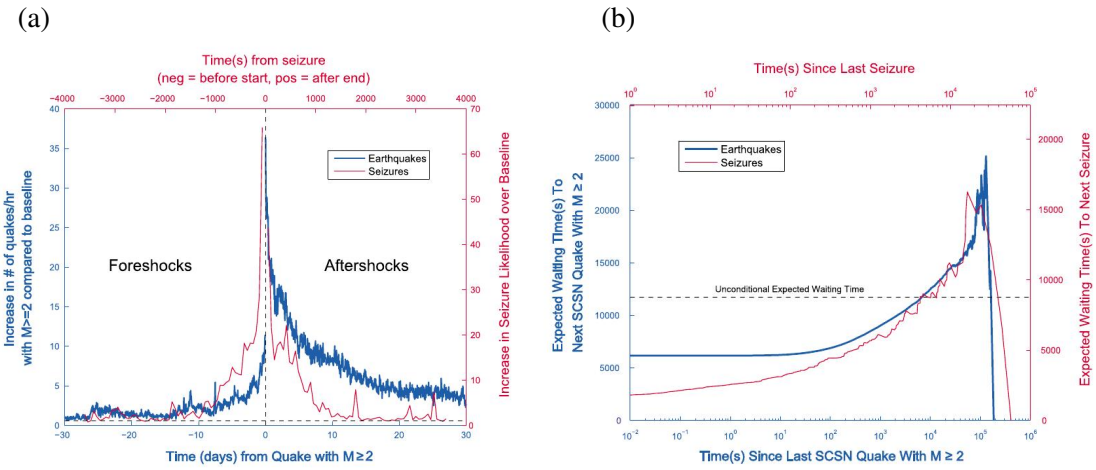

Figure 6.9.: (a) shows the aftershock- and foreshock-rates for earthquakes and epileptic seizures. As one can see, both have a similar behaviour. In (b) the expected waiting time is shown for epileptic seizures and earthquakes. Again a similar behaviour for both systems can be observed. Both figures are taken from [OFS+10].

but the starting points are used for the calculations. By this, the Omori-Law and inverse Omori-Law was reproduced with the experimental data, as can be seen in figure 6.9(a). As one can see in figure 6.9(a), the aftershock- and foreshock-rates for earthquakes and epileptic seizures underlie the same behaviour. The shock-rate is proportional to the inverse of the time-difference to the main event. This indicates that the Omori- and inverse Omori-Law applies to both systems (see chapter 3.6.5), whereas the parameter setting differs. The only difference between the systems is that the shock-rates are symmetric for epileptic seizures and non-symmetric for earthquakes, but this was already considered in chapter 3.6.5.
As the Omori- and inverse Omori-Law states, the event rate depends on the time-distance to the last event. If the time-distance is smaller, the event-rate and hence the probability for another state of enhanced activity to occur is higher, than for larger time distances. Therefore, another interesting question is how the expected waiting time depends on the time that has already passed by, since the last event. The expected waiting time is the time that has to pass by until the next event occurs. It was calculated by [OFS+10] for epileptic seizures and earthquakes and is plotted in figure 6.9(b). It can be observed that both systems have the same behaviour. First, the increase of the expected waiting time with the time that passed by since the last event is governed by a power-law. After the expected waiting time reached its maximum, it rapidly drops down, until it becomes zero. Consequently, there is a maximal interevent waiting time in both systems. This is a well known finite-size effect. A system with a limited size is loaded and it has to unload after a certain time, since the contained

energy can not be stored any more. This is valid for earthquakes and epileptic seizures. Due to the finite-size effect the *PDFs* aberrates from the power-law behaviour for large event sizes.
The statistical attributes that were considered by Osorio *et al.* [OFS$^+$10] are reproduced for states of enhanced activity. The theoretical data is created by long time simulations.
For this a network of 100 neurons is set up and the damping constant γ is set to 1.0. The other system parameters stay fixed. The time step dt for the applied fourth-order Runge-Kutta method is 0.1
The occurring states of enhanced activity are identified by a threshold mechanism. It is based on the value of the mean dendritic current. As can be seen in figure 6.2, the dendritic current ψ is large during a state and outside close to zero. Consequently, a threshold θ_ψ for the dendritic current can be chosen so that the system is in a state of enhanced activity if the mean dendritic current is above the threshold θ_ψ. Vice versa, no state of enhanced activity takes place if the mean dendritic current is below this threshold θ_ψ.
All-in-all around $10,000$ events were measured. This is around half of the events measured by Osorio *et al.* [OFS$^+$10] for epileptic seizures, but one has to keep in mind that the numerical costs to produce these data are immense and 27 runs of the program were performed, whereby each of them lasted more than a month.
The duration, the interevent waiting time and the energy are calculated, whereupon the energy is proportional to the square of the dendritic current. The probability density functions for the energy, the event duration and the interevent waiting time are estimated via a histogram. Furthermore, the Omori- and inverse-Omori-Law are reproduced and the conditional expected waiting time is calculated.

6.2.1. Power-law-like behaviour

In the calculated *PDF*s, a power-law (chapter 3.6.4) is fitted by using a least square fit. The aim of this is to determine the scaling coefficient. It can be compared with the experimental scaling-coefficients calculated by Osorio *et al.* [OFS$^+$10] and by this, the theoretical results can be relayed with experimental data.

Interevent waiting time

The interevent waiting time is the interval length between two subsequent states of enhanced activity. For this quantity Omori *et al.* [OFS$^+$10] discovered that the *PDFs* of earthquakes and epileptic seizures are governed by a power-law and they determined the scaling coefficient as $\alpha^{(I)}_{\text{Earth}} = -1.1$ and $\alpha^{(I)}_{\text{Epi}} \approx -\frac{3}{2}$, respectively. If the theoretical data is plotted and a power-law is fitted into it, as it is done in figure 6.10, the scaling coefficient is given by $\alpha^{(I)}_{\text{Theo}} \approx -1.555 \pm 0.044$. It is therefore similar to the experimental results for seizures.
It is obvious that the data points are well described by a power-law for smaller interevent waiting times. For larger event times, the points are scattered around the fitted power-law.

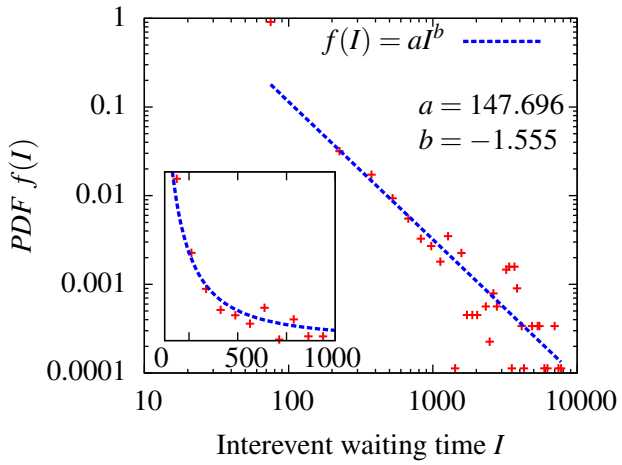

Figure 6.10: The probability density function estimate of the interevent-intervals of the states of enhanced activity is plotted. The axes in the main plot is logarithmic scaled. The inset shows the same data points for standard scaling. A power-law is fitted to the data.

An possible explanation is the lack of fluctuation or that the produced statistic is not yet converged for large values, since the amount of data points is limited. Unfortunately, the numerical costs to get more data are in no relation to the gained information. To measure one event with the maximal interevent time of of $10,000$, which denotes $100,000$ numerical steps, around $100,000,000$ numerical steps are necessary. This is due to the fact that the probability for this event is approximately 0.001. This illustrate the range of the numerical costs.

Gutenberg-Richter-Law

[OFS+10] calculated the power-law-exponents for the energy distribution $\alpha^{(E)}_{\text{Earth}} \approx -5/3$ for earthquakes and with $\alpha^{(E)}_{\text{Epi}} \approx -5/3$ for epileptic seizures. Therefore, both systems have the same scaling behaviour for the energy. The probability density function for the energy of the states of enhanced activity is plotted in figure 6.11. The fitted coefficient is -1.667 ± 0.011 and hence it is consistent with the experimental results. The *PDF* has a slight tail for large energies, whereat the data points have the tendency to be below the power-law-fit. If one assumes that the power-law occurs due to *Self-organized-criticality*, a possible explanation is that the events after a certain size, lose their self similarity, due to the limited system size. If this is true, the power-law would be valid over a wider range for larger systems and therefore could be an indicator for the size of the system that produces the states of enhanced activity. This would also explain the derivation from the power-law for larger event sizes for the *PDF* of the interevent waiting time.

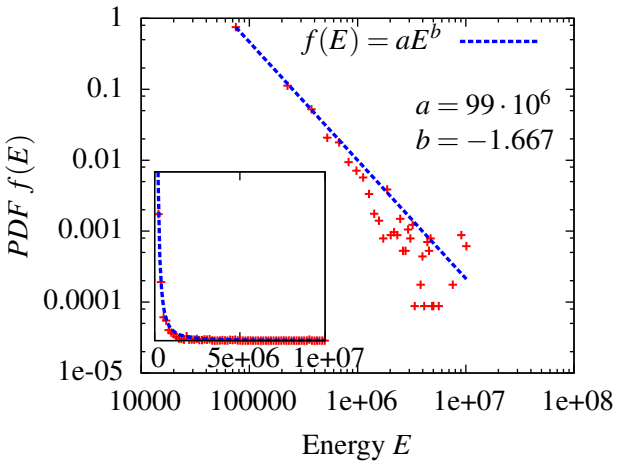

Figure 6.11: The probability density function estimate of the total energy of the states of enhanced activity is shown. A power-law was fitted in there, with a least-square fit and the coefficient is approximately -1.667 ± 0.011.

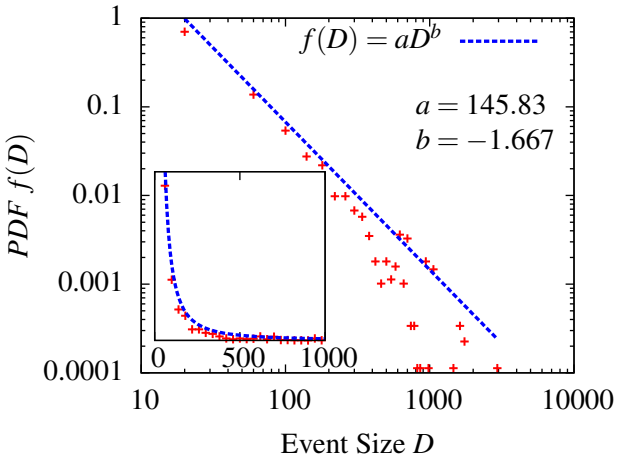

Figure 6.12: The probability density function estimate of the duration of the states of enhanced activity is plotted. By the power-law fit the scaling coefficient is determined as approximately -1.667, which is congruent to the power-law exponent of the energy *PDF*.

The energy of the seizures has been calculated by the sum of the intensities of the state of enhanced activity, which are given by the squares of all dendritic currents $\psi(t_n)$ times the resistance R, normalized by the number of neurons M. It reads:

$$E(S) = \frac{R}{M} \sum_{n,m} \psi_m(t_n)^2 = \frac{R}{M} \sum_{n,m} I_m(t_n), \tag{6.1}$$

where $I_m(t_n)$ is the intensity. If one considers the probability density function of the duration of states of enhanced activity, an interesting attribute of these is revealed. The *PDF* is plotted in figure 6.12.
The value of the scaling coefficient for the probability density function is -1.667. As can be seen, the scaling factor of the probability density functions of the energy and the duration are

nearly identical. This indicates that the distribution of the energy is proportional to the *PDF* of the duration. The proportionality constant is the intensity $< I >$ of the state of enhanced activity.

$$E(S) = \frac{R}{M} \sum_{n,m} \psi_m(t_n)^2 =< I > \; D(S) \tag{6.2}$$

This equation states that an event with a longer duration has a higher energy. This is not surprising, but it reveals that all states in this model have, independent of their duration, the same distribution of the intensity $< I >$. Hence, the distribution of the dendritic current ψ is independent of the length, too. If the mean value of the intensity would depend on the length of the state, a step would occur in the probability density function for the energy. Since this is not the case, one can conclude that the underlying mechanism producing the states of enhanced activity is the same for all events.

6.2.2. Omori Law and Inverse Omori Law

The foreshock- and aftershock-rates of states of enhanced activity are calculated with the method introduced by Osorio *et al.* [OFS$^+$10]. By this, the Omori-Law and the inverse Omori-Law is reproduced with the theoretical data, as can be seen in figure 6.13.
The foreshock- and aftershock-rate is plotted against the time distance to the main event. The coordinate system is scaled double logarithmic and the Omori-Law is fitted into the data points. As can be seen, it describes the theoretical data-points for the aftershock- and foreshock-rate well. Similar to the Omori-Law calculated by Osorio *et al.* [OFS$^+$10] for epileptic seizures, the aftershock- and foreshock-rates are in opposite to the one for earthquakes, symmetric.

6.2.3. Expected waiting time

Osorio [OFS$^+$10] *et al.* showed that the expected waiting times of earthquakes and seizures underlie the same behaviour. The results of the numerical simulations are shown in figure. 6.14. As one can see, the expected waiting time strongly depends on the time distance to the last event and is similar to the behaviour of and seizures that is shown in figure 6.9(b). In the beginning, the increase of the expected waiting time underlies a power-law. After it reaches its maximum, the expected waiting time rapidly drops down until it reaches zero.

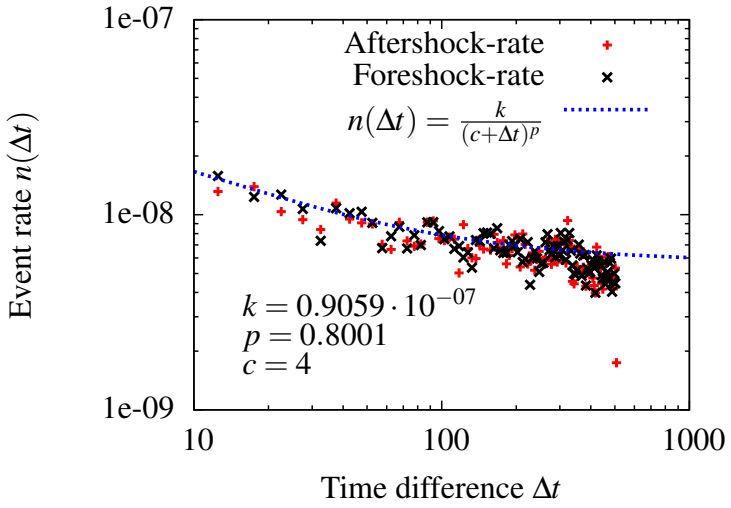

Figure 6.13.: The foreshock- and aftershock-rates for states of enhanced activity are shown in a double logarithmic scale. The x-axis shows the time distance t to the main event and it is given by $\Delta t = |t_{main} - t_{side}|$. This has the advantage that the foreshock- and aftershock-rate fit into the same time window. The Omori-Law is fitted into the data points with the shown fitting parameters.

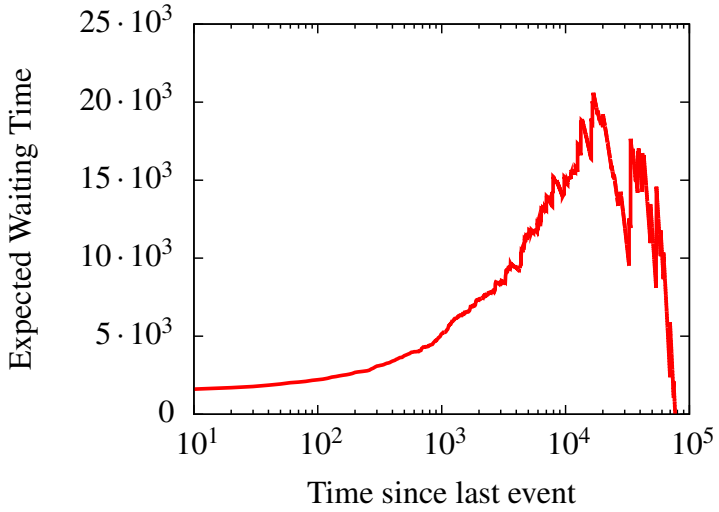

Figure 6.14.: The averaged waiting time to the next state of enhanced activity in dependency of the time distance to the last event is shown.

	Earthquakes	Epileptic seizures	Simulations
Energy	$-5/3$	$-5/3$	-1.667 ± 0.011
Interevent waiting time	-1.1	$-3/2$	-1.555 ± 0.044

Table 6.1.: The scaling coefficients gained from the experimental and numerical data are shown. The experimental coefficients for earthquakes and epileptic seizures were calculated by [OFS+10].

6.2.4. Discussion

In this section the results of the previous chapters are summed up. The scaling coefficients of the power-laws that govern the probability density functions for the energy, duration and interevent waiting time were calculated and compared with experimental data [OFS+10]. An overview is given in table 6.1. The coefficient for the duration is omitted, since it was not considered by [OFS+10].
It was demonstrated that all probability density functions for the state of enhanced activity underlie a power-law. In addition, the scaling coefficients are similar to the experimental results for epilepsy gained by Osorio *et al.* [OFS+10] and even for earthquakes a good consistency was found. The found consistency with the experimental results is astonishing. Both events, epileptic seizures and states of enhanced activity have the same statistical behaviour in many aspects, despite the fact that the Lighthouse Model is a simplistic model, that reduces a neuron to two attributes.
A possible explanation of the occurring power-law behaviour of the states of enhanced activity in the expanded Lighthouse Model is *Self-organized-criticality*. This phenomenology was introduced by [Bak99]. It can occur in dynamic systems that contain an internal threshold. An external force has to be applied on the system, by which energy is stored in the system. If the energy exceeds this threshold, the system reaches criticality, which is a state of marginal stability. A local perturbation can either have a very small effect, or propagate through the whole system. This is denoted as scale-free behaviour and can give rise to a power-law distribution, like it is shown for earthquakes and epileptic seizures [BCDS02, OFS+10].
Since the simulated neural network consists of threshold oscillators, a critical threshold is embedded in the system. The threshold of the single Lighthouse Neuron is given by the Naka-Rushton relation. An external force is applied on the system, by which the system can reach a critical state. It is possible that this state is reached when an adequate number of phases of neurons are close to 2π, since the system is very sensitive to any kind of perturbation. Of course the *Self-organized-criticality* is just one way to explain the occurrence of the power-law behaviour and other explanations are possible.
For instance, one can imagine that the states of enhanced activity are represented by a fixed point in the phase space, where the system is driven to by the external force. At least one of the eigenvalues of this fixed point has to be positive, since the system leaves the orbit of this fixed point. This is caused by an unstable manifold and happens on different trajectories.

Different sets of trajectories could exist, whereby each set represents a state of enhanced activity with a different duration and energy.
A very important aspect, which is worth further investigations, is the parameter range in that these states occur. It was pointed out that the damping γ has to be in a certain range to allow the rise and the termination of states of enhanced activity, but this is still a very superficial investigation. A wider range of parameters can be altered, for instance the values of the coupling matrix were not considered. The only observation that was made is that the coupling weights are tending towards a base level during a state of enhanced activity and they stay at this level, even if more states occur.
Another point to consider is, if the settings of the learning parameter influence the occurrence and rise of a state of enhanced activity. It was shown that the state does not terminate without synaptic plasticity and maybe a parameter setting can be found, for that the occurrence of states of enhanced activity are repressed.
Another important influence is the structure of the network itself. By removing several connections and varying the network structure, the occurrence of states of enhanced activity could be disabled, since the connectivity is important for the occurrence of a state. These are some questions that have to be considered in future work.

6.3. Spreading of states of enhanced synchrony through networks of networks

It is well known that epileptic seizures emerge in foci spread locally and can even spread to other regions of the brain. This was investigated, for instance by Brazier *et al.* [Bra72] and Frederico *et al.* [FM96]. Motivated by this, the spreading of states of enhanced activity through networks of networks is considered. As can be observed in figure 2.4, areas in the brain exist in that nearly all neurons are coupled with each other. On the other hand, the number of connections to spatial separated regions in the brain is in comparison low.
In the following, a network of networks is considered to investigate the spreading of states of enhanced activity through it. The network of networks consists of smaller systems, in which the connectivity between the neurons is very large and an all-to-all coupling exists. These networks are connected to each other by only a few synaptic connections.

6.3.1. Spreading of states of enhanced activity between two networks

The aim of this chapter is to become a first impression for the time τ, which is necessary for the state of enhanced activity to spread to the second system. This knowledge could be helpful if the spreading of states of enhanced activity between huge networks of networks is investigated, to be able to explain the complex interactions that can occur.
Two neural networks are observed. Both are set up as before, but now the system consists of 50 neurons and the damping constant γ is set to 0.4. One of them is set up to create states

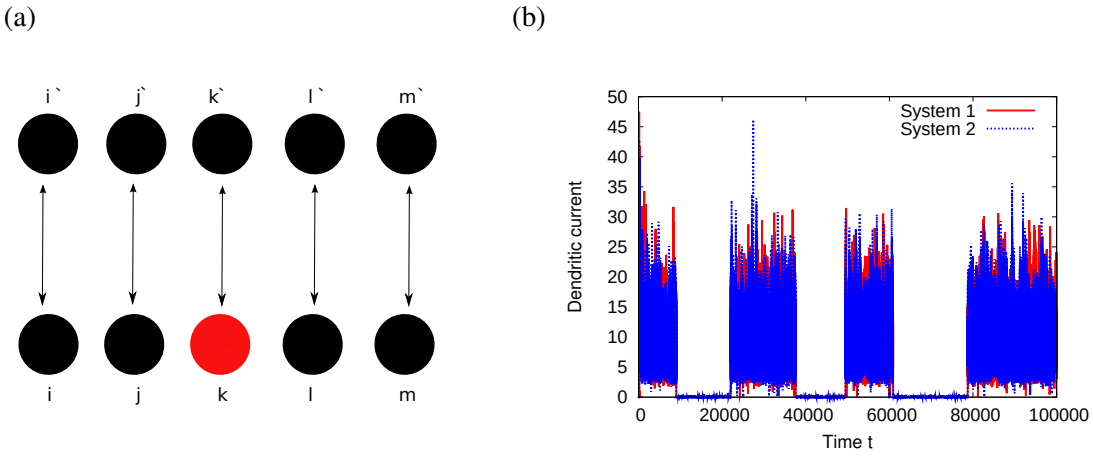

Figure 6.15.: (a) The set up of the two networks is shown. One network generates states of enhanced activity, since one neuron of it receives an external signal. This neuron is highlighted red. The connection between the networks consists of single synaptic connections between neurons of different networks. The number of connections N can be altered and also the coupling strength ζ. (b) The dendritic current of two neurons is shown, whereas each of them is part of another neuronal system.

of enhanced activity. The networks are connected via fixed synaptic links. All synaptic connections between the networks have the same strength. The general setup is shown in figure 6.15 (a).
To get a first impression, two networks are considered. The maximal number of connections between the networks is chosen in combination with a strong synaptic connection. The dendritic current of the systems is shown in figure 6.15 (b).
As one can see, the first system generates a state of enhanced activity, which spreads to the other network after a time τ and from this point in time, the state of enhanced activity in both systems is synchronized. Therefore, the start and termination times in both networks are equal. Since the coupling between the networks is strong, it is not astonishing that the state spreads quickly and that synchronization occurs. For weaker coupling the states do not synchronize and the delay time increases.
In the following, the delay time τ is considered in dependency of the number of couplings N and the coupling strength ζ. To gain statistics, several runs are made for each parameter setting. The initial values for the dendritic currents, the phases of the neurons and the coupling weights of each network are randomly picked. The system parameters of the networks are identical, except that one neuron of one system is driven by an external input. The calculated delay times in dependency of the coupling strength and number of couplings are shown in figure 6.16.

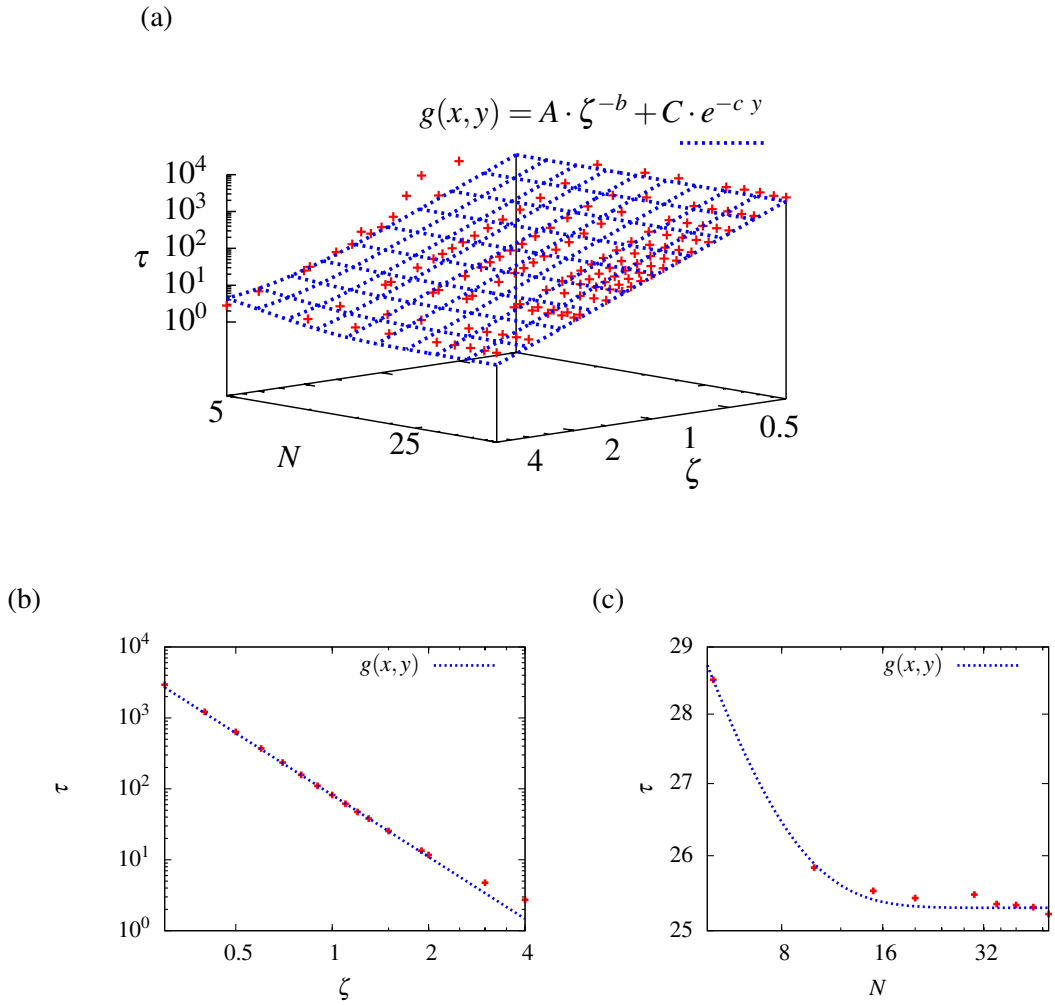

Figure 6.16.: In (a) the delay time τ is plotted in dependency of the number of connections N and the coupling strength ζ in a double logarithmic scale. A curved plane, which is described by equation (6.3), is fitted into the data. The following parameter settings were used: $A = 70$, $b = 2.9$,$c = -0.33765$ and $C = 17.3164$. It describes the delay times for most regions well, except for weak coupling in combination with sparse connections between the system. For strong connectivity between the systems the delay time seems to be independent of the number of connections N. (b) and (c) show transverse sections for a fixed number of connections N (a) and a constant coupling strength ζ (c). As one can see in (a), the data differs slightly from the power-law behaviour for strong couplings weights ζ.

As one can see, the delay time τ has an exponential dependency on the number of connections N for a small connectivity, and tends towards a constant value for a stronger connection between the networks. The delay time has a power-law dependency on the coupling strength ζ and the function describing the delay time reads:

$$\tau \approx A \cdot \zeta^{-b} + C \cdot e^{-c\,y}, \tag{6.3}$$

whereas the parameters can be determined by fitting this equation to the theoretical data. Derivations of this behaviour can be seen for small coupling weights and for a small number of connections. This region spreads if γ increases, since the emergence of a state of enhanced activity in the driven system is inhibited and secondly the second system becomes more sensitive to the received input, too.

7. Summary and outlook

In this diploma thesis the Lighthouse Model was used, which distinguishes from other neural models due to its unique phase relation. In addition, it was combined with an up-to-date mechanism for synaptic plasticity. The results of this work are briefly summarized in the following, whereas the diploma thesis can be divided into two parts.

The first part had the aim to get more familiar with the underlying extended Lighthouse Model. The saturation of the coupling weights were considered in chapter 4. It was analytically shown that saturation occurs under certain conditions. Additionally, it was pointed out that it is rather an oscillation about a fixed value. It should be possible to find the underlying equation that describes the oscillation. Afterwards, this knowledge was applied in chapter 5.1 to demonstrate that the connections of the network can be structured by an external signal. Furthermore it was shown that information can be stored in a network due to this and the system develops an associative memory. This is helpful to demonstrate how the memorization of knowledge in the human brain works and how information is stored.
In chapter 5.2, bumps in a neural network were considered and the findings of Carson Chow *et al.* [CC06] were reproduced. It was pointed out that the behaviour of bumps changes for altered parameter settings. In addition, it was shown that a wandering bump can be localized by spike time dependent plasticity. This phenomena was explained by the emerging structure in the coupling weight matrix. Since it is assumed that these bumps contain information [CC06], the underlying mechanism becomes even more important. Another interesting question is, if the underlying equation for the movement of a bump can be changed. Chow *et al.* [CC06] pointed out that the movement underlies a two mull potential, but by synaptic plasticity this could be altered.

The second part was considering collective states of the network that are linked to the synchronization of neurons. They were denoted as states of enhanced activity and are considered in chapter 6. They were characterized by the fact that all neurons of the network were active at once, whereby their spiking frequency was close to the saturation frequency ν, given by the Naka-Rushton relation.
The statistical attributes of them were considered and it was pointed out that the probability density functions for the energy and interevent waiting time are governed by a power-law. The occurring of collective states with this features is quite new for neural models [LHG09, MG09]. The power-law behaviour is an indicator for the occurrence of *Self-organized-criticality*, since the system fulfils the general requirements for it. But further

investigations are necessary to pinpoint the mechanism, since the power-law behaviour could also be explained by the unstable manifold of a fixed point 6.2.4.
In addition to the *PDFs*, even more statistical attributes were considered, like the aftershock-rate of states of enhanced activity. These were compared with the statistical attributes of epileptic seizures, pointed out by Osorio *et al.* [OFS$^+$10]. Astonishingly it was shown that both systems have a similar behaviour. For instance, the scaling coefficient for the *PDFs* are similar. Therefore it could be possible to transfer knowledge about states of enhanced activity about their occurrence and termination to epileptic seizures. The contributions mentioned above [LHG09, MG09] that also discovered the power-law behaviour did not investigate the additional statistical features, since the states discovered by them, underlie restrictions or had different characteristics.
The underlying dynamic of states of enhanced activity was investigated, but still unresolved questions exist concerning the mechanisms for the emergence and termination of these states. It was shown that the emergence is due to a piling of the phases, similar to the underlying mechanism for earthquakes. By this, the system could reach a critical point, so that scale-free behaviour can occur. Furthermore, it was shown that the termination occurs at a maximum of the phase synchronization of the system. If one compares this behaviour to epileptic seizures, a similarity is observed, hence it is suspected [SBH$^+$08, LBH$^+$09] that synchronization catalyses the termination of states of enhanced activity. A first explanation was given on the system scale to understand the underlying mechanism for the termination and it was pointed out that it is based on spike time dependent plasticity and would not occur without it. Due to the plasticity, the spike order of the neurons is swapped and by this the mean connectivity reaches a minimum, so that the system is barely able to exchange signals. But again, this mechanism has to be investigated in a greater detail and it holds a large potential for future works.
An interesting topic is if an order parameter of the system can be found, which indicates the rise of a state of enhanced activity, before it actually starts. This could be used to predict the occurrence of states of enhanced activity and this information could be transferred to the biological system.
Another point that has to be investigated is the dependency of these states on the learning parameters. For instance, whether a state of enhanced activity can be suppressed, by the right setting of learning parameters. This is connected to the question, why a brain that produced a seizure once, does not always produce more seizures, since nearly every person has a seizure during his life time [LBH$^+$09].

Motivated by the analogy of states of enhanced activity and epileptic seizures, the spreading of states of enhanced activity through a network of networks was investigated in chapter 6.3. The spreading between two networks was observed. The time needed by a state of enhanced activity to reach the second system was considered and a relation between the delay time, the number of couplings and the coupling strength between the networks was found.

To sum up, this contribution investigated states of enhanced activity and pointed out that these have similar attributes to epileptic seizures and earthquakes. The emergence, termination and spreading was explored and maybe some of these points can be investigated in greater detail. Especially the propagating of these states between networks of networks could one day be useful to understand the spreading, termination and occurrence of epileptic seizures in the human brain.

Bibliography

[ABPV+05] J. A. Acebrón, L. L. Bonilla, C. J. Pérez Vicente, F. Ritort, and R. Spigler. The kuramoto model: A simple paradigm for synchronization phenomena. *Reviews of Modern Physics*, 77, Apr 2005.

[AVSN97] L. F. Abbott, J. A. Varela, Kamal Sen, and S. B. Nelson. Synaptic depression and cortical gain control. *Science*, 275, 1997.

[Bak99] P Bak. *how nature works: the science of self-organized criticality*. Springer, 1 edition, 5 1999.

[BCDS02] P. Bak, K. Christensen, L. Danon, and T. Scanlon. Unified scaling law for earthquakes. *Physical Review Letters*, 88, 2002.

[BHSG99] C. C. Bell, V. Z. Han, Y. Sugawara, and K. Grant. Synaptic plasticity in the mormyrid electrosensory lobe. *The Journal of Experimental Biology*, 202, 1999.

[Bra72] M. A. B. Brazier. Spread of seizure discharges in epilepsy: Anatomical and electrophysiological considerations. *Experimental Neurology*, 36, 1972.

[Bur06] A. Burkitt. A review of the integrate-and-fire neuron model: I. homogeneous synaptic input. *Biological Cybernetics*, 95, 2006.

[Car92] N. A. Carlson. *Foundations of Physiological Psychology*. Massachusetts: Simon and Schuster, 1992.

[CC06] C. C. Chow and S. Coombes. Existence and wandering of bumps in a spiking neural network model. *Journal on Applied Dynamical Systems*, 5, 2006.

[CDSB02] K. Christensen, L. Danon, T. Scanlon, and P. Bak. Unified scaling law for earthquakes. *Proceedings of the National Academy of Sciences of the United States of America*, 99, 2002.

[CJ10] C.-C. Chen and D. Jasnow. Mean-field theory of a plastic network of integrate-and-fire neurons. *Physical Review E*, 81, 2010.

[CLL+11] M. Chacron, T. Lewis, J. Lewis, A. Longtin, L. Maler, J. Rubin, and J.-P. Thivierge. *5th Computaional Neuroscience Summer School*. uOttawa Centre for Neuronal Dynamics, 2011.

[CLM04] M. J. Chacron, A. Longtin, and L. Maler. To burst or not to burst? *Journal of Computational Neuroscience*, 17, 2004.

[Coo05] S. Coombes. Waves, bumps, and pattern in neural field theories. *Biological Cybernetics*, 93, 2005.

[CS07] B. Cessac and M. Samuelides. From neuron to neural networks dynamics. *The European Physical Journal - Special Topics*, 142, 2007.

[DHF05] O. David, L. Harrison, and K. J. Friston. Modelling event-related responses in the brain. *NeuroImage*, pages 756–770, 2005.

[Doi07] N. Doidge. *The Brain That Changes Itself: Stories of Personal Triumph from the Frontiers of Brain Science (James H. Silberman Books)*. Penguin (Non-Classics), 1 reprint edition, 12 2007.

[DP06] Y Dan and M. Poo. Spike timing-dependent plasticity: From synapse to perception. *Physiol Rev*, 86, 2006.

[DWG+05] L. G. Dominguez, R. A. Wennberg, W. Gaetz, D. Cheyne, C. Snead, and J. L. P. Velazquez. Enhanced synchrony in epileptiform activity? local versus distant phase synchronization in generalized seizures. *The Journal of Neuroscience*, 25, 2005.

[FA11] J. Fell and N. Axmacher. The role of phase synchronization in memory processes. *Nature Reviews Neuroscience*, 12, 2011.

[FBB+05] R. S. Fisher, W. v. E. Boas, W. Blume, C. Elger, P. Genton, P. Lee, and Engel. Epileptic seizures and epilepsy: Definitions proposed by the international league against epilepsy (ilae) and the international bureau for epilepsy (ibe). *Epilepsia*, 46, 2005.

[Fen01] J. Feng. Is the integrate-and-fire model good enough?—a review. *Neural Networks*, 14, 2001.

[FM96] P. Frederico and B. Macviar. Imaging the induction and spread of seizure activity in the isolated brain of the guinea pig: The roles of gaba and glutamate receptors. *Journal of Neurophysiology*, 76, 1996.

[GC04] Y. Guo and C. C. Chow. Existence and stability of standing pulses in neural networks : I existence. *SIAM Journal on Applied Dynamical Systems*, 4, 2004.

[GvH92] W. Gerstner and J. L. van Hemmen. Associative memory in a network of 'spiking' neurons. *Network: Computation in Neural Systems*, 3, 1992.

[Hak95] H. Haken. *Principles of Brain Functioning: A Synergetic Approach to Brain Activity, Behavior and Cognition (Springer Series in Synergetics)*. Springer, 1 edition, 1995.

[Hak06] H. Haken. *Brain Dynamics: Synchronization and Activity Patterns in Pulse-Coupled Neural Nets with Delays and Noise (Springer Series in Synergetics)*. Springer, 2006.

[Heb49] D. O. Hebb. The organization of behaviour. *New York : Wiley*, 18, 1949.

[Heb02] D. O. Hebb. *The Organization of Behavior: A Neuropsychological Theory*. Psychology Press, new edition edition, 2002.

[HGMJ06] A. V. M. Herz, T. Gollisch, C. K. Machens, and D. Jaeger. Modeling single-neuron dynamics and computations: A balance of detail and abstraction. *Science*, 314, 2006.

[HH52] A. L. Hodgkin and A. F. Huxley. A quantitative description of membrane current and its application to conduction and excitation in nerve. *Journal of Physiology*, 17, 1952.

[HH95] J. J. Hopfield and A. V. Herz. Rapid local synchronization of action potentials: toward computation with coupled integrate-and-fire neurons. *Proceedings of the National Academy of Sciences of the United States of America*, 92, 1995.

[HO11] C. Himpe and M. Ohlberger. Implementation and analysis of dynamic causal modeling for eeg/meg data. *WWU*, 2011.

[Jen98] H. J. Jensen. *Self-Organized Criticality: Emergent Complex Behavior in Physical and Biological Systems (Cambridge Lecture Notes in Physics)*. Cambridge University Press, 1 1998.

[JR95] B. H. Jansen and V. G. Rit. Electroencephalogram and visual evoked potential generation in a mathematical model of coupled cortical columns. *Biological Cybernetics*, 73, 1995.

[KSJ00] E. R. Kandel, J. H. Schwartz, and T. M. Jessell. *Principles of Neural Science*. New York: McGraw-Hill, 2000.

[LBH+09] K. Lehnertz, S. Bialonski, M. T. Horstmann, D. Krug, A. Rothkegel, M. Staniek, and T. Wagner. Synchronization phenomena in human epileptic brain networks. *Journal Neuroscience Methods*, 183:42–48, 2009.

[LHG09] A. Levina, J. M. Herrmann, and T. Geisel. Phase transitions towards criticality in a neural system with adaptive interactions. *Physical Review Letters*, 102, 2009.

[MG09] C. Meisel and T. Gross. Adaptive self-organization in a realistic neural network model. *Physical Review E*, 80, Dec 2009.

[MTK05] R. G. M. Morris, L. Tarassenko, and M. Kenward. *Cognitive Systems - Information Processing Meets Brain Science*. Academic Press, 1 edition, 2005.

[oA12] Epilepsy Foundation of America. http://www.epilepsyfoundation.org/aboutepilepsy, 25. January. 2012.

[OFS+10] I. Osorio, M. G. Frei, D. Sornette, J. Milton, and Y.-C. Lai. Epileptic seizures: Quakes of the brain? *Physical Review E*, 82, 2010.

[Omo94] F. Omori. On the aftershocks of earthquakes. *Journal of the College of Science*, Imperial University of Tokyo 7, 1894.

[PF12] C. Petrovic and R. Friedrich. Spiking neural networks - pattern formation and plasticity. *WWU*, 2012.

[Pop00] S. B. Pope. *Turbulent Flows*. Cambridge University Press, 1 edition, 10 2000.

[Pre07] W. Press. *Numerical Recipes*. Cambridge University Press, 2007.

[RL11] A. Rothkegel and K. Lehnertz. Recurrent events of synchrony in a complex network of pulse-coupled oscillators. *Europhysics Letters*, 95, 2011.

[Run89] J. B. Rundle. Derivation of the complete gutenberg-richter magnitude-frequency relation using the principle of scale invariance. *Reviews of Modern Physics*, 94, Apr 1989.

[SBH+08] K. A. Schindler, S. Bialonski, M. T. Horstmann, C. E. Elger, and K. Lehnertz. Evolving functional network properties and synchronizability during human epileptic seizures. *Chaos*, 18, 2008.

[She94] G. M. Shepherd. *Neurobiology*. Oxford University Press, USA, 3 edition, 5 1994.

[Sor10] D. Sornette. Dragon-kings, black swans and the prediction of crisis. *International Journal of Terraspace Science and EngineerfCooing*, 2010.

[Spe10] *Spektrum der Wissenschaft*, November 2010.

[Squ87] L. R. Squire. *Memory and Brain*. Oxford University Press, USA, 1 edition, 1987.

[STR04] R. Shcherbakov, D. L. Turcotte, and J. B. Rundle. A generalized omori's law for earthquake aftershock decay. *Geophysical research letters*, 31, 2004.

[TDH+11] W. Truccolo, J. A. Donoghue, L. R. Hochberg, E. N. Eskandar, J. R. Madsen, W. S. Anderson, E. N. Brown, E. Halgren, and S. S. Cash. Single-neuron dynamics in human focal epilepsy. *Nature Neuroscience*, 14, 2011.

[TM97] M. V. Tsodyks and H. Markram. The neural code between neocortical pyramidal neurons depends on neurotransmitter release probability. *Proceedings of the National Academy of Sciences of the United States of America, Neurobiology*, 94, 1997.

[UOM95] T. Utsu, Y. Ogata, and R. S. Matsu'ura. The centenary of the omori formula for a decay law of aftershock activity. *Journal of Physics of the Earth*, 43, 1995.

[vRBT00] M. C. W. van Rossum, G. Q. Bi, and G. G. Turrigiano. Stable hebbian learning from spike timing-dependent plasticity. *The Journal of Neuroscience*, 81, 2000.

Danksagung

"So long and thanks for all the fish."

Douglas Adams, The Hitchhiker's Guide to the Galaxy

Zuerst einmal möchte ich mich bei Prof. Friedrich bedanken. Für die gebotene Betreuung, die stets offene Tür und die hilfreichen Ratschläge. Auch für die gegebenen Gelegenheiten, Tagungen oder Summer schools zu besuchen, möchte ich mich bei ihm bedanken.
Außerdem möchte ich Dr. Wolters meinen Dank aussprechen sowohl dafür, dass er sich als Zweitgutachter bereitgestellt hat, als auch für das gezeigte Interesse an meiner Arbeit.
Bedanken möchte ich mich des weiteren bei Michael Wilczek für die nette Betreuung im Seminar, sowie für die gegebenen Ratschläge. Auch bei Oliver Kamps möchte ich mich bedanken, für die stets anspornenden und motivierenden Gespräche und als auch für die gemeinsam gesungenen Lieder. Natürlich gebührt auch der anderen Hälfte des Büros, Christoph Berling, mein Dank, besonders die gemeinsamen Muffinmontage. Svetlana Gurevich danke ich für die Motivation und den Kaffee, Katrin Schmietendorf für ein offenes Ohr, Johannes Lülff für die Beratung bei LaTeX und Nintendo Problemen und Christoph Honisch und Golo Strickmann für eine schöne Zeit in Oldenburg. Natürlich ist auch Cornelia Petrovic nicht zu vergessen, als auch die restliche Arbeitsgruppe.

Des weiteren möchte ich mich bei Marc Osthues, Christian Diddens und Michael Grevenstette aus Büro 406 bedanken, "zu dem ich auch irgendwie dazugehöre", sowie Michael Bengfort und Karsten Dreimann. Um auch niemanden zu vergessen, möchte ich auch Dirk Sandbrink und Helmsby erwähnen, die stets Zeit für Kaffee hatten und auch Computerprobleme schnell und zuverlässig gelöst haben.
Fürs Korrekturlesen möchte ich mich bei Tobias Eschen, Felix Huerkamp, Hans-Georg Pietruck, der Wg an der Oase und auch noch einmal bei Oliver Kamps bedanken.
Zum Schluss möchte ich mich auch bei meinen Eltern und Geschwistern bedanken, dafür dass sie stets für mich da sind, zu jeder Tages- und Nachtzeit, und für die Unterstützung und das entgegengebrachte Vertrauen in allen nur erdenklichen Situationen.

Vielen Dank für alles.

Erklärung zur Diplomarbeit
Hiermit versichere ich, diese Arbeit selbstständig angefertigt und außer den angegebenen keine weiteren Hilfsmittel verwendet zu haben.

Daniel Ritterskamp
Münster, im Januar 2011